DYNAMICAL SYMMETRY-BREAKING AND THE MEAN-FIELD APPROACH IN MICROSCOPIC NUCLEAR THEORY

Edward David Davis

A Thesis submitted to the Faculty of Science,
University of the Witwatersrand, Johannesburg,
in Fulfilment of the Requirements
for the Degree of Doctor of Philosophy.

Johannesburg 1986

ABSTRACT

The "phase transitions" predicted within finite microscopic systems by Hartree-Fock-Bogoliubov (HFB) and aspects of the use of the associated broken-symmetry bases in the random-phase approximation (RPA) are considered using soluble models. Evidence is presented in support of the conjecture that the success of these techniques lies in the fact that they mimic singularities in the dependence on interaction strengths of the exact solution. This conjecture provides a natural explanation for why such methods fail close to a point where a phase transition occurs and indicates possible directions for improvement.

Phase diagrams at both zero and finite temperature are determined, and simple analytic expressions for the way in which critical strengths scale with particle number are found. It is shown that the "phase transitions" predicted at finite temperature are relevant. A connection between the singularities referred to above and real phase transitions found in the thermodynamic limit is discussed.

It is found that only stable bases can be used in an RPA calculation. This is in particular true for those RPA modes which are not associated with the onset of instability of the basis; these modes do not describe any excited state when the basis is unstable.

Outside transitional regions certain undesirable features of HFB are unearthed, notably that the HFB ground state energy is not necessarily an upper bound to the exact ground state energy. The effectiveness in this regime of the Hartree-Fock Seniority approximation as a substitute to projection methods is evaluated.

DECLARATION

I declare that this dissertation is my own, unaided work. It is being submitted for the degree of Doctor of Philosophy in the University of the Witwatersrand, Johannesburg. It has not been submitted before for any degree or examination in any other university.

E D Davis

Edward David Davis

12th day of August, 1986.

To the memory of my father

EDWARD DAVIS

(1906 - 1974)

CONTENTS

ACKNOWLEDGEMENTS

I am happy to have this opportunity to thank the many physicists, fellow graduate students, other colleagues, friends and members of my family who, in different ways, have contributed to this work. I wish to express my indebtedness to, in particular:

* Dieter Heiss, my supervisor, for his insightful guidance and unflagging encouragement;
* Hank Miller, for the numerous instructive and stimulating discussions, and the salient suggestion to consider finite temperature "phase transitions";
* Michael Gering for his interest and the fine example he set;
* Lyn for all her sacrifices on my behalf;
* my Mother for her support.

In addition, access to the computing facilities of the Wits-CSIR Schonland Research Centre for Nuclear Sciences is gratefully acknowledged.

Finally, my thanks go to Hester Wolmarans and Phillip Anagnostaras for their efforts in the physical production of this thesis.

Some of the material in this thesis appears in two papers, namely (DH 86) (which is based on chapters 2, 3 and 6) and (DM 86) (which is a condensation of chapters 4 and 5).

LIST OF TABLES

LIST OF ILLUSTRATIONS

CHAPTER ONE

INTRODUCTION

A challenge common to many areas of physics is to understand the properties of an interacting system having large or infinite numbers of degrees of freedom. Among these complex many-body problems, the ground state structure and low-energy collective dynamics of atomic nuclei occupy a unique place: the wealth of experimental information on nuclear properties makes the nucleus by far the best laboratory for the study of quantal collective phenomena (AW 85 and references therein).

The past 35 years have seen the development in importance of the self-consistent mean-field approximation in the microscopic description of the nuclear many-body problem. Beginning with the early bewilderment that something like the shell model could be good in a strongly interacting system, continuing through the discovery (BL 55, Br 55) of a suitable treatment of short-range correlations, and then the discovery (BCS 57, BMP 58) of a suitable treatment of pairing correlations, it was ultimately established that an adequate quantitative description of ground state properties can be afforded by a (static) self-consistent mean-field approximation of, in the most general case, the Hartree-Fock-Bogoliubov type with an effective interaction derived from first principles (NV 72, FN 75). More recently an ambitious programme involving the time-dependent generalisation of mean-field theory has been launched (BKN 76, CMM 78, FKW 78) with a view to providing a microscopic description of nuclear collisions (at an energy of a few MeV per nucleon above the Coulomb barrier) and large-amplitude collective motion; collective variables and their dynamics are fully specified by the nuclear Hamiltonian and the physical process under consideration, and not decided upon on an ad hoc basis. This theory presents a formidable computational effort as it leads to a set of highly non-linear coupled integro-differential equations, but the solutions have demonstrated an unexpectedly rich behaviour and good agreement with experiment has been found (Ne 82, DDK 85, KG 85).

The mean-field approximation does not accommodate energy-dependent (or dynamic) effective interactions. The significance and physical relevance of dynamic interactions, as well as their proper treatment within the Green's function formulation of the many-body problem, have been discussed at length in (EHH 77) and (Ge 85). A formally important property emerging from these investigations is the crossing-symmetry required of an exact four point vertex function Γ, which reflects the complexity of a many-body system in mathematical terms. Direct attempts to construct a crossing-symmetric Γ in the general case have been unsuccessful (He 80, 81), but insight has been gained from the model study in (GH 84a), which, in fact, suggests that the implementation of crossing-symmetry becomes important in the region of the "phase transitions" within nuclei predicted by the self-consistent mean-field approximation. This claim rests on the conjecture that the "phase transitions" are related to the presence of branch point singularities in the dependence on interaction strengths of the exact solution. The desire to present more evidence in support of this conjecture was the starting point of the present study.

Two topics are explored in this work. The first concerns the "phase transitions" predicted by the self-consistent mean-field approximation when applied to finite microscopic systems both at zero and at finite temperature. In chapter 5, evidence is presented in support of the conjecture discussed above (which refers to zero temperature phase transitions). In particular attention is paid to what can reasonably be expected to happen to the distribution of branch point singularities as the dimensions of the system increase, specifically as the particle number $N \to \infty$ (and the thermodynamic limit is attained), to see whether these singularities can account for (as they must) the occurrence of non-analytic behaviour in the real phase transitions found in this limit.

These investigations imply that, contrary to the findings of (Go 84) and (ERI 85), a "phase transition" predicted in a finite system should remain visible at finite temperature. Accordingly, this issue is also taken up (again in chapter 5), but, instead of studying order parameters as in (Go 84) and (ERI 85), the specific heat C_V is considered; it has the advantage of being a direct measure of thermal fluctuations, which are claimed to be responsible for the "washing out" of the "phase transitions", and at the same time, it behaves in a distinctive (singular) way in real phase transitions.

The second topic is intimately related to the first: aspects of the use (at zero temperature) of self-consistent mean-fields with broken symmetry are addressed. The conjectured relationship between phase transitions and branch point singularities is seen to imply that broken-symmetry bases which are stable (in the sense of section 3.1) mimic appropriately the effects of the singularities. Thus, while they may be inadequate in the vicinity of a phase transition, their quality ought to improve outside of the transition region. Confirmation of this is presented in chapter 6, which considers RPA calculations in the vicinity of phase transitions and beyond. Both stable and unstable bases are employed in order to highlight this.

In chapter 7, some unexpected and undesirable consequences of using broken-symmetry bases, which can arise in regions far removed from phase transitions, are discussed. In addition, the effectiveness in this regime of an approximate treatment, which has been proposed recently (GP 86) as a substitute to complex projection methods, is evaluated.

To accomplish all this, the exactly soluble Agassi model (Ag 68, DH 86), which is similar to the Pairing-plus-Quadrupole model, is employed. It is chosen because a variety of phase transitions can be studied within it. Chapters 2 - 4 prepare the foundations for the subsequent considerations by discussing the exact properties of this model and results of the application of Hartree-Fock-Bogoliubov (HFB) at zero and finite temperature. In chapter 2, the model is described; its exact solution using the quasi-spin method and qualitative features of the solution are discussed. Zero temperature and finite temperature HFB are applied in chapters 3 and 4, respectively, with the purpose of establishing the appropriate phase diagrams.

Conclusions emerging from this work are presented in chapter 8. With the exception of chapter 8, each of the succeeding chapters possesses an introductory section in which the contents of the particular chapter is outlined. These complement the discussion in this chapter of the global structure of the thesis by pointing out specific results which are felt transitions", and at the same time, it behaves in a distinctive (singular) way in real phase transitions.

The second topic is intimately related to the first: aspects of the use (at zero temperature) of self-consistent mean-fields with broken symmetry are addressed. The conjectured relationship between phase transitions and branch point singularities is seen to imply that broken-symmetry bases which are stable (in the sense of section 3.1) mimic appropriately the effects of the singularities. Thus, while they may be inadequate in the vicinity of a phase transition, their quality ought to improve outside of the transition region. Confirmation of this is presented in chapter 6, which considers RPA calculations in the vicinity of phase transitions and beyond. Both stable and unstable bases are employed in order to highlight this.

In chapter 7, some unexpected and undesirable consequences of using broken-symmetry bases, which can arise in regions far removed from phase transitions, are discussed. In addition, the affectiveness in this regime of an approximate treatment, which has been proposed recently (GP 86) as a substitute to complex projection methods, is evaluated.

To accomplish all this, the exactly soluble Agassi model (Ag 68, DH 86), which is similar to the Pairing-plus-Quadrupole model, is employed. It is chosen because a variety of phase transitions can be studied within it. Chapters 2 - 4 prepare the foundations for the subsequent considerations by discussing the exact properties of this model and results of the application of Hartree-Fock-Bogoliubov (HFB) at zero and finite temperature. In chapter 2, the model is described; its exact solution using the quasi-spin method and qualitative features of the solution are discussed. Zero temperature and finite temperature HFB are applied in chapters 3 and 4, respectively, with the purpose of establishing the appropriate phase diagrams.

Conclusions emerging from this work are presented in chapter 8. With the exception of chapter 8, each of the succeeding chapters possesses an introductory section in which the contents of the particular chapter is outlined. These complement the discussion in this chapter of the global structure of the thesis by pointing out specific results which are felt to be novel or interesting and by citing, where appropriate, relevant developments in the literature. In addition, there are several appendices. As in most cases their contents is relevant to no more than one chapter, they have been formatted to appear as integral parts of the chapters concerned.

CHAPTER TWO

THE AGASSI MODEL

The Agassi model (Ag 68) consists of N identical fermions which occupy two levels, each with degeneracy Ω (Ω even). Adopting the BCS phase convention, the Hamiltonian is

$$H = \frac{\varepsilon}{2} \sum_{\sigma m} \sigma\, c^{\dagger}_{\sigma m} c_{\sigma m} - \frac{V}{2} \sum_{\sigma, m, m'} c^{\dagger}_{\sigma m} c^{\dagger}_{\sigma m'} c_{-\sigma m'} c_{-\sigma m}$$

$$- g \sum_{\substack{\sigma,\sigma' \\ m,m' > 0}} c^{\dagger}_{\sigma m} c^{\dagger}_{\sigma -m} c_{\sigma' -m'} c_{\sigma' m'} \tag{2.1}$$

where σ labels the levels, m the states within a level and $c^{\dagger}_{\sigma m}$ creates a fermion in the single-particle state $|\sigma m\rangle$. In this work σ is taken to be +1(-1) for the upper (lower) level, and m to have the range $m = \pm 1, \pm 2, \ldots, \pm\Omega/2$. Also V and g are assumed to be non-negative, and N to be even.

The Agassi model is by design a schematic version of the phenomenologically successful Pairing-plus-Quadrupole model (KG 84). While the pairing interaction (with strength g) is retained, the complex quadrupole interaction is replaced by the simpler monopole interaction (with strength V) familiar from the LMG model (LMG 65). It is well known (GLM 65, ALM 66) that this interaction is responsible for effects which are formally similar to those induced by the quadrupole interaction. The two levels together may be interpreted as the equivalent of the valence shell in a nucleus. In application of the Pairing-plus-Quadrupole model, the single-particle levels used are typically (GD 66) just those in this shell.

Familiarity with the LMG model and the 2-Level Pairing model (RR 64) immediately suggests that the Hamiltonian of the Agassi model can be rewritten as

$$H = \varepsilon J_0 - \frac{V}{2}(J_+^2 + J_-^2) - g(L_+ + S_+)(L_- + S_-) \tag{2.2}$$

in which

$$S_+ = (S_-)^\dagger = \sum_{m>0} c^\dagger_{-1m} c^\dagger_{-1-m} , \quad L_+ = (L_-)^\dagger = \sum_{m>0} c^\dagger_{1m} c^\dagger_{1-m} ,$$

$$J_+ = (J_-)^\dagger = \sum_m c^\dagger_{1m} c_{-1m} , \qquad J_o = L_o - S_o, \tag{2.3}$$

where

$$L_o = \tfrac{1}{2}(\sum_m c^\dagger_{1m} c_{1m} - \Omega/2) \quad \text{and} \quad S_o = \tfrac{1}{2}(\sum_m c^\dagger_{-1m} c_{-1m} - \Omega/2).$$

The L, S and J operators separately form SU(2) algebras. Obviously the L and S operators commute. Consideration of the commutation relations of the J operators with the L and S operators shows that a closed Lie algebra is obtained by introducing the operators M_+ and $M_- = (M_+)^\dagger$ where

$$M_+ = \sum_{\substack{\sigma,m \\ m>0}} c^\dagger_{\sigma m} c^\dagger_{-\sigma-m}. \tag{2.4}$$

The M operators also form an SU(2) algebra: the operator M_o is given by $M_o = L_o + S_o$.

The non-trivial commutators of the 10 independent operators introduced above are given in Appendix 2.2; they demonstrate that these operators form the Lie algebra of the group SO(5) (Pa 65, Ge 81). This means that H can only have a non-zero matrix element between two states if a component of each belongs to the same irreducible representation of SO(5). The irreducible representations of SO(5) contain states of different particle numbers. The dimension of the N-particle subspaces within these irreducible representations is at most cubic in N. (by contrast, the dimension of the full Hilbert space involved grows exponentially with N.) Accordingly, adopting a basis which consists of these N-particle subspaces makes exact diagonalization (by computer) of the <u>entire</u> Hamiltonian matrix feasible even when N is quite large.

In succeeding chapters the Agassi model will be considered at both zero and finite temperatures. The approach adopted at finite temperature is however influenced by insights arrived at in the zero temperature case. So, this chapter will be devoted to material relevant to the exact solution at zero temperature. (The finite temperature case will be taken up in Chapter 5.)

At zero temperature, only the ground state of the Agassi model and its most collective (low-lying) excitations are of interest. These are all spanned by a single irreducible representation of the "quasi-spin" group SO(5), whatever the value of N. (Recall N is assumed to be even.) For obvious reasons, the N-particle subspace of this irreducible representation will subsequently be referred to as the "collective subspace" of the N-particle system. The dimension of the subspace is a quadratic in N.

The introduction of the quasi-spin group SO(5) dramatically simplifies the problem of determining the most collective states of the Agassi model. The use of SO(5) in the Agassi model is an illustration of a completely general approach to the nuclear man problem. The rationale behind this approach is discussed extens (KCL 82). A spin-off is that it suggests a method whereby a ty of exactly soluble but non-trivial models can be generated.

The information necessary to construct the Hamiltonian matrix in the collective subspace of the Agassi model is presented in Section 2.1 of this chapter. In particular, the group theoretical basis for the collective subspace will be considered. While all of this material is implicit in the literature (Ag 68, He 65, Pa 65), this discussion makes the thesis self-contained (and serves as an accessible prescription for anyone who would like to use the Agassi model).

Section 2.2 is devoted to the small and large interaction strength limits of the Agassi model. This discussion establishes what the salient qualitative features of the exact solution are. Finally, there are two appendices to this chapter. The first contains useful matrix elements of the operators in the SO(5) algebra in the group theoretical basis for the collective subspace, and the second, as already mentioned, the non-trivial commutators of these quasi-spin operators.

SECTION 2.1: INGREDIENTS FOR THE EXACT SOLUTION OF THE AGASSI MODEL

The L and S operators introduced in Eq. (2.3) can be used to construct a set of four commuting operators, namely L^2, S^2, L_o and S_o. The mathematically natural choice of basis for an irreducible representation of SO(5) consists of simultaneous eigenstates of these four operators (Section 2 in (He 65)). In fact, the eigenvalues of these operators are sufficient to label the members of the basis completely. Furthermore the maximum values attained within the irreducible representation by the eigenvalues of L_o and S_o unambiguously specify the representation. If these are denoted by L_m and S_m respectively, then the basis states are $|(L_mS_m)L,S,M_L,M_S\rangle$, where $M_L(M_S)$ is the eigenvalue of $L_o(S_o)$, and $L(L + 1)$ and $S(S + 1)$ are the eigenvalues of L^2 and S^2 respectively.

The basis used in (RR 64) to diagonalise the 2-level Pairing model is very similar. When both levels have the same degeneracy Ω, the states in the basis are

$$|LS\ M_L\ M_S\rangle = |L\ M_L\rangle\ |S\ M_S\rangle$$

where

$$L = S = \Omega/4$$

and

$$M_L = -\Omega/4,\ -\Omega/4 + 1,\ \ldots,\ -\Omega/4 + N/2\ (M_S = (N - \Omega)/2 - M_L).$$

These span the interacting ground state of this model. If the limit (i.e. $V \to 0$) in which the Agassi model coincides with the 2-level Pairing model is uniform, the irreducible representation of SO(5) which contains the collective subspace of the Agassi model must contain states for which $L = S = \Omega/4$. This is only possible if L_m, $S_m \geq \Omega/4$. On the other hand, from the definitions of L_o and S_o in Eq. (2.3), their eigenvalues M_L, $M_S \leq \Omega/4$, implying L_m, $S_m \leq \Omega/4$. Combining these inequalities leads to the result that, for the irreducible representation of interest, $L_m = S_m = \Omega/4$, whatever the value of N.

The assumption required to derive this conclusion falls away if it can be shown that the irreducible representation selected spans the ground state of the LMG model. This model possesses the same single-particle level scheme as the Agassi model but the number of particles present is automatically equal to Ω. An obvious member of the basis spanning the ground state is the state in which all Ω particles occupy the lower level. This state is also found in the irreducible representation with $L_m = S_m = \Omega/4$, where it is denoted by

$$|(\Omega/4\ \Omega/4)\ \Omega/4,\ \Omega/4,\ -\Omega/4,\ \Omega/4>.$$

As the remainder of the basis for the ground state of the LMG model is generated by acting on this state with the "ladder" operator J_+ (introduced in Eq. (2.3)), the desired result follows.

Because $L_m = S_m$ in the irreducible representation of interest, the basis consists of states in which $L = S$ (Eq. (11) in (He 65)). The range of values of L (and S) is given by $L = \Omega/4 - m/2$ where $m = 0, 1, 2, \ldots, \Omega/2$. In states containing N particles, the eigenvalues M_L and M_S must satisfy the constraint

$$M_L + M_S = (N - \Omega)/2 = \Delta. \tag{2.6}$$

This is possible provided $2L = \Omega/2 - m \geq |\Delta|$, or equivalently, $m \leq m_u$ where

$$m_u = \Omega/2 - |\Delta| = \begin{cases} N/2 & N \leq \Omega \\ (2\Omega - N)/2 & N > \Omega \end{cases} \tag{2.7}$$

The constraint in Eq. (2.6) implies that M_L and M_S can be written as

$$M_L = \Delta/2 + z \quad , \qquad M_S = \Delta/2 - z \tag{2.8}$$

where the unconstrained variable $z = -z_u, -(z_u - 1), -(z_u - 2), \ldots, z_u - 1, z_u$ with

$$2z_u = m_u - m, \tag{2.9}$$

Thus the group theoretical basis for the N-particle collective subspace of the Agassi model is the set of states

$$|m,z\rangle$$

$$= |(L_m = S_m = \Omega/4)\ L = S = \Omega/4 - m/2,\ M_L = \Delta/2 + z,\ M_S = \Delta/2 - z\rangle$$

where the ranges of m and z are given above. Clearly the dimension of this subspace is

$$D_c = \sum_{m=0}^{m_u} (2z_u + 1) = \tfrac{1}{2}(m_u + 1)(m_u + 2),$$

which is a quadratic in either N or $2\Omega - N$, whichever is smaller. In circumstances where it is necessary to specify the particle number of the state $|m,z\rangle$ it will be denoted by $|m,z,\Delta\rangle$.

Inspection of the Hamiltonian in Eq. (2.1) shows that it transforms a state containing an even number of particles in the upper level into (in general) a linear combination of such states; a similar result holds for states containing an odd number of particles in the upper level. The formal reason for this property is that the Hamiltonian commutes with the "parity" operator $P = \exp(i\pi J_0)$ familiar from the LMG model. States which contain an even/odd number of particles in the upper level, and linear combinations of these states, are said to possess positive/negative parity. Because the state $|m,z\rangle$ is an eigenstate of L_0, it must have good parity; in fact it is easily shown that $|m,z\rangle$ has positive parity if m is even and negative parity if m is odd. The parity symmetry of the Agassi Hamiltonian implies that the Hamiltonian matrix in the basis $|m,z\rangle$ is not of dimension D_c. Instead it consists of two submatrices, one of which couples the positive parity (even m) basis states, while the other couples the negative parity (odd m) basis states. The dimensions of these submatrices are given in Table 2.1. It is clear that the eigenstates which emerge from the diagonalisation of this Hamiltonian matrix automatically have good parity.

Expressions for the non-zero matrix elements of the Agassi Hamiltonian H in the basis $|m,z\rangle$ can be deduced from Eqs. (A2.4) - (A2.7) of Appendix 2.1. The members of the basis are assumed to be ordered so that m increases from left-to-right or top-to-bottom in a matrix and, for given m, z varies in the same way. Since the Hamiltonian matrix is hermitian, only the matrix elements $\langle m',z'|H|m,z\rangle$ in which $(m',z') \geq (m,z)$, have to be calculated. Expressions for three of these matrix elements can be written down immediately from Eqs (A2.4) - (A2.7). They are:

1) $$\langle m,z|H|m,z\rangle = \langle m,z|\ \varepsilon J_o - g(L_+L_- + S_+S_-)\ |m,z\rangle$$

$$= 2z\,\varepsilon - \left\{\frac{1}{2}\left(\frac{\Omega}{2} - m\right)\left(\frac{\Omega}{2} - m + 2\right) - 2z^2 - \Delta\left(\frac{\Delta}{2} - 1\right)\right\}g; \tag{2.10a}$$

2) $$\langle m,z+1|H|m,z\rangle = -\langle m, z+1|g\,L_+S_- + \frac{V}{2}J_+^2|m,z\rangle$$

$$= -(g + b(m)V)\ \alpha(z+1)\ \alpha(-z) \tag{2.10b}$$

where

$$\alpha(x) = \tfrac{1}{2}(m_u - m + 2x)^{\frac{1}{2}}\ (m_u - m + 2|\Delta| + 2x)^{\frac{1}{2}}$$

and

$$b(m) = (a(m))^2 + (a(m-1))^2$$

in which

$$a(m) = \left\{ \frac{2(m+1)(\Omega - m + 2)}{(\Omega - 2m)(\Omega - 2m + 2)} \right\}^{\frac{1}{2}};$$

3) $$\langle m+2, z+1|H|m,z\rangle = -V/2\ \langle m+2, z+1|J_+^2|m,z\rangle$$

$$= a(m+1)\ a(m)\ \alpha(-z)\ \alpha(-z-1)\ V. \tag{2.10c}$$

The fourth (and final) non-zero matrix element of H of this type follows from the observation that $\langle m-2, z+1|J_+^2|m,z\rangle$ is non-zero (cf. Eq. (A2.7)), which implies, through hermitian conjugation, that

$$<m + 2, z - 1|J^2_-|m,z>$$

is non-zero. Thus, using the reality of matrix elements of $J^2_{\pm}$,

$$\begin{aligned} <m + 2, z - 1|H|m,z> &= - V/2 <m + 2, z - 1|J^2_-|m,z> \\ &= - V/2 <m,z|J^2_+|m + 2, z - 1> \qquad (2.10d) \\ &= - a(m + 1)\ a(m)\ \alpha(z)\ \alpha(z - 1)\ V. \end{aligned}$$

The parity-conserving property of H is contained in the fact that $<m',z'|H|m,z>$ is non-zero only if $m' - m$ is even.

In the non-interacting limit, it is obvious the properties of the $(\Omega + 2k)$-particle system where ($k = 1, 2, \ldots, \Omega/2$) are trivially related to those of the $(\Omega - 2k)$-particle system, if the description of states in the $(\Omega + 2k)$-particle system is reformulated in terms of the $(\Omega - 2k)$ single-particle states which are unoccupied. Consideration of Eqs. (2.7) and (2.9) shows that the bases $|m, z, \Delta = k>$ and $|m, z, \Delta = -k>$ possess the same ranges of m and z. This suggests a fundamental connection between the systems containing $(\Omega - 2k)$ and $(\Omega + 2k)$ particles persists in the (interacting) Agassi model. Inspection of Eq. (2.10) confirms this suspicion, for it implies

$$\begin{aligned} &<m', z', \Delta = k\ |H|\ m, z, \Delta = k> \\ &\qquad = <m', z', \Delta = -k\ |H|\ m, z, \Delta = -k> - 2kg\ \delta_{m',m}\ \delta_{z'z}, \end{aligned}$$

which means the two Hamiltonian matrices have exactly the same eigenvectors, while the eigenenergies of the $(\Omega + 2k)$-particle system are obtained by subtracting 2kg from each of the eigenenergies of the $(\Omega - 2k)$-particle system. Equations (A2.1) - (A2.4) (of Appendix 2.1) demonstrates that the equivalence of these two systems also embraces the matrix elements of the individual quasi-spin operators. Thus, in what follows, $N \leq \Omega$ unless otherwise specified. Furthermore, as only a 2 x 2 matrix has to be diagonalised when $N = 2$, it will be assumed that $\Omega \geq 4$.

SECTION 2.2: QUALITATIVE FEATURES OF THE SOLUTION TO THE AGASSI MODEL

In subsections 2.2.1 and 2.2.2 of this section, the solution to the Agassi model for small and large interaction strengths respectively will be considered. The discussion will take advantage of results available analytically. Attention will be focussed on the properties of the ground state, the global structure of the spectrum of excitation energies and the matrix elements of quasi-spin operators between the ground state and other states. It is convenient to characterise the ground state by the expectation values of combinations of quasi-spin operators. These expectation values convey the essential physics of the ground state without any redundant information. (In fact, just this is exploited in the elegant Sum-rule alternatives to full RPA calculations (BLM 79).) In this regard, it is useful to introduce the combinations

$$J_x = (J_+ + J_-)/2, \quad J_y = (J_+ - J_-)/2i, \quad Y_\pm = L_\pm + S_\pm, \tag{2.11}$$

which, because the Agassi Hamiltonian can be written as

$$H = \varepsilon J_o - V(J_x{}^2 - J_y{}^2) - gY_+Y_-, \tag{2.12}$$

are particularly appropriate to the limits of large g and V.

With regard to notation (here and elsewhere), the eigenstates of H will be denoted by $|j,\pi>$. The label π is +1/-1 for positive/negative parity states; for states of a given parity, j increases with increasing energy, with j = 1 for the state of lowest energy. For succinctness, the ground state will usually be denoted by $|0>$. When the particle number of eigenstates is needed, they will be denoted by $|j,\pi,N>$ (or, in the case of the ground state, $|0,N>$).

2.2.1 Behaviour when g and V small

It is useful in discussing this regime to distinguish that the part of the pairing interaction which acts within a level from the rest (which scatters particles from one level to the other). This can be done by introducing, instead of the Agassi Hamiltonian, the more general Hamiltonian

$$H = \varepsilon J_o - V/2\ (J_+{}^2 + J_-{}^2) - g_1(L_+L_- + S_+S_-) - g_2(L_+S_- + S_+L_-). \tag{2.13}$$

From Eq. (2.10), the expressi for the eigenenergies of H contain terms which are linear in g_1, an g_2 and V appear to higher powers. Thus in studying the limit of sm l interaction strengths in the Agassi model, a reasonable first step is the set $V = g_2 = 0$. This immediately simplifies the problem since the states $|m,z>$ are then the eigenstates of H with eigenenergies

$$E(m,z) = 2z\,\varepsilon - \left\{\frac{1}{2}\left(\frac{\Omega}{2} - m\right)\left(\frac{\Omega}{2} - m + 2\right) - 2z^2 - \delta\left(\frac{\delta}{2} + 1\right)\right\}g_1 \tag{2.14}$$

where $\delta = (\Omega - N)/2 = |\Delta|$. In all of these eigenstates the number of particles in the upper level is a good quantum number. This feature is usually typical of non-interacting systems. These states are however very different from those of a non-interacting system, being special superpositions (in general) of several Slater determinants. (Only the states $|m = 0,\ z = \pm z_u,\ \Delta = 0>$ comprise just one Slater determinant.)

As g_1 is increased from zero, a level-crossing involving the lowest two positive parity state occurs. For g_1 less than this value, the state with the lowest energy (i.e. the ground state) is $|0> = |m = 0,\ z = -z_u = -N/4>$. The energies of the remaining states relative to the ground state are given by

$$\begin{aligned} &E(m,z) - E(m = 0,\ z = -N/4) \\ &\quad = m\big(\varepsilon + (\delta + 1)g_1\big) + k\big(2\varepsilon - (N - 2m - 2k)g_1\big) = \Delta E(m,k) \end{aligned} \tag{2.15}$$

where $k = z + z_u = 0, 1, 2, \ldots, N/2 - m$. Figure 2.1 contains a typical plot of $\Delta E(m,k)$ for some of the low-lying excited states. If m and k are small in comparison to N, then it is a good approximation to write

$$\Delta E\ (m,k) \cong m\,E^\circ_{mon} + k\,E^\circ_{pr} \tag{2.16a}$$

where

$$E^{\circ}_{mon} = \varepsilon + (\delta + 1)g_1 , \qquad E^{\circ}_{pr} = 2\varepsilon - (N - 2)g_1. \qquad (2.16b)$$

Equation (2.16) shows that the spectrum of excited states can be easily understood if it is supposed that the N-particle system supports two independent vibrational modes: one has a negative parity quantum of energy E°_{mon} and the other has a positive parity quantum of energy E°_{pr}. The excited states contain different numbers of these two quanta. This description also makes the collective nature of the spectrum clear.

The spectrum in Fig. 2.2a is typical of those found in the full Agassi model when $\chi(\equiv(\Omega -1)V/\varepsilon)$ is small and $\Sigma(\equiv(\Omega - 1)g/\varepsilon)$ is varied. It is noticeable how similar Figs. 2.2a and 2.1 are in the range $0 \leq \Sigma \leq 0.75$. The description of the spectrum in terms of two vibrational modes of opposite parity (with energies E_{mon} and E_{pr}) is still feasible in this regime, with the level-repulsions at $\Sigma \approx 0.25$ being in effect level-crossings. Comparison of the energies in Fig. 2.2a in the limit $\Sigma \to 0$ with Eq. (2.16) suggests that, for small χ, E_{mon} decreases with increasing χ, while E_{pr} is essentially independent of χ. This is confirmed by the spectrum in Fig. 2.2b, for which Σ is now small and χ is varied. Furthermore, it too is vibrational (provided $\chi \leq 1$). The two modes of energy E_{mon} and E_{pr} are the counterparts of the monopole vibration in the LMG model and the pairon-holon vibration in the 2-level Pairing model respectively. (The terms pairon and holon are defined in the introduction to (EHH 77).) Thus the excitations in the Agassi model, when Σ and χ are small, are precisely those expected intuitively of a model which is obtained by combining the LMG model with the 2-level Pairing model. (Features in the spectra in Fig. 2.2 when Σ, $\chi >> 1$ will be discussed in Section 2.2.2.)

The success of Eq. (2.15) in reproducing the essential features of the spectrum when V and $g_2 = g_1$ are non-zero but small implies that assuming the eigenstates to be $|m,z\rangle$ will yield useful order of magnitude estimates for the ground state expectation values and transition matrix elements of quasi-spin operators. Expressions for these can be inferred directly from Appendix 2.1.

The expectation values in $|0\rangle = |\, m = 0,\ z = -N/4\rangle$ of the simple combinations of quasi-spin operators discussed in Appendix 2.1 are listed in Table 2.2. As all N particles are in the lower level in $|0\rangle$, the expectation values of L_+L_-, L_+S_-, J_+^2, J_+J_- and M_+M_- must be zero. The expectation values of S_+S_- and J_o (and any combination thereof) are also trivial because $|0\rangle$ is an eigenstate of these operators. From Eqs. (A2.4) and (A2.8),

$$J_o|0\rangle \;=\; -\,N/2|0\rangle$$

and

$$S_+S_-|0\rangle \;=\; N/2\ (\delta + 1)\ |0\rangle\,.$$

(Actually these results are implicit in Eq. (2.14).) Since $N \geq 2$, $\langle 0|S_+S_-|0\rangle \geq \Omega/2$. Combining all of these results and Eq. (2.11), one can deduce the expectation values of J_x^2, J_y^2 and Y_+Y_-. When $N = \Omega$, $|0\rangle$ is a single Slater determinant; even when $N < \Omega$ (and $|0\rangle$ is superposition of several Slater determinants) only the expectation values involving S_+S_- differ from those of any Slater determinant in which all N particles are in the lower level.

Of the quasi-spin operators which conserve particle number, only $J_\pm$ (or J_x and J_y) can connect $|0\rangle$ with other states. Since none of the particles in $|0\rangle$ are in the upper level, $J_-|0\rangle = 0$. From Eq. (A2.2),

$$J_+|0\rangle \;=\; \sqrt{N}/2\ |m = 1,\ z = -\,N/4 + \tfrac{1}{2}\rangle \;=\; \sqrt{N}/2\ |m = 1,\ z = -z_u\rangle$$

which implies

$$\langle j,\pi|J_+|0\rangle \;=\; \sqrt{N}/2\quad \delta_{j,1}\ \delta_{\pi,-1}\,.$$

Adopting J_x and J_y instead of $J_\pm$, these results become

$$\langle j,\pi|J_x|0\rangle \;=\; i\ \langle j,\pi|J_y|0\rangle \;=\; \sqrt{N}/2\ \delta_{j,1}\ \delta_{\pi,-1}\,. \qquad (2.17a)$$

The independent non-zero matrix elements of $S_\pm$, $L_\pm$ and $M_\pm$ between $|0,N>$ and other states are (using Eqs. (A2.1) and (A2.3)):

$$<0,\ N-2|S_-|0,N> \;=\; \sqrt{N(\delta+1)/2}$$

$$<j=2,\ \pi=+1,\ N+2|L_+|0,N> \;=\; \sqrt{\Omega/2}, \qquad (2.17b)$$

$$<j=1,\ \pi=-1,\ N+2|M_+|0,N> \;=\; \sqrt{2\delta}\ .$$

The remaining non-zero matrix elements can be inferred by hermitian conjugation.

Because the quasi-spin operators are SO(5) generators, the matrix elements of any combination Q of quasi-spin operators satisfy the sum rule

$$\Sigma\ |<\ell|Q|0>|^2 \;=\; <0|Q^\dagger\, Q|0>\ ,$$

where $|\ell>$ is any basis for the collective subspace. The results in Eq. (2.17a) may be summarised by saying that, as χ, $\Sigma \to 0$, the matrix element involving the lowest negative parity eigenstate exhausts the sum rules for J_x and J_y (cf. Table 2.2). Similarly, the sum rules for $S_\pm$, $L_\pm$ and $M_\pm$ are in each case exhausted by one matrix element in the sum.

2.2.2 Behaviour when g and V large

In this subsection, the limit $g \to \infty$ (V fixed) is considered first, and then the limit $V \to \infty$ (g fixed).

When $g >> V,\varepsilon$, the Agassi Hamiltonian becomes in effect

$$H \;=\; -g\, Y_+Y_- \;=\; -g(Y^2 - Y_o^2 + Y_o),$$

where $Y_o = L_o + S_o$ ($= M_o$) and $Y_\pm$ form a SU(2) algebra. This Hamiltonian only couples states $|m,z>$ and $|m',z'>$ if $m = m'$ (cf. Eq. (2.10)). So its eigenstates are linear combinations of the states $|m,z>$, m fixed, which are eigenstates of Y^2. (By construction, each state $|m,z>$ is an eigenvector of Y_o with eigenvalue $M_y = \Delta$.) Since the operators $\bar{L}$, $\bar{S}$ and

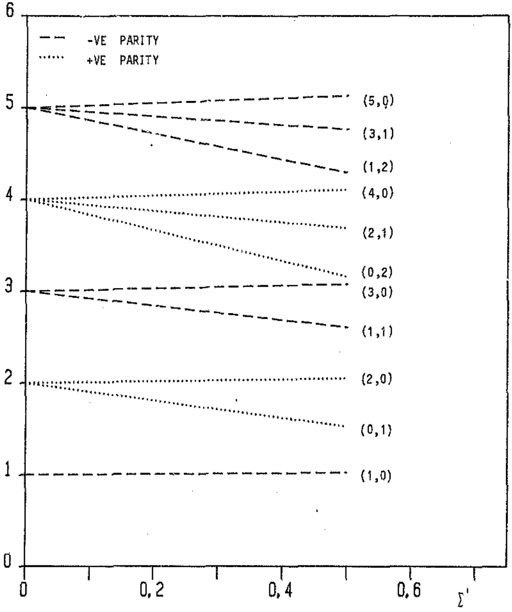

Fig. 2.1 Excitation energies (in units of ε) of low-lying states when only g_1 non-zero ; $N = \Omega = 20$, $\Sigma' \equiv (\Omega - 1)(g_1/\varepsilon)$. Each level is labelled by the orderd pair (m, k), where m and k refer to Eq. (2.15).

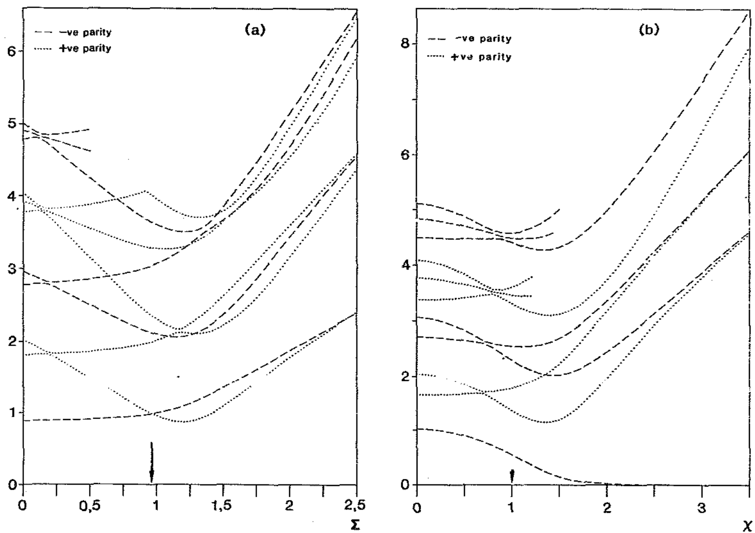

Fig. 2.2 Low-lying members of exact collective excitation spectrum of Agassi model when $N = \Omega = 20$; in part (a), $\chi = \frac{1}{2}$ (Σ varied), while, in part (b), $\Sigma = 0.35$ (χ varied).

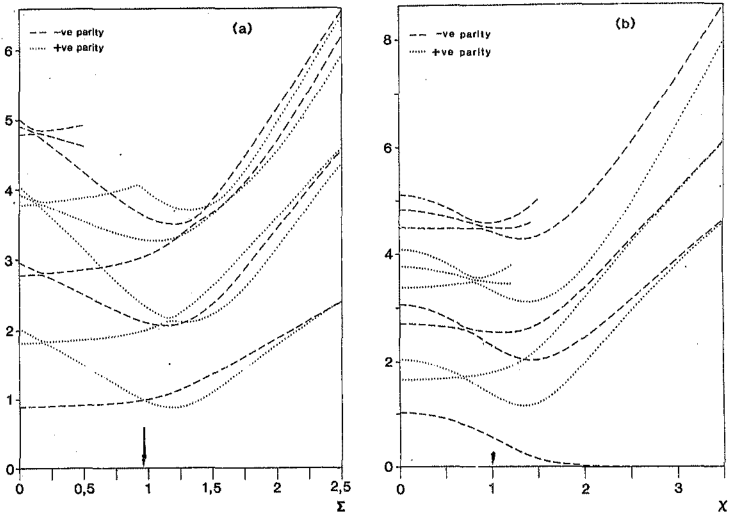

Fig. 2.2 Low-lying members of exact collective excitation spectrum of Agassi model when $N = \Omega = 20$; in part (a), $\chi = \frac{1}{2}$ (Σ varied), while, in part (b), $\Sigma = 0.35$ (χ varied).

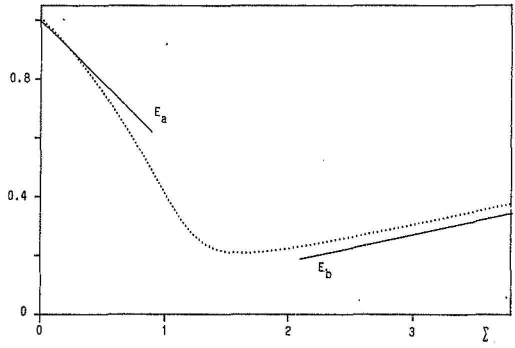

<u>Fig. 2.3</u> Ground state energy of N = 20 system relative to ground state energy of N = Ω = 22 system (χ = 0.4); E_a and E_b are approximations to this given in Eq. (2.22).

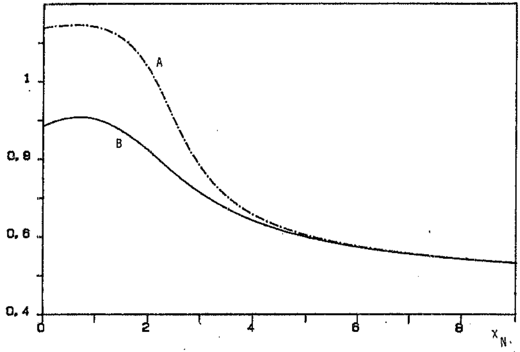

Fig. 2.4 Expectation value of Y_+Y_- in the positive parity ground state (curve A) and the lowest negative parity state (curve B) when $N = 14$, $\Omega = 22$ and $\Sigma_N = 1.5$. (The expectation values have been scaled by a factor of $4/N\Omega$).

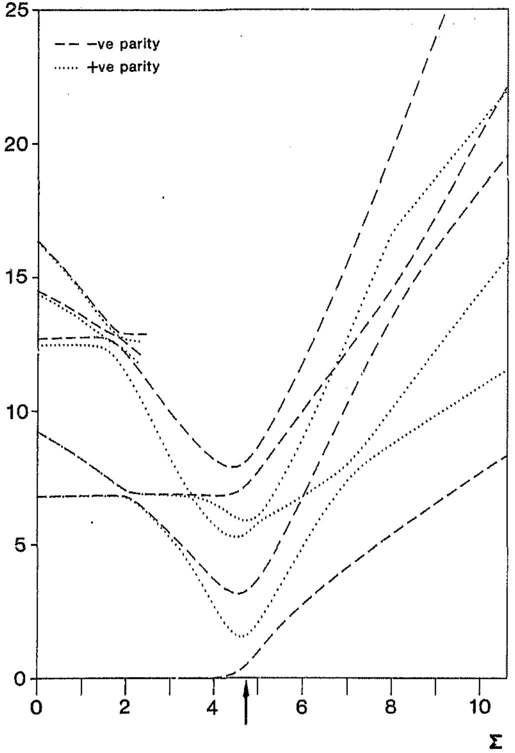

Fig. 2.5 Low-lying members of exact collective excitation spectrum of Agassi model when $\chi = 5$, $N = \Omega = 20$.

$\bar{Y}$ have the formal properties of angular momentum operators and $\bar{Y} = \bar{L} + \bar{S}$, these combinations follow from standard angular momentum coupling techniques. Thus the eigenstates of H are

$$|Y,m\rangle = |Y, M_y = \Delta, L = S = \Omega/4 - m/2\rangle$$

$$= \sum_{z=-z_u}^{z_u} C_{Ymz} |m,z\rangle \qquad (2.18)$$

in which C_{Ymz} is the Clebsch-Gordon coefficient

$$C_{Ymz} = \left(L = \frac{\Omega}{4} - \frac{m}{2},\ S = \frac{\Omega}{4} - \frac{m}{2},\ M_L = \frac{\Delta}{2} + z,\ M_S = \frac{\Delta}{2} - z \middle| Y, M_y\right)$$

and $Y = \delta, \delta + 1, \delta + 2, \ldots, \Omega/2 - m$. The eigenenergy of $|Y,m\rangle$ is

$$E_Y = -(Y(Y + 1) - \delta(\delta + 1))g, \qquad (2.19)$$

from which it is clear that the ground state of the system is the single state for which $Y = \Omega/2$ - i.e. $|0\rangle = |Y = \Omega/2, m = 0\rangle$. As a result, in the 2-level Pairing model only states in which $m = 0$ are considered. (The set of states $|m = 0,z\rangle$ coincides with the basis in Eq. (2.8).)

In this limit the ground state expectation value of Y_+Y_- attains its maximum value, namely

$$\begin{aligned} \langle 0|Y_+Y_-|0\rangle &= N/2\ (\Omega/2 + \delta + 1) \\ &= \Omega^2\ (N/2\Omega)\ (1 - N/2\Omega + 1/\Omega). \end{aligned} \qquad (2.20a)$$

On the other hand, when $g\ (,V) \to 0$, then, from Table 2.2,

$$\langle 0|Y_+Y_-|0\rangle = \Omega^2/4\ N/\Omega\ (1 - N/\Omega + 2/\Omega). \qquad (2.20b)$$

Both results depend on the sum over all states of the product of the probability that a single-particle state is occupied with the probability that it is unoccupied. Whereas, for N small, the expression in

Eq. (2.20a) is only a factor of 2 greater than the expression in Eq. (2.20b), it becomes a factor of $\Omega/2$ greater as $N \to \Omega$. It is the drop in the probability that any single-particle state is unoccupied when particles are confined to one level (i.e. the factor of $(1 - N/\Omega)$ in Eq. (2.20b)), which accounts for this trend.

Since $g_2 \to \infty$, it is plausible that both levels contain the same number of particles in the state $|0\rangle$ - i.e. $\langle 0|J_o|0\rangle = 0$. Symmetry properties of the Clebsch-Gordon coefficients imply that $C_{Ymz} = (-)^{Y-Y_m} C_{Ym(-z)}$, where $Y_m = \Omega/2 - m$. It follows that

$$\langle 0|J_o|0\rangle \;=\; 2 \sum_z z \,(C_{Y = \Omega/2,\ m = 0,\ z})^2 \;=\; 0$$

or that $\langle 0|L_o|0\rangle = \langle 0|S_o|0\rangle = -\delta/2$ as anticipated. (What is perhaps a little surprising is that this result holds for all states $|Y,m\rangle$.)

The calculation of the remaining ground state expectation values in the limit $g \to \infty$ is lengthy but straightforward; it is facilitated by the use of standard techniques (in the theory of Angular Momentum) for the matrix elements of products of irreducible tensors in coupled bases (e.g. Chapter 7 of (YLV 62)). (Recall that $\vec{L}$ and $\vec{S}$ are "angular momenta" coupled to total "angular momentum" $\vec{Y}$.) One obtains the following results:

$$\begin{aligned}
\langle 0|S_+S_-|0\rangle \;=\; \langle 0|L_+L_-|0\rangle \;&=\; \mu\,(\Omega/2)^2 - \mu\,\Omega/2 + N/4\ , \\
\langle 0|L_+S_-|0\rangle \;&=\; \mu\,(\Omega/2)^2\ , \\
\langle 0|J_x^2|0\rangle \;=\; \langle 0|J_o^2|0\rangle \;=\; \mu\,\Omega \;&=\; N/2\,(1 - N/2\Omega) + \mu\ , \qquad (2.21) \\
\langle 0|J_y^2|0\rangle \;&=\; 0\ , \\
\langle 0|M_+M_-|0\rangle \;&=\; N/\Omega\ N/4 \;-\; \mu\ ,
\end{aligned}$$

where

$$\mu \;=\; \Omega/(\Omega - 1)\ N/2\Omega\ (1 - N/2\Omega)\ .$$

Consistent with intuitive anticipations, the expectation values of L_+L_-, S_+S_- and L_+S_- are to a good approximation equal. Their value in this limit is thus determined by $\langle 0|Y_+Y_-|0\rangle$. The results for J_o^2 and J_y^2 indicate that both their expectation values decrease significantly as g increases from zero (cf. Table 2.2).

From Eq. (2.19) the energies of excited states relative to the energy of the ground state are

$$E(s) = E_{Y = (\Omega/2 - s)} - E_{Y = \Omega/2} = s\,(\Omega + 1 - s)\,g$$

where $s = 1, 2, 3, \ldots, N/2$. There are $s + 1$ states with excitation energy $E(s)$. In addition states of opposite parity are degenerate. (The number of positive parity states with energy $E(s)$ is $(s + 1)/2$ if s is odd, and $s/2 + 1$ if s is even.) For the low-lying states (s small), the spacing between energy levels is almost constant. This suggests these states are essentially non-interacting vibrational states; such a description, which requires two modes with quanta of opposite parity but the same energy, provides a natural way of accounting for the number of positive and negative parity states of a given excitation energy.

The structure in the spectrum implied by these results is not restricted to the limit g (or Σ) $\to \infty$. Reference to Fig. 2.2a shows that, when χ is small, it is already visible for $\Sigma \approx 2$.

The spectra for a <u>specific number</u> of particles when V and g are small and when g is large (V fixed) are qualitatively similar in that both are vibrational. However qualitative differences are found when the energies of corresponding states (e.g. ground states) in systems of different particle number are compared. Using Eqs. (2.14) and (2.19), the ground state energy of the N-particle system relative to the ground state energy of the Ω-particle system is, to leading order in g,

$$E_n = \delta(\varepsilon - (\Omega/2 - 1 - \delta)g) \tag{2.22a}$$

when g is small, and

$$E_b \;=\; \delta(\delta + 1)g \tag{2.22b}$$

when $g \to \infty$. Provided χ is small, these expressions provide useful estimates of the splitting of ground state energies in the two regimes (cf. Fig. 2.3). For small δ (i.e. N close to Ω), the former expression implies the ground states belong to a pairing vibrational band (BB 66) while the latter implies they belong to a pairing rotational band (Sc 72). Similarly, each excited state of the N-particle system is a member of, in the first limit, a vibrational band and, in the second limit, a rotational band extending over systems of different particle number. Every state in a particular vibrational band has the same values of m and k (cf. Eq. (2.16a)), while, for a rotational band, the values of Y and m are constant.

The significance of the pairing rotational bands becomes apparent when the matrix elements of $Y_\pm$ between different eigenstates are considered. When $g \to \infty$, Y_+ and Y_- can only connect the ground state of the N-particle system to the ground states of the (N + 2)- and (N − 2)-particle systems respectively (i.e. to other members of the ground state pairing rotational band), whereas in the limit of small interaction strengths, Y_+ and Y_- connect the ground state of the N-particle system to both the ground states and the first excited states of positive parity in the (N + 2)- and (N − 2)-particle systems (cf. Eq. (2.17b)). Exactly the reverse of this pattern is seen in the matrix elements of S_-. The selectivity of $S_\pm$ in the limit of small g and V (cf. Eq. (2.17b)) is a characteristic of pairing vibrations.

Explicit calculation (using Eq. (2.18)) shows that the matrix elements of quasi-spin operators which do not change the number of particles can also display distinctive behaviour. When g and V are small, $\langle k = 1, \pi = +1|J_y|0\rangle$ is non-zero, but, as $g \to \infty$, it must vanish (since $\langle 0|J_y^2|0\rangle \to 0$). Likewise $\langle k = 2, \pi = +1|J_o|0\rangle$, which vanishes if only $g_1 \neq 0$, exhausts the (non-zero) sum rule $\langle 0|J_o^2|0\rangle$ when g is large.

In the limit $V \to \infty$, the eigenstates of H must be eigenstates of J^2. Unfortunately these eigenstates are not available analytically as the monopole interaction term contains both J_x and J_y which do not commute (cf. Eq(2.12)). Nevertheless it is possible to infer some results by semi-classical arguments, without performing numerical diagonalisation.

When only $g_1 \neq 0$, the ground state $|0\rangle$ is an eigenstate of J^2 and J_o with eigenvalues $J = -M_J = N/2$; classically, this state has quasi-spin $\vec{J} = -(N/2)\hat{z}$. The form of the monopole interaction term implies that switching on V will cause the quasi-spin of this state to rotate in such a way that $\langle 0|J_x^2|0\rangle$ is increased (without changing $\langle 0|J_y^2|0\rangle$), thereby lowering the ground state energy. Thus, in the limit $V \to \infty$, one would expect the ground state to have the following expectation values:

$$\langle 0|J_x^2|0\rangle = N^2/4 \quad , \quad \langle 0|J_o|0\rangle = 0 \quad , \tag{2.23a}$$

and, because the system is not classical,

$$\langle 0|J_y^2|0\rangle = \langle 0|J_o^2|0\rangle = N/4 \tag{2.23b}$$

Numerical calculations, for example the plots in Fig. 5.2a (in Chapter 5) of $4(\langle 0|J_x^2|0\rangle - N/4)/N^2$ for an open-shell configuration of the Agassi model, confirm these are useful order of magnitude estimates for large V. (The variables χ_N and Σ_N in Fig. 5.2a are in effect V and g; they are defined in Chapter 3, Eq. (3.43).) So the ground state in the regime of large V is characterised by a considerable enhancement in the value of $\langle 0|J_x^2|0\rangle$, being $O(N^2/4)$ as compared to $O(N/4)$ when $V \equiv 0$ (cf. Table 2.2).

The operators J_x and J_y are the equivalent in the Agassi model of the components of the quadrupole operator in the Pairing-plus-Quadrupole model. The enhancement in $\langle 0|J_x^2|0\rangle$ is similar to the increase in the ground state expectation value of the scalar product of the quadrupole operator with itself found in "deformed" 0^+ nuclei. Thus an analogue of quadrupole deformation exists within the Agassi model Instead of rotational bands, parity doublets emerge in the spectrum (cf. Fig. 2.2b). Not only do the energies of the two members of a parity doublet coincide, but also their expectation values of quasi-spin operators (cf. Fig. (2.4)).

The dependence of the excited parity doublets on interaction strengths suggests that again there exist two different fundamental excitations. The energies of all excited doublets are sensitive to the value of χ (cf. Fig. 2.2b). However if one considers the dependence on Σ of the energies of the two lowest-lying excited parity doublets, then one finds, as demonstrated by Fig. 2.5, that, although one of these decreases rapidly with Σ (Σ small), the other is unchanged. This pattern is reminiscent of the behaviour of the energies of the monopole and pairon-holon vibrations introduced in the earlier discussion of Fig. 2.2a. Hence the former doublet can be viewed as a "pairon-holon" excitation and the latter doublet as a "monopole" excitation. If one ignores (in the first approximation) the splitting of the higher-lying doublets in Fig. 2.5 (Σ small), then they can be interpreted as superpositions of both of these different modes; thus the spectrum is approximately harmonic (just as in the other limits considered). Observe that the splitting is smallest in the pairon-holon doublet and its higher harmonics, despite the fact that these excitations are absent in the LMG model.

The increase in $\langle 0|J_x^2|0\rangle$ as $V \to \infty$ implies that the transition matrix elements of J_x between the ground state and other states increase. In fact, numerical calculations show that the lowest negative parity state exhausts the associated (non-energy-weighted) sum rule when it becomes part of the ground state parity doublet - i.e.

$$|k = 1,\ \pi = -1\rangle \to n\, J_x|0\rangle,$$

where n is a normalisation constant. This result, when coupled with the fact that $\langle 0|J_0|0\rangle \to 0$, implies another signature of the large V regime: $\langle k = 1,\ \pi = -1|J_y|0\rangle$ vanishes.

The very different behaviour of ground state expectation values of quasi-spin operators in the two limits $V \to \infty$ (g fixed) and $g \to \infty$ (V fixed) indicates that the monopole and pairing interactions compete. This is reinforced by the spectrum in Fig. 2.5. As Σ is increased beyond [illegible], the parity doublets - including the ground state parity doublet [illegible]lit. For $\Sigma > 7$, the ordering of levels expected in the infinite g limit begins to emerge. It is the competition between these two regimes which distinguishes the Agassi model from other simpler one-parameter models like the LMG model. Although the computational effort entailed is considerably greater, the richer structure is desirable, for it leads to several insights not possible within one-parameter models.

Finally, an interesting way of discussing the properties of the Agassi model not considered here is to vary N keeping g, V and Ω fixed (Section 2 of (Ag 68)). It demonstrates how the Agassi model can simulate the properties of the Pairing-plus-Quadrupole model when applied to the isotopes of a medium-to-heavy nucleus.

APPENDIX 2.1: MATRIX ELEMENTS OF QUASI-SPIN OPERATORS IN THE COLLECTIVE SUBSPACE

In this appendix expressions for the action of several combinations of quasi-spin operators on the basis state $|m,z,\Delta\rangle$ are given. The matrix elements of these combinations follow trivially. The presentation of certain results can be simplified if the states $|m,z,\Delta\rangle$ and $|m,z,-\Delta\rangle$ are treated on the same footing. This is achieved by introducing the notation $|m,z;\Delta_o,\pm\rangle$, which is such that $|m,z;\Delta_o,\pm\rangle = |m,z,\pm\Delta_o\rangle$. In what follows $\Delta_o = 0, 1, 2, \ldots, \Omega/2$.

Individual quasi-spin operators ($L_\pm$, $S_\pm$, $J_\pm$, $M_\pm$)

The expressions for $L_\pm|m,z,\Delta\rangle$ and $S_\pm|m,z,\Delta\rangle$ are well known from elementary treatments of angular momentum in quantum mechanics. However in terms of the variables m and z used in this work they become

$$A_\pm|m,z;\Delta_o,\pm\rangle = (z_u - z)^{\frac{1}{2}} (z_u + z + \Delta_o + 1)^{\frac{1}{2}} |m, z+\tfrac{1}{2}; \Delta_o + 1, \pm\rangle,$$

$$A_\mp|m,z;\Delta_o,\pm\rangle = (z_u - z + \Delta_o)^{\frac{1}{2}} (z_u + z + 1)^{\frac{1}{2}} |m, z + \tfrac{1}{2}; \Delta_o - 1, \pm\rangle,$$

$$\text{(A2.1)}$$

$$A_\pm^\dagger|m,z;\Delta_o,\pm\rangle = (z_u - z + 1)^{\frac{1}{2}} (z_u + z + \Delta_o)^{\frac{1}{2}} |m, z-\tfrac{1}{2}; \Delta_o - 1,\pm\rangle,$$

$$A_\mp^\dagger|m,z;\Delta_o,\pm\rangle = (z_u - z + \Delta_o + 1)^{\frac{1}{2}} (z_u + z)^{\frac{1}{2}} |m, z - \tfrac{1}{2}; \Delta_o + 1, \pm\rangle,$$

where $A_+ = L_+$, $A_- = S_-$ and $2z_u = \Omega/2 - \Delta_o - m$ (≥ 0).

There exists a simple relation between the infinitesimal generators $F_{\alpha\beta}$ used in (He 65) and the operators $J_{\pm}$ and $M_{\pm}$ (Pa 65, Ag 68). Thus expressions for $J_{\pm}|m,z,\Delta>$ and $M_{\pm}|m,z,\Delta>$ can be obtained by specialising results for $F_{\alpha\beta}|(L_m S_m)L,S,M_L,M_S>$ implicit in Sections 2 and 4 of (He 65) and listed explicitly in the appendix to (Ag 68). (In both these works the symbols J and Λ are used instead of L and S respectively.) One finds that

$$J_{\pm}|m,z,\Delta> \;=\; A(m)\;\alpha(\mp z)\;|m+1,\; z\pm\tfrac{1}{2},\;\Delta>$$

$$+\;A(m-1)\;\alpha(1\pm z)\;|m-1,\; z\pm\tfrac{1}{2},\;\Delta>,$$

where (A2.2)

$$A(m) \;=\; 2\left\{\frac{(m+1)\;(\Omega-m+2)}{(\Omega-2m)(\Omega-2m+2)}\right\}^{\frac{1}{2}} \;,$$

and

$$\alpha(x) \;=\; (z_u+x)^{\frac{1}{2}}\;(z_u+|\Delta|+x)^{\frac{1}{2}}.$$

Similarly

$$\pm M_{\pm}|m,z;\Delta_o,\pm> \;=\; A(m)\;\beta(0)\;|m+1,\;z;\;\Delta_o+1,\;\pm>$$

$$-\;A(m-1)\;\beta(\Delta_o+1)\;|m-1,\;z;\;\Delta_o+1,\;\pm>,$$

$$\mp M_{\mp}|m,\;z;\;\Delta_o,\;\pm> \;=\; A(m)\;\beta(\Delta_o)\;|m+1,\;z;\;\Delta_o-1,\;\pm>$$

(A2.3)

$$-\;A(m-1)\;\beta(1)\;|m-1,\;z;\;\Delta_o-1,\;\pm>,$$

where $\beta(x) = (z_u - z + x)^{\frac{1}{2}}\,(z_u + z + x)^{\frac{1}{2}}$. Consistent with their definitions (in Eqs. (2.3) and (2.4)), $J_{\pm}$ and $M_{\pm}$ couple states of positive parity (even m) to states of negative parity (odd m).

Combinations of quasi-spin operators in the Agassi Hamiltonian

To calculate the matrix of the Agassi Hamiltonian it is sufficient to consider the following operators:

(1) J_o

From Eq: (2.8), $$J_o|m, z, \Delta\rangle = 2z\,|m, z, \Delta\rangle. \tag{A2.4}$$

(2) $S_+S_- + L_+L_-$

Using relations like $S_+S_- = S^2 - S_o^2 + S_o$,

$$S_+S_- + L_+L_- = S^2 + L^2 - (S_o + L_o)\,((S_o + L_o) - 1) + 2S_oL_o.$$

Thus

$$\begin{aligned}(S_+S_- + L_+L_-)\,&|m, z, \Delta\rangle \\ &= \left(\tfrac{1}{2}(\Omega/2 - m)\,(\Omega/2 - m + 2) - 2z^2 - \Delta(\Delta/2 - 1)\right)\,|m, z, \Delta\rangle.\end{aligned} \tag{A2.5}$$

(3) L_+S_-

Using Eq. (A 2.1),

$$L_+S_-|m,z,\Delta\rangle = \alpha(z + 1)\,\alpha(-z)\,|m, z + 1, \Delta\rangle \tag{A2.6}$$

where $\alpha(x)$ is defined in Eq. (A2.2).

(4) J_+^2

Using Eq. (A2.2),

$$\begin{aligned}(J_+)^2|m,z,\Delta\rangle \\ &= A(m + 1)\,A(m)\,\alpha(-z)\,\alpha(-z - 1)\,|m + 2, z + 1, \Delta\rangle \\ &+ ((A(m))^2 + (A(m - 1))^2)\,\alpha(z + 1)\,\alpha(-z)\,|m, z + 1, \Delta\rangle \\ &+ A(m - 1)\,A(m - 2)\,\alpha(z + 2)\,\alpha(z + 1)\,|m - 2, z + 1, \Delta\rangle.\end{aligned} \tag{A2.7}$$

Other combinations of quasi-spin operators (for expectation values)

If J_o is excluded, then the simplest combinations of quasi-spin operators which have non-zero expectation values are products of two quasi-spin operators which conserve particle number and parity. Those of interest are:

(1) Y_+Y_- (cf. Eq. (2.11))

The results given in Eqs. (A2.5) and (A2.6) are sufficient to calculate expectation values of Y_+Y_-.

(2) L_+L_-, S_+S_-

Because of Eq. (A2.5), it is enough to consider

$$S_+S_- - L_+L_- = S^2 - L^2 + (L_o - S_o)(L_o + S_o - 1).$$

It follows

$$(S_+S_- - L_+L_-)\ |m,z,\Delta\rangle = (\Delta - 1)\ 2z\ |m, z, \Delta\rangle, \tag{A2.8}$$

(3) J_x^2, J_y^2

From Eq. (2.11),

$$\left.\begin{array}{l} 4J_x^2 \\ 4J_y^2 \end{array}\right\} = 2J_+J_- - 2J_o \pm (J_+^2 + J_-^2).$$

To calculate expectation values require, in addition to Eqs. (A2.4) and (A2.7),

$$\begin{aligned} J_+J_-\ &|m,z,\Delta\rangle \\ &= A(m+1)\ A(m)\ \alpha(z)\ \alpha(-z)\ |m+2, z, \Delta\rangle \\ &\quad + \{(A(m))^2\ \alpha^2(z) + (A(m-1))^2\ \alpha^2(1-z)\}\ |m \quad ,z,\Delta\rangle \\ &\quad + A(m-1)\ A(m-2)\ \alpha(1+z)\ \alpha(1-z)\ |m-2, z, \Delta\rangle \end{aligned} \tag{A2.9}$$

which follows from Eq. (A2.2).

(4) M_+M_-

Using (A2.3),

$$M_+M_- \; |m,z,\Delta\rangle$$

$$= \; - A(m + 1)\, A(m)\, \alpha(z)\, \alpha(-z)\, |m + 2,\, z,\, \Delta\rangle$$

$$+ \{(A(m))^2\, \beta(0)^2 \qquad \text{(A2.10)}$$

$$+ (A(m - 1))^2\, \beta(\Delta + 1)^2\}\, |m,z,\Delta\rangle$$

$$- A(m - 1)\, A(m - 2)\, \alpha(1 + z)\, \alpha(1 - z)\, |m - 2,\, z,\, \Delta\rangle.$$

The similarity between (A2.9) and (A2.10) is not a fortuitous feature of working within the basis $|m,z,\Delta\rangle$. The operator $A = \frac{1}{2}(M_+M_- + J_+J_-)$ is related to the quadratic Casimir operator G of SO(5) by

$$A \; = \; G - L^2 - S^2 + \tfrac{1}{2}(Y_o + J_o) \qquad \text{(Eq. (16) in (He 65).)}$$

Hence A must be diagonal in the basis $|(L_mS_m)L,S,M_L,M_S\rangle$, whatever the values of L_m and S_m.

The matrix elements of J_o^2 are trivial (cf. Eq. (A2.4)), while any expectation value of J_xJ_y and J_yJ_x can be written in terms of the expectation value of J_o in the same state.

APPENDIX 2.2: COMMUTATORS OF QUASI-SPIN OPERATORS

The 10 independent operators forming the SO(5) algebra are taken to be the L and S operators, and $J_\pm$ and $M_\pm$. The non-vanishing commutators involving these operators (excluding the trivial SU(2) commutators) are:

$$[L_+,J_-] = -M_+ \qquad [L_o,J_+] = \tfrac{1}{2}J_- \qquad [L_+,M_-] = J_+$$

$$[L_o,M_+] = \tfrac{1}{2}M_+ \qquad [S_+,J_+] = -M_+ \qquad [S_o,J_+] = -\tfrac{1}{2}J_+$$

$$[S_+,M_-] = J_- \qquad [S_o,M_+] = \tfrac{1}{2}M_+ \qquad [J_+,M_+] = 2L_+$$

$$[J_+,M_-] = -2S_-$$

together with the hermitian conjugate commutators.

TABLE 2.1: DIMENSIONS OF HAMILTONIAN SUBMATRICES

	D_+	D_-
$\frac{N}{2}$ even	$\frac{(m_u + 2)^2}{4}$	$\frac{m_u(m_u + 2)}{4}$
$\frac{N}{2}$ odd	$\frac{(m_u + 1)(m_u + 3)}{4}$	$\frac{(m_u + 1)^2}{4}$

D_+ (D_-) is the dimension of positive (negative) parity submatrix; m_u is defined in Eq. (2.10). (If $N \leq 3$, $m_u = N/2$.)

TABLE 2.2: GROUND STATE EXPECTATION VALUES OF QUASI-SPIN OPERATORS (Only $g_1 \neq 0$)

Operator	Y_+Y_-	S_+S_-	L_+L_-	M_+M_-	J_o	J_x^2	J_y^2
	$\frac{N}{2}(\delta + 1)$	$\frac{N}{2}(\delta + 1)$	0	0	$-\frac{N}{2}$	$\frac{N}{4}$	$\frac{N}{4}$

CHAPTER THREE

SELF-CONSISTENT MEAN-FIELDS
(at zero temperature)

It is well known that the pairing and monopole interactions in the Agassi model give rise to non-trivial solutions of the zero temperature Bardeen-Cooper-Schrieffer (BCS) and Hartree-Fock (HF) equations respectively (RR 64, ALM 66). Thus it is necessary to employ the Hartree-Fock-Bogoliubov (HFB) formalism, which generalises and unifies the BCS and HF theories, to determine the self-consistent mean-fields appropriate to the Agassi model. In this chapter the application of HFB at zero temperature is considered, and in the next, the application at finite temperature.

The first section of this chapter is devoted to a brief description of HFB at zero temperature (Ma 75, Go 79a), with the emphasis on the (formal) properties of the HFB approximation to the ground state. Section 3.2 presents the form to which the transformation determining the HFB ground state can be restricted within the Agassi model. A modification of a parametrisation first used in (BFS 69) is introduced to simplify subsequent manipulations. It is shown that, if $N \neq \Omega$, the transformation must automatically break particle number symmetry. The various solutions of the corresponding equations for the HFB ground state when $N = \Omega$ and $N < \Omega$ are discussed in Sections 3.3 and 3.4 respectively. In particular the conditions are determined under which these solutions are stable. (The notion of stability is defined in the last paragraph of Section 3.1.) This information is summarised in "phase diagrams" - i.e. plots in the gV-plane showing which solutions are stable where. A feature of the phase diagram for the closed-shell ($N = \Omega$) system is the absence of a genuine HFB solution (or phase).

The calculation of expectation values in the most general form of HFB ground state appropriate to the Agassi model is outlined in Appendix 3.1 to this chapter. Only expectation values of the combinations of quasi-spin operators discussed in Chapter 2 are considered. Appendix 3.2 contains material required in Appendix 3.1.

SECTION 3.1: RESUMÉ OF RELEVANT PROPERTIES OF HFB

HFB is the most general form of self-consistent mean-field approximation for an interacting non-relativistic fermion many-body system with Hamiltonian

$$H = \sum_{ij} t_{ij} b_i^\dagger b_j + \tfrac{1}{4} \sum_{ijkl} \bar{v}_{ijkl} b_i^\dagger b_j^\dagger b_l b_k \tag{3.1}$$

where $b_i^\dagger$, b_i are the particle creation and annihilation operators associated with any complete single-particle basis, and $\bar{v}_{ijkl}$ are the anti-symmetrised matrix elements of the interaction in this basis. The self-consistent mean-field approximation seeks quasi-particle creation and annihilation operators $\beta_i^\dagger$, β_i in terms of which the Hamiltonian H can be recast (without any approximation) into the following simpler form:

$$H = E_o + \sum_i E_i \beta_i^\dagger \beta_i + H_{res} , \tag{3.2}$$

where H_{res} is the (residual) interaction between quasi-particles which, by design, is as small as possible (in a sense explained below), given the restriction that the quasi-particle operators are related to the "bare" operators $b_i^\dagger$, b_i by a unitary transformation. (In the Agassi model the most convenient set of "bare" operators is that used in Eq. (2.1).) The determination of the transformation which accomplishes this requires the self-consistent solution of a set of non-linear equations. In most systems, including the Agassi model, the solution is such that all the energies E_i in Eq. (3.2) are positive. (A careful discussion of this point is given in Sections 7.3 and 7.7 of (RS 80).) Whereas in HF the unitary transformation is also required to conserve particle number, in HFB the most general form is permissible, namely

$$\beta_i^\dagger = \sum_j (U_{ji} b_j^\dagger + V_{ji} b_j). \tag{3.3}$$

In this way, short-range pairing correlations can be incorporated (Va 61). However it also implies that a subsidiary condition must be introduced which ensures that the corresponding approximation to the ground state conserves particle number on the average. This can be done by considering, instead of H in Eq. (3.2), $H' = H - \mu\hat{N}$, where $\hat{N}$ is the particle number operator and the chemical potential μ is fixed so that the ground state expectation value of $\hat{N}$ is equal to N, the number of particles in the system. (This procedure is easily generalised to constraints involving the ground state expectation values of other operators (Go 79a), but in the present work only $\hat{N}$ needs to be considered.) Since the transformation is unitary, the quasi-particles are also fermions.

Ideally H_{res} is negligible, in which case H is effectively diagonalised by the quasi-particle basis. Whatever the case, this basis is the optimal one for the pur of the sole (but important) approximation made, namely that H_{res} can be ignored. The ground state of the system (i.e. the state of lowest energy) when each E_i is positive is then, from Eq. (3.2), the state containing no quasi-particles or the quasi-particle vacuum $|v\rangle$. (In what follows, unless otherwise specified, $|v\rangle$ is normalised.) A consequence of Wick's theorem is that $|v\rangle$ is specified (to within an arbitrary phase factor) by the set of all contractions

$$\rho_{ij} = \langle v|b_j^\dagger b_i|v\rangle, \qquad \kappa_{ij} = \langle v|b_j b_i|v\rangle, \tag{3.4}$$

which are the matrix elements of the single-particle density ρ and the pairing tensor κ in the "bare" basis respectively. The definition of $|v\rangle$ implies that all the contractions of the quasi-particle operators (in this state) vanish except

$$\langle v|\beta_i\beta_j^\dagger|v\rangle = \delta_{ij} . \tag{3.5}$$

Substituting the inverse of Eq. (3.3) into Eq. (3.4) and using Eq. (3.5), one finds that

$$\rho_{ij} = \sum_k V_{ik}^* V_{jk}$$

and (3.6)

$$\kappa_{ij} = \sum_k V_{ik}^* U_{jk} ,$$

where V^*_{ij} is the complex conjugate of V_{ij}.

Under a change of single-particle basis - i.e. the unitary transformation

$$b^\dagger_i \rightarrow \sum_k u_{ki}\, b^\dagger_k \,, \qquad\qquad b_i \rightarrow \sum_k u^*_{ki}\, b_k \,,$$

ρ_{ij} and κ_{ij} transform like the matrix elements of an operator and of a second order tensor respectively (BM 62). (Hence the term pairing tensor for κ.) Furthermore, from Eq. (3.4), ρ is hermitian and κ is anti-symmetric. Thus there exists a single-particle basis in which ρ is diagonal, while the simplest form to which the matrix for κ can be reduced is the canonical form

$$\begin{bmatrix} 0 & & & & & & \\ & 0 & a_1 & & & & \\ & -a_1 & 0 & & & & \\ & & & 0 & a_2 & & \\ & & & -a_2 & 0 & & \\ & & & & & & \ddots \end{bmatrix}$$

where the first square consists of zeros, the a_i are real and the entries outside the squares on the diagonal vanish (Zu 62). It is demonstrated in (BM 62) that, for ρ and κ to describe one and the same quasi-particle vacuum, they must satisfy the relations

$$\kappa\kappa^\dagger = \rho - \rho^2 \qquad (3.7a)$$

and

$$\rho\kappa = \kappa\rho^* \,. \qquad (3.7b)$$

It follows that the single-particle basis which diagonalises ρ can be chosen in such a way that κ is simultaneously brought into its canonical form (BM 62). *This very special and important single-particle basis is* termed the canonical basis.

The matrix elements of ρ and κ in the canonical basis will be denoted by ρ_i^c (since ρ diagonal) and κ_{ij}^c. As κ is canonical in form, this basis can be divided into "paired" and "blocked" states: for any blocked state $|a\rangle$,

$$\kappa_{aj}^c = 0 \quad (\text{for all } j),$$

and, for any paired state $|b\rangle$,

$$\kappa_{bj}^c = \delta_{j\bar{b}}\, \kappa_b^c,$$

where $|\bar{b}\rangle$ is the state which is canonically conjugate to $|b\rangle$ or "partners" $|b\rangle$. (From the previous paragraph, $\kappa_{\bar{b}}^c = -\kappa_b^c$.) It follows from Eq. (3.7a) that, for a blocked state $|a\rangle$, ρ_a^c is either 1 or 0.

As is well-known, the existence of the canonical basis implies that any HFB transformation can be decomposed into three successive transformations of simpler structure (the Bloch-Messiah theorem (BM 62)). These are:

1) First, a unitary transformation U_1 from the bare basis to the canonical basis of the form

$$a_i^\dagger = \sum_j (U_1)_{ji}\, b_j^\dagger,$$

where the particle creation operators $a_i^\dagger$ refer to the canonical basis;

2) Second, a special Bogoliubov-Valatin transformation B_{sp} of the operators $a_i^\dagger$, a_i, which, for blocked states, is of the form

$$\alpha_k^\dagger = \begin{cases} a_k^\dagger & \rho_k^c = 0 \\ a_k & \rho_k^c = 1 \end{cases}$$

and, for paired states, of the form

$$\alpha_k^\dagger = u_k\, a_k^\dagger - v_k\, a_{\bar{k}},$$

where u_k and v_k are real, $u_k = u_{\bar{k}}$, $v_k = -v_{\bar{k}}$ and $u_k^2 + v_k^2 = 1$;

3) Finally, in general, a unitary transformation U_2 among the quasi-particle operators $\alpha_i^\dagger$ to obtain the quasi-particle operators

$$\beta_i^\dagger = \sum_j (U_2)_{ji}\, \alpha_j^\dagger .$$

The ground state $|v\rangle$ is a priori determined (to within an arbitrary phase factor) by the requirement that

$$\beta_i\, |v\rangle = 0 \qquad \text{(for all } i\text{).}$$

This can however be replaced by the condition

$$\alpha_i\, |v\rangle = 0 \qquad \text{(for all } i\text{),}$$

which demonstrates that all physically important properties of $|v\rangle$ are determined by the first two transformations, U_1 and B_{sp}, alone. In fact one can replace the expressions for ρ_{ij} and κ_{ij} in Eq. (3.6) by

$$\rho_{ij} = \sum_k (U_1)_{ik}\, (U_1)_{jk}^*\, \rho_k^c$$

and (3.8)

$$\kappa_{ij} = \sum_k{}' \, (U_1)_{ik}\, (U_1)_{j\bar{k}}\, \kappa_k^c,$$

where Σ' is the sum over the paired states in the canonical basis. Observe that the expectation value of $\hat{N}$

$$\langle v|\hat{N}|v\rangle = \sum_i \rho_{ii} = \sum_k \rho_k^c \qquad (3.9)$$

depends only on the nature of the second transformation.

If the formal expressions for the operators $b_i^\dagger$, b_i in terms of the operators $\alpha_i^\dagger$, α_i are substituted into H' and the result is rewritten in terms of normally-ordered products (with respect to $|v\rangle$), then one finds in general that

$$H' = E_o' + \sum_{ij} H_{ij}^{11} \alpha_i^\dagger \alpha_j$$

$$+ \tfrac{1}{2} \sum_{ij} (H_{ij}^{20} \alpha_i^\dagger \alpha_j^\dagger + \text{h.c.}) + H_4 ,$$

where H^{11} is a hermitian matrix, H^{20} is anti-symmetric (h.c. denotes hermitian conjugate), and H_4 consists of normally-ordered products containing four quasi-particle operators. (For the purposes of the present discussion explicit expressions for H^{11}, H^{20} and H_4 are unnecessary; however these are given in all generality in Appendix E of (RS 80), while expressions for H^{11} and H^{20} appropriate to the Agassi model are given in appendix 6.1.) The transformations U_1 and B_{sp} are determined by the requirement that

$$H^{20} \equiv 0, \tag{3.10a}$$

along with the subsidiary condition that

$$\mathrm{Tr}\ (\rho) = N, \tag{3.10b}$$

where Tr denotes trace. It is in this way that the role of the interaction in the system of quasi-particles is minimised. Given the solution of Eq. (3.10), H^{11} can be explicitly calculated. The transformation U_2 follows trivially: in order to obtain the form of H' in Eq. (3.2), U_2 is chosen so that it diagonalises H^{11} - i.e. $U_2^\dagger H^{11} U_2$ is diagonal. Hence this transformation is important for the description of excited states. When the normally-ordered products in H_4 are expressed in terms of the operators $\beta_i^\dagger$, β_i, it coincides with H_{res} in Eq. (3.2).

The transformation U_1 is analogous to that determining the ground state in HF. Indeed, in the limit in which $\kappa \equiv 0$, inspection of the detailed expression for H^{20} shows that it satisfies the same set of equations. Likewise the form of B_{sp} is familiar from BCS and, in a limit similar to

$\kappa \equiv 0$ but not quite as restrictive, B_{sp} satisfies the BCS equations. As is to be expected from the marriage of HF and BCS, the ground state of a full HFB solution describes a system in which pairing takes place between particles moving in a deformed HF-like field. An essential ingredient of this description is that it allows for the self-consistent influence of the pairing on the deformation and vice versa. Despite the conceptual similarity between HFB and the coupled HF-BCS approximation (BGG 69), the two methods should not be confused for they are in general different (Go 79a). (The coupled HF-BCS approximation ignores certain contributions to H^{20} and H^{11} which are usually non-zero; various studies have shown neglecting these terms has undesirable consequences (Go 79a).)

Applying Wick's theorem to Eq. (3.1) and using Eq. (3.4), one deduces that the HFB approximation to the ground state energy is given by

$$E_o = \sum_{ij} t_{ij}\,\rho_{ij} + \tfrac{1}{2}\sum_{ijkl} (\rho^*_{ik}\,\bar{v}_{ijkl}\,\rho_{lj} + \tfrac{1}{2}\kappa^*_{ij}\,\bar{v}_{ijkl}\,\kappa_{kl}), \tag{3.11}$$

where ρ_{ij} and κ_{ij} are evaluated once Eq. (3.10) has been solved. On the other hand, E_o can also be regarded as a functional of the unknown coefficients in U_1 and B_{sp}, and can then be used to determine their values. Not all variations in these coefficients are permissible: they must be such that U_1 and B_{sp} remain unitary and the trial state $|v\rangle$ has expectation value $\langle v|\hat{N}|v\rangle = N$. The variational principle

$$\delta_c\, E_o = 0, \tag{3.12}$$

where $\delta_c\, E_o$ denotes the constrained variation of E_o discussed above, is, along with the necessary constraint conditions, exactly equivalent to Eq. (3.10). (See, for example, (DMP 66).)

Since the equations determining U_1 and B_{sp} are non-linear, they possess in general more than one solution. The recognition that these equations follow from a variational principle of the Rayleigh-Ritz type involving E_o, suggests that only solutions corresponding to a local minimum of E_o

can be relevant. Such solutions are termed "stable". (It is important to realise that the local minimum under consideration is only required to be a local minimum for variations which *satisfy the constraints* discussed (OS 83), a point which has been overlooked in, for example, (Ca 65).) In what follows, stability will be sufficient to select one solution from any others. *For systems where this is not the case*, the stable solution of lowest energy is usually adopted.

SECTION 3.2: FORM OF THE HFB TRANSFORMATION

In the Agassi model the transformation to the canonical basis U_1 accommodates the monopole interaction. This transformation differs from its HF counterpart only in that HFB allows for the self-consistent influence of pairing. Therefore U_1 must have the same form as its HF counterpart, namely (from the HF calculations in (ALM 66))

$$a^{\dagger}_{\sigma m} = \sum_{\sigma'} (U_1)_{\sigma',\sigma}\, c^{\dagger}_{\sigma' m} , \tag{3.13}$$

where $a^{\dagger}_{\sigma m}$ and $c^{\dagger}_{\sigma m}$ are the creation operators in the canonical and bare bases respectively. Like the bare basis, the canonical basis consists of two levels each of degeneracy Ω. As V, g > 0, U_1 can be assumed to be orthogonal (Section 5.4 in (RS 80)). So the transformation in Eq. (3.13) can be rewritten without any loss of generality as

$$a^{\dagger}_{\sigma m} = \cos\phi/2\; c^{\dagger}_{\sigma m} + \sigma \sin\phi/2\; c^{\dagger}_{-\sigma m} \tag{3.14}$$

where $|\phi| \leq \pi$.

The transformation within the canonical basis allows for correlations which may be induced by the pairing interaction. It too should be formally similar to its BCS counterpart. The application of BCS to the 2-level Pairing model (RR64) thus implies this transformation is

$$\alpha^{\dagger}_{\sigma m} = u_{\sigma}\, a^{\dagger}_{\sigma m} - \mathrm{sgn}(m)\, v_{\sigma}\, a_{\sigma -m}, \tag{3.15}$$

where sgn(m) is the sign of m and u_{σ}, v_{σ} are non-negative. The coefficients u_{σ}, v_{σ} are subject to the constraint

$$u_\sigma^2 + v_\sigma^2 = 1 \tag{3.16}$$

to ensure that the transformation in Eq. (3.15) is unitary.

The matrix elements of ρ and κ in the canonical basis are

$$\begin{aligned} \rho^c_{\sigma m,\sigma' m'} &= \langle v|a^\dagger_{\sigma' m'}\, a_{\sigma m}|v\rangle = \rho^c_\sigma\, \delta_{\sigma,\sigma'}\, \delta_{m,m'} \\ \kappa^c_{\sigma m,\sigma' m'} &= \langle v|a_{\sigma' m'}\, a_{\sigma m}|v\rangle = \mathrm{sgn}(m)\, \kappa^c_\sigma\, \delta_{\sigma,\sigma'}\, \delta_{m,-m'} \end{aligned} \tag{3.17a}$$

in which

$$\rho^c_\sigma = v_\sigma^2, \qquad \kappa^c_\sigma = u_\sigma\, v_\sigma, \tag{3.17b}$$

and $|v\rangle$ is the (normalized) trial HFB ground state, which is such that $\alpha_{\sigma m}|v\rangle = 0$ (for all σ,m).

Combining Eqs. (3.17) and (3.9), the particle number constraint reads

$$v_{-1}^2 + v_1^2 = N/\Omega \quad . \tag{3.18}$$

Equations (3.16) and (3.18) imply it is possible to write u_σ, v_σ as

$$\begin{aligned} v_{-1} &= (N/\Omega)^{\frac{1}{2}} \cos\psi/2 & u_{-1} &= (1 - N/\Omega \cos^2\psi/2)^{\frac{1}{2}} \\ v_1 &= (N/\Omega)^{\frac{1}{2}} \sin\psi/2 & u_1 &= (1 - N/\Omega \sin^2\psi/2)^{\frac{1}{2}} \end{aligned} \tag{3.19}$$

where ψ is an arbitrary variable lying in the interval $0 \leq \psi \leq \pi$. In the Agassi model one must have $\rho^c_{-1} \geq \rho^c_1$; hence ψ can in fact be restricted to the range $0 \leq \psi \leq \pi/2$.

If $N = \Omega$, then, when $\psi = 0$, the transformation in Eq. (3.15) becomes

$$\alpha^\dagger_{1m} = a^\dagger_{1m}$$

$$a^{\dagger}_{-1m} = -\mathrm{sgn}(m)\; a_{-1m},$$

which shows that it can encompass the class of HF solutions. By contrast, when $N < \Omega$, the coefficients v_{-1} and u_{-1} are confined to the ranges

$$N/2\Omega \leq v_{-1} \leq N/\Omega \quad , \quad (1 - N/\Omega)^{\frac{1}{2}} \leq u_{-1} \leq (1 - N/2\Omega)^{\frac{1}{2}} \; .$$

The transformation in Eq. (3.15) thus automatically breaks particle number symmetry. The exclusion of mean-fields which conserve particle number is necessary. If fixed particle number N is retained in the mean-field description, then only N states in the lower level of the canonical basis can be occupied. Clearly, as $N < \Omega$, there is no unique choice of these states, which means that the ansatz for the approximate ground state is not unique. This is both physically and formally undesirable (Da 67). The problem is circumvented when particle number symmetry is broken.

Expressions for ρ and κ in the bare basis can be deduced by combining Eqs. (3.8), (3.14) and (3.17). One finds that

$$\begin{aligned} \rho_{\sigma m,\sigma' m'} &= \langle v| c^{\dagger}_{\sigma' m'}\, c_{\sigma m} |v\rangle = \rho_{\sigma,\sigma'}\, \delta_{m,m'} \\ \kappa_{\sigma m,\sigma' m'} &= \langle v| c^{\dagger}_{\sigma' m'}\, c_{\sigma m} |v\rangle = \mathrm{sgn}(m)\, \kappa_{\sigma,\sigma'}\, \delta_{m,-m'} \end{aligned} \tag{3.20a}$$

where

$$\begin{aligned} \rho_{\sigma,\sigma} &= \rho_{\sigma} = \frac{(\rho^{c}_{-1} + \rho^{c}_{1})}{2} - \sigma\, \frac{(\rho^{c}_{-1} - \rho^{c}_{-1})}{2} \cos\phi \\ &= N/2\Omega\, (1 - \sigma \cos\psi \cos\phi) \\ \rho_{\sigma,-\sigma} &= -\rho_{o} = \frac{-\,(\rho^{c}_{-1} - \rho^{c}_{1}) \sin\phi}{2} = \frac{-N}{2\Omega} \cos\psi \sin\phi \end{aligned} \tag{3.20b}$$

and

$$\kappa_{\sigma,\sigma} = \kappa_\sigma = \frac{(\kappa^c_{-1} + \kappa^c_1)}{2} - \sigma\,\frac{(\kappa^c_{-1} - \kappa^c_1)\cos\phi}{2}$$

$$\kappa_{\sigma,\bar\sigma} = \kappa_0 = \frac{-(\kappa^c_{-1} - \kappa^c_1)\sin\phi}{2} \quad . \tag{3.20c}$$

Just as $\rho^c_{-1} \geq \rho^c_1$, so $\rho_{-1} \geq \rho_1$, implying $|\phi| \leq \pi/2$. The sign of ϕ determines the signs of ρ_0 and κ_0 which are arbitrary. Hence ϕ can be restricted to $0 \leq \phi \leq \pi/2$.

The trial ground state $|v\rangle$ can break two symmetries of the Agassi Hamiltonian, namely parity symmetry whenever ρ_0 is non-zero, and particle number symmetry whenever $\bar\kappa = (\kappa_{-1} + \kappa_1)/2$ is non-zero. These two parameters, ρ_0 and $\bar\kappa$, conveniently specify the physical character of the ground state. *Because parity symmetry is the analogue in the Agassi model of rotational invariance in the Pairing-plus-Quadrupole model*, a ground state for which $\rho_0 \neq 0$ is termed deformed; a ground state for which $\bar\kappa \neq 0$ is superconducting. Four different types of ground state can be identified:

(i) spherical - $\rho_0 = \bar\kappa = 0 \leftrightarrow \psi = \phi = 0$, $N = \Omega$ (HF state);

(ii) deformed - $\rho_0 \neq 0$, $\bar\kappa = 0 \leftrightarrow \psi = 0$, $0 < \phi \leq \pi/2$, $N = \Omega$ (HF state);

(iii) superconducting - $\rho_0 = 0$, $\bar\kappa \neq 0 \leftrightarrow 0 \leq \psi < \pi/2$ (equality when $N < \Omega$), $\phi = 0$ (BCS state), or $\psi = \pi/2$, ϕ arbitrary (Full HFB state);

(iv) deformed-superconducting - ρ_0, $\bar\kappa \neq 0 \leftrightarrow 0 \leq \psi < \pi/2$ (equality when $N < \Omega$), $0 < \phi \leq \pi/2$.

The deformed and deformed-superconducting states are interpreted as describing both members of the ground state parity doublet found when $V \to \infty$, g fixed (cf. Section 2.2.2). Observe that, when $N < \Omega$, only superconducting or deformed-superconducting states are possible. (This is one of the reasons why the cases $N = \Omega$ and $N < \Omega$ are discussed separately in Sections 3.3 and 3.4 respectively.)

Applying Wick's theorem to the Agassi Hamiltonian H (Eq. (2.1)) and using Eq. (3.20), lead to the result

$$\xi = \frac{2}{\Omega}\left(\frac{\langle v|H|v\rangle}{-\varepsilon}\right)$$

$$= (\rho^c_{-1} - \rho^c_1)\cos\phi + \Sigma_1(2\rho^c_{-1}\rho^c_1) + \Sigma_2(2\kappa^c_{-1}\kappa^c_1) \qquad (3.21)$$

$$+ \tfrac{1}{2}(\chi(\rho^c_{-1} - \rho^c_1)^2 + V/\varepsilon\,(\kappa^c_{-1} - \kappa^c_1)^2)\sin^2\phi + n\, g/\varepsilon$$

where

$$\Sigma_1 = \Sigma_2 - \frac{g}{\varepsilon} - \frac{V}{\varepsilon} = \left(\frac{\Omega}{2} - 1\right)\frac{g}{\varepsilon}, \quad \chi = (\Omega - 1)\frac{V}{\varepsilon}, \quad n = \frac{N}{\Omega}\left(\delta + \frac{N}{\Omega}\right).$$

(A less direct derivation of this essential result is discussed in Appendix 3.1.) Since, by choice, ϕ and ψ automatically satisfy all the relevant constraints, the variational principle in Eq. (3.12) implies that it is necessary to find ϕ_o, ψ_o such that

$$\frac{\partial\xi}{\partial\phi}\Big|_{\phi = \phi_o,\ \psi = \psi_o} = \frac{\partial\xi}{\partial\psi}\Big|_{\phi = \phi_o,\ \psi = \psi_o} = 0$$

(There are, of course, no subsidiary conditions.) Also, in the present case, the corresponding state is stable if

$$\frac{\partial^2\xi}{\partial\phi^2},\ \frac{\partial^2\xi}{\partial\psi^2} < 0 \quad \text{and} \quad \frac{\partial^2\xi}{\partial\phi^2}\,\frac{\partial^2\xi}{\partial\psi^2} > \frac{\partial^2\xi}{\partial\phi\partial\psi}, \qquad (3.22)$$

where the partial derivatives are evaluated at $\phi = \phi_o$, $\psi = \psi_o$. The parametrisation of the transformations (Eqs. (3.14) and (3.19)) simplifies considerably the determination of the HFB ground state, and, in particular, the application of the stability criterion.

SECTION 3.3: HFB GROUND STATE WHEN $N = \Omega$

Setting $N = \Omega$ in Eq. (3.19), one finds that

$$v_{-1} = u_1 = \cos\psi/2 , \qquad u_{-1} = \text{[illegible]} = \sin\psi/2 \tag{3.23a}$$

which implies

$$\rho^c_\sigma = \tfrac{1}{2}(1 - \cos\psi), \qquad \kappa^c_\sigma = \tfrac{1}{2} \sin\psi, \tag{3.23b}$$

so that ξ assumes the form

$$\xi = \cos\psi \cos\phi + \tfrac{1}{2}\Sigma_o \sin^2\psi + \tfrac{1}{2}\chi \cos^2\psi \sin^2\phi + g/\varepsilon \tag{3.24}$$

where $\Sigma_o = \Sigma_1 + \Sigma_2$. The equations determining the HFB ground state are

$$\frac{\partial\xi}{\partial\phi} = 0 = \cos\psi \sin\phi \,(1 - \chi \cos\psi \cos\phi),$$

$$\frac{\partial\xi}{\partial\psi} = 0 = \sin\psi \,(\cos\phi + \chi \cos\psi \sin^2\phi - \Sigma_o \cos\psi).$$

The solutions of these equations can be found analytically. Their multiplicity depends on the values of χ and Σ_o.

If $\chi \neq \Sigma_o$, there are four different solutions, which are as follows.

(1) $\psi = \phi = 0$. This exists for any values of χ, Σ_o and is a spherical HF solution. It is also a trivial solution of the HF equations in the LMG model and the BCS equations in the 2-level Pairing model (when $N = \Omega$).

(2) $\psi = \phi = \pi/2$. Again, the existence of this solution is independent of the values of χ and Σ_o. It is an example of that peculiar type of superconducting state for which $\phi = \pi/2$.

(3) $\psi = 0$, $\cos\phi = 1/\chi$ provided $\chi > 1$. This is the deformed (strictly parity-mixed) HF solution found in the LMG model.

(4) $\phi = 0$, $\cos\psi = 1/\Sigma_o$ provided $\Sigma_o > 1$. This is a BCS solution. It corresponds to the superconducting solution of the 2-level Pairing model.

For the special case $\chi = \Sigma_o > 1$, there is another (infinite) class of *solutions consisting of all the values of ψ, ϕ which satisfy the single* equation

$$\cos\psi \cos\phi = 1/\chi. \tag{3.25}$$

Only members of this class of solutions are deformed-superconducting.

The evaluation of the second derivatives of ξ for these solutions is straightforward. Employing Eq. (3.22), one finds that:

(i) the spherical HF stable is stable only if both $\chi, \Sigma_o < 1$;

(ii) the deformed HF (BCS) solution is stable provided $\chi > \Sigma_o$ ($\Sigma_o > \chi$);

(iii) the solution $\psi = \phi = \pi/2$ is never stable.

Accordingly this last solution can hereafter be ignored.

These results are conveniently summarised in *Fig. 3.1. It shows what* the stable self-consistent mean-field is in any part of the $\Sigma\chi$ - plane (where $\Sigma = (\Omega - 1)g/\varepsilon$). For $g = 0$ and $V = 0$ the diagram is consistent with the results of HF and BCS calculations in the LMG and Pairing Models respectively. Figure 3.1 demonstrates that the class of solutions satisfying Eq. (3.25) has no practical relevance.

The absence of a genuine HFB solution is probably a general feature of $N = \Omega$ systems. The most general "physical" Hamiltonian for a two-level model which has quasi-spin group SO(5) and conserves parity is given by (EK 71)

$$H_{gen} = \epsilon J_o - \frac{V_1}{2}(J_+J_- + J_-J_+ - \hat{N}) - \frac{V_2}{2}(J_+^2 + J_-^2)$$

$$- g_1 (L_+L_- + S_+S_-) - g_2(L_+S_- + S_+L_-) .$$

(The Agassi Hamiltonian corresponds to the choice $V_1 = 0$, $V_2 = V$, $g_1 = g_2 = g$.) For attractive interactions, the form of the transformation determining the HFB ground state is the same for this system as it is for the Agassi model. In terms of the parameters ψ and ϕ, the HFB variational functional when $N = \Omega$ is

$$\xi_{gen} = \frac{2}{\Omega} \frac{(\langle v|H_{gen}|v\rangle)}{-\epsilon} = \cos\psi \cos\phi + \tfrac{1}{2} \Sigma_{gen} \sin^2\psi$$

$$+ \tfrac{1}{2} \chi_{gen} \cos^2\psi \sin^2\phi + g_1/\epsilon$$

where

$$\Sigma_{gen} = \left(\frac{\Omega}{2} - 1\right) \frac{g_1}{\epsilon} + \frac{\Omega}{2} \frac{g_2}{\epsilon} + \frac{V_2}{\epsilon} - \frac{V_1}{\epsilon}$$

$$\chi_{gen} = (\Omega - 1) \left(\frac{V_1}{\epsilon} + \frac{V_2}{\epsilon}\right) + \frac{g_2}{\epsilon} - \frac{g_1}{\epsilon} \tag{3.26}$$

From comparison of ξ_{gen} with ξ in Eq. (3.24), one can immediately deduce that, again, the relevant solutions are either HF or BCS states. The same result has been found in realistic calculations in closed-shell nuclei (SGB 69).

Expressions, appropriate to the three regions in Fig. 3.1, for ρ_o, $\bar{\kappa}$, the approximate ground state energy and expectation values of various combinations of quasi-spin operators are collected together in Table 3. The parameters ρ_o and $\bar{\kappa}$ and the approximate ground state energy are easily calculated using Eqs. (3.20b), (3.23b) and (3.24). The other expectation values follow straightforwardly from Eqs. (A3.3) - (A3.5) in Appendix 3.1.

Inspection of Table 3 shows that, in certain respects, the BCS and deformed HF solutions are formally similar, with Σ_0 performing the same role in the BCS solution as χ does in the deformed HF solution. However, as the expectation values of all the quasi-spin operators (except J_0) demonstrate, these two solutions are physically very different. The considerable enhancement in the expectation values of J_x^2 in the deformed region and Y_+Y_- in the superconducting region demonstrates that these solutions accommodate the monopole and pairing interactions, respectively.

A feature of the transition from one region in Fig. 3.1 to another is the non-analytic change of various quantities in Table 3. In some cases the quantities themselves are discontinuous at the boundary between two regions, and in others only their first derivatives with respect to ξ and g. This type of non-analytic behaviour in physical observables is a characteristic of phase transitions. It is for this reason that a stable quasi-particle basis is commonly referred to as a "phase" (Chapter 11 of (RS 80)). Similarly, Fig. 3.1 is a phase diagram, which indicates the phase transitions predicted by HFB; ρ_0 and $\bar{\kappa}$ are <u>order parameters</u> for these transitions.

In the thermodynamic description of phase transitions, the phase is determined by the value of the chemical potential μ. Transitions are classified as either continuous or discontinuous depending on whether derivatives of μ (with respect to the relevant thermodynamic variables) are continuous or discontinuous. (The chemical potential itself is continuous through a transition.) In the present context, ξ fulfils the role of μ. Hence the analogous classification scheme implies that the spherical-to-deformed and spherical-to-superconducting transitions in Fig. 3.1 are continuous. By contrast, the deformed-to-superconducting transition is discontinuous <u>despite</u> the presence of the class of solutions of Eq. (3.25).

The correlations promoted <u>strongly</u> by the monopole and pairing interactions respectively are quite different, as evidenced by the very different mean-fields which accommodate them. The competition between these two different types of correlations is seen in the fact that the monopole interaction strength required to cause the deformed-to-superconducting transition increases linearly with the pairing interaction strength (cf. Fig. 3.1). However, the mean-fields involved do not cater directly for this competition (because neither are full HFB solutions). For example, $\bar{\kappa}$, the measure of pairing correlations, increases instead of decreasing as V is increased and the superconducting-to-deformed transition line in Fig. 3.1 is approached from below. This trend arises because a small fraction of the correlations induced by the monopole interaction resemble those induced by the pairing interaction. (The similar contribution to the correlations induced by the monopole interaction from part of the pairing interaction is fortuitously cancelled by the remainder of the pairing interaction - cf. χ_{gen} in Eq. (3.26).) The fact that the monopole interaction promotes other correlations is seen only in the "independent" comparison of the ground state energies of the BCS and deformed HF states. Hence the discontinuity of the deformed-to-superconducting transition.

In line with the earlier stability analysis, the phases which supplant the spherical phase have lower ground state energies (cf. Table 3). Consider the spherical-to-deformed transition. In the spherical phase, the Ω particles fill the lower level of the non-interacting basis. In the deformed phase both the upper and lower levels are populated. To create this distribution one must excite the system with an energy $E_e = (\Omega\ \rho_1)\varepsilon$. However the m^{th} state of the upper level and the m^{th} state of the lower level now interact. Such an interaction causes an energy drop of magnitude $e_c = \alpha V$, where α is some constant. The magnitude of the overall drop, which is obtained by summing over all distinct pairs of these correlations, is then $E_c = \frac{1}{2}\Omega(\Omega - 1)e_c$. Thus χ is essentially the magnitude of the ratio of E_c to E_e. This recognition provides a simple explanation for the location of the spherical-to-deformed transition. It also illustrates the collective character of the factor $(\Omega - 1)$ appearing in χ. A similar analysis can be applied to the spherical-to-superconducting transition.

The presence of ε in Σ_o and χ is a non-trivial feature. The larger the level spacing ε of the non-interacting basis, the larger the interaction strengths must be for the spherical phase to become unstable. A similar trend is observed in the application of HFB to the Pairing - plus - Quadrupole model (BS 68): the lower the level density (or the larger

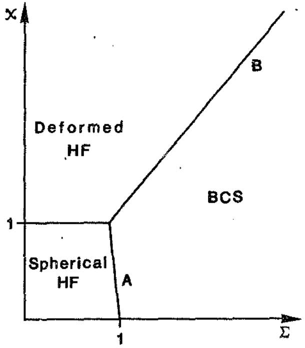

Fig. 3.1 Zero temperature HFB phase diagram for Agassi model when $N = \Omega$. Transition line A is given by $\chi = (\Omega - 1)(1 - \Sigma)$ and transition line B by $\chi = ((\Omega - 1)/(\Omega - 2))\ \Sigma$.

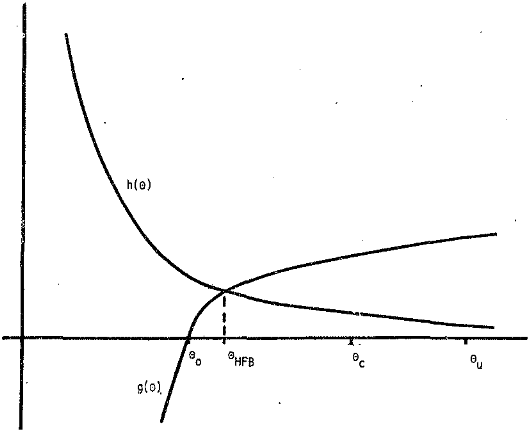

Fig. 3.2 Schematic graphical equivalent of Eq. (3.37a) when the conditions for the existence of θ_{HFB} are satisfied. The funtion $h(\theta)$ is independent of interaction strengths, while $g(\theta)$ increases monotonically with V.

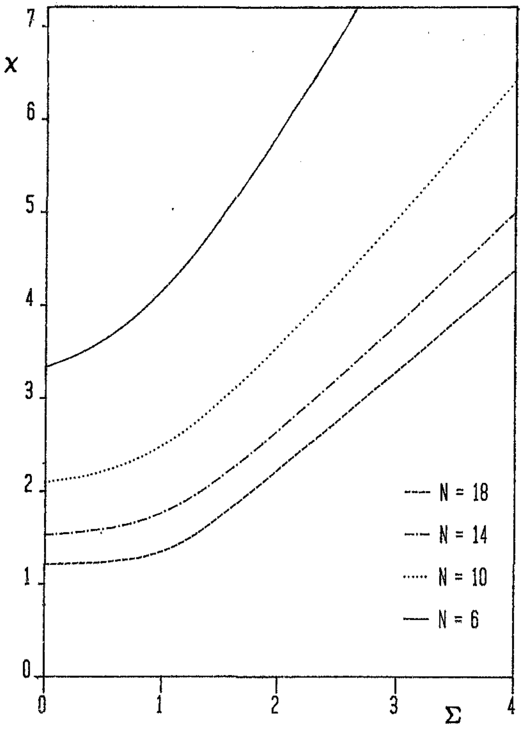

Fig. 3.3 Superconducting - to - deformed - superconducting transition line for different particle numbers N when Ω = 22. The superconducting (BCS) solution is stable below these lines.

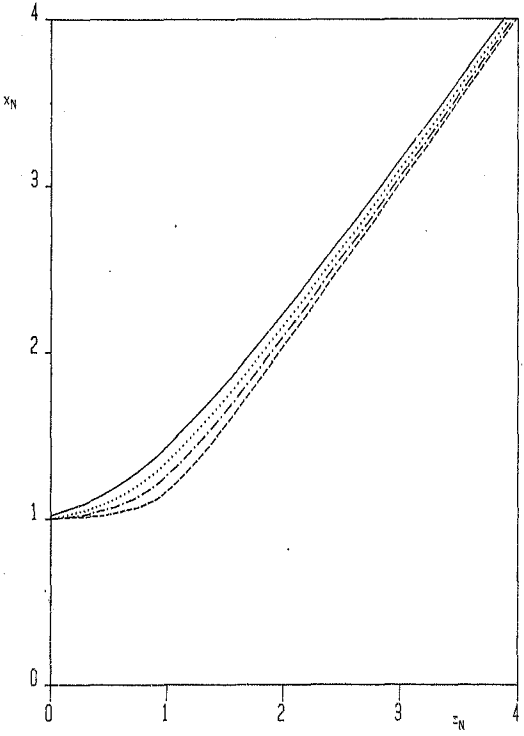

Fig. 3.4 The superconducting - to - deformed - superconducting transition lines of Fig. 3.3 when replotted using Σ_N and x_N (defined in Eq. (3.43)) instead of Σ and χ ; the key to curves is the same as in Fig. 3.3.

the level spacing) near the Fermi level of the underlying <u>spherical</u> shell model basis, the stronger the residual interaction strengths must be for a symmetry-breaking solution to be found.

SECTION 4: HFB GROUND STATE WHEN $N < \Omega$

When $N < \Omega$, the dependence of ξ in Eq. (3.21) on ψ is quite complex. A tractable expression for $\partial\xi/\partial\psi$ is obtained by introducing the variable θ related to ψ by the transformation

$$\cos\psi = (1 + \beta - \beta \sec\theta)^{\frac{1}{2}}$$

in which

$$\beta = 2(1 - N/\Omega) \,/\, (N/\Omega)^2$$

and, as $0 \le \psi \le \pi/2$, $0 \le \theta \le \theta_u = \arccos(\beta/(1 + \beta)) < \pi/2$. In terms of this new variable,

$$2\rho^c_{-1}\,\rho^c_1 = (1 - N/\Omega)\,(\sec\theta - 1), \quad 2\kappa^c_{-1}\,\kappa^c_1 = (1 - N/\Omega)\tan\theta$$

and (3.27)

$$\rho^c_{-1} - \rho^c_1 = N/\Omega(1 + \beta - \beta\sec\theta)^{\frac{1}{2}} .$$

With the aid of

$$(\kappa^c_\sigma)^2 = \rho^c_\sigma\,(1 - \rho^c_\sigma) \quad \text{and} \quad \rho^c_{-1} + \rho^c_1 = N/\Omega, \tag{3.28}$$

the coefficient of $\sin^2\phi$ in Eq. (3.21) becomes

$$\chi(\rho^c_{-1} - \rho^c_1)^2 + \frac{V}{\varepsilon}(\kappa^c_{-1} - \kappa^c_1)^2$$

(3.29)

$$= \frac{N}{\Omega}\left(\frac{N}{\Omega}\chi + \left(1 - \frac{N}{\Omega}\right)\frac{V}{\varepsilon}\right) - \left(2\chi - \frac{V}{\varepsilon}\right) \qquad \frac{V}{\varepsilon}(2\kappa^c_{-1}\,\kappa^c_1) .$$

Substituting from Eqs. (3.27) and (3.29) into Eq. (3.21), one finds that

$$\xi \;=\; N/\Omega \cos\phi \; (1 + \beta - \beta \sec\theta)^{\frac{1}{2}} \qquad (3.30a)$$
$$+ \;(1 - N/\Omega)\; \{\sigma_1(\phi) \sec\theta \;+\; \sigma_2(\phi) \tan\theta\}$$

where

$$\sigma_1(\phi) \;=\; \Sigma_1 \;-\; (\chi \;-\; \tfrac{1}{2}\, V/\varepsilon) \sin^2\phi \qquad (3.30b)$$

$$\sigma_2(\phi) \;=\; \Sigma_2 \;-\; \tfrac{1}{2}\, V/\varepsilon \sin^2\phi \;=\; \tfrac{1}{2}(\Omega g/\varepsilon + V/\varepsilon) \;+\; \tfrac{1}{2}\, V/\varepsilon \cos^2\phi \qquad (3.30c)$$

and terms independent of θ have been dropped. It follows that

$$\frac{\partial\xi}{\partial\psi} \;=\; \frac{\partial\xi}{\partial\theta}\frac{\partial\theta}{\partial\psi} \;=\; 0 \;=\; (\sec\theta - 1)^{\frac{1}{2}} \qquad (3.31)$$
$$\times\{N/\Omega\; (1 + \beta - \beta \sec\theta)^{\frac{1}{2}}\; (\sigma_1(\phi) + \sigma_2(\phi) \operatorname{cosec}\theta) - \cos\phi\}$$

Study of the limit $\theta \to 0$ shows that, whatever the value of ϕ, $\theta = 0$ does not satisfy this equation. Thus the factor of $(\sec\theta - 1)^{\frac{1}{2}}$ can be discarded. From Eq. (3.21),

$$\frac{\partial\xi}{\partial\phi} \;=\; 0 \;=\; \sin\phi \qquad (3.32)$$
$$\times\{(\rho^c_{-1} - \rho^c_1) - \left(\chi(\rho^c_{-1} - \rho^c_1) + V/\varepsilon\, (\kappa^c_{-1} - \kappa^c_1)^2\right) \cos\phi\}$$

which through Eqs. (3.27) and (3.29) is an expression in θ and ϕ.

Inspection of Eqs. (3.31) and (3.32) shows that the choice $\phi = \pi/2$ is a solution for all interaction strengths provided $\psi = \pi/2$ $(\theta = \theta_u)$ and vice versa. Like its counterpart when $N = \Omega$, it too is of no interest because it is always unstable. There remain two other solutions, both of which are physically relevant.

(1) A <u>superconducting</u> solution, for which $\phi = 0$ and θ satisfies (from Eqs. (3.30b,c) and (3.31))

$$\frac{N}{\Omega}(1 + \beta - \beta\sec\theta)^{\frac{1}{2}} = \frac{1}{\Sigma_1 + \Sigma_2\,\mathrm{cosec}\,\theta} \tag{3.33}$$

The graphical equivalent of Eq. (3.33) demonstrates immediately that a solution θ_{BCS} always exists, is unique and confined to the open interval $0 < \theta_{BCS} < \theta_u$ ($\Rightarrow 0 < \psi_{BCS} < \pi/2$).

A remarkable feature of Eq. (3.33) is that the left-hand side does not depend on the interaction strengths g and V, while the right-hand side does not depend on N. This makes it simple to deduce that θ_{BCS} increases with increasing g, V and N. It follows that $\bar{\kappa}$, which, from Eqs. (3.27) and (3.28), is given by

$$\begin{aligned}\bar{\kappa} &= \tfrac{1}{2}\sqrt{N/\Omega\,(1 - N/\Omega) + 2\rho^c_{-1}\,\rho^c_1 + 2\kappa^c_{-1}\,\kappa^c_1} \\ &= \tfrac{1}{2}\sqrt{(1 - N/\Omega)\,(\sec\theta + \tan\theta - (1 - N/\Omega))},\end{aligned} \tag{3.34}$$

increases with g in the superconducting phase, as one would expect.

(2) A <u>deformed - superconducting</u> solution in which $0 < \phi < \pi/2$, $0 < \theta < \theta_u$. Equation (3.32) implies that the values of ϕ and θ for any solution of this kind are related to each other by the expression

$$\begin{aligned}\cos\phi &= \frac{\rho^c_{-1} - \rho^c_1}{((\Omega - 1)\,(\rho^c_{-1} - \rho^c_1)^2 + (\kappa^c_{-1} - \kappa^c_1)^2)V/\varepsilon} \\ &= \frac{(1 + \beta - \beta\sec\theta)^{\frac{1}{2}}}{h_1(\theta)\;V/\varepsilon} = S(\theta)\end{aligned} \tag{3.35a}$$

where, from Eqs. (3.27) and (3.29),

$$\begin{aligned}h_1(\theta) &= 1 - N/2\Omega\,(1 + \beta\tan\theta) \\ &\quad + N/\Omega\,(\Omega - 3/2)\,(1 + \beta - \beta\sec\theta).\end{aligned} \tag{3.35b}$$

The function $S(\theta)$ is positive and increases monotonically with θ; it diverges as $\theta \to \theta_u$. Clearly the equality in Eq. (3.34a) can only hold if

$$S(0) = \frac{1}{(N + 1 - 2N/\Omega)V/\varepsilon} < 1 \tag{3.36}$$

Furthermore, even when Eq. (3.36) is satisfied, it is necessary to restrict θ to the interval $0 < \theta < \theta_c$, where θ_c ($< \theta_u$) is such that $S(\theta_c) = 1$.

Elimination of ϕ in Eq. (3.31) using Eq. (3.35a) yields the equation which must be satisfied by θ, namely

$$g(\theta) = h_2(\theta)/(h_1(\theta))^2 \tag{3.37a}$$

where

$$g(\theta) = \frac{N}{2\Omega}\frac{V}{\varepsilon}(\Sigma o + g/\varepsilon)\left\{1 + 2\left(\frac{\chi - \Sigma_o}{\Sigma_o + g/\varepsilon}\right) - \operatorname{cosec}\theta\right\} \tag{3.37b}$$

$$h_2(\theta) = \frac{N}{2\Omega}((1 + \beta - \beta\sec\theta)\operatorname{cosec}\theta + 1 + \beta\tan\theta) - 1 \tag{3.37c}$$

and $h_1(\theta)$ is defined in Eq. (3.35b). By inspection, $g(\theta)$ is a monotonically increasing function of θ, which, whatever the interaction strengths, is negative for θ small enough; $h(\theta) = h_2(\theta)/(h_1(\theta))^2$ is positive and decreases monotonically. Thus the solution θ_{HFB} of Eq (3.37) is unique and exists when Eq. (3.36) and the condition

$$g(\theta_c) > h(\theta_c) \tag{3.38}$$

are satisfied.

Figure 3.2 is a schematic drawing of the graphical equivalent of Eq. (3.37a) under these conditions. It demonstrates that θ_{HFB} is in fact confined to the interval $\theta_o < \theta_{HFB} \leq \theta_c$ where, from Eq. (3.37b),

$$\operatorname{cosec}\theta_o = 1 + 2\,(\chi - \Sigma_o)\,/\,(\Sigma_o + g/\varepsilon). \tag{3.39}$$

An inference from Eq. (3.39), which is interesting in view of the earlier results for $N = \Omega$, is that Eq. (3.38) cannot be satisfied if $\Sigma_o \geq \chi$ (for then $g(\theta) \leq 0$). The dependence of θ_o, θ_c and θ_{HFB} on V is easily determined. While θ_c increases with increasing V, θ_o and θ_{HFB} decrease. As, from Eq. (3.35a), $\cos\phi_{HFB} = S(\theta_{HFB})$, this implies the intuitively pleasing trend that ϕ_{HFB} increases with increasing V; similarly, from Eq. (3.30), $\bar{\kappa}$ decreases. As $V \to \infty$ (g fixed), both θ_{HFB} and θ_o tend not to zero but to $\theta_\infty = \arcsin(1/(2\Omega - 3))$.

Evaluation of the second derivatives of ξ shows that the full HFB state is stable whenever it exists, but that the BCS state is stable only if $S(\theta_{BCS}) > 1$. It follows that a necessary condition for the instability of the BCS state is that Eq. (3.36) is satisfied, which is one of the criteria for the existence of the HFB state. Now, by employing the results given above, it is also possible to prove that the other criterion, Eq(3.38), is satisfied only when the BCS state is unstable. Thus one arrives at another intuitively satisfying result, namely that the instability of the BCS solution is equivalent to the existence of the HFB solution. It follows that the phase diagram for the Agassi model when $N < \Omega$ contains just these two solutions. The BCS-to-HFB transition line is the locus of points for which $\theta_{BCS} = \theta_c$. Because $S(\theta)$ is (fortuitously) independent of g, this line is easily determined for given N and Ω. Fixing V (at some value which satisfies Eq. (3.36)) allows one to solve for θ_c. After substituting θ_c into the equation determining θ_{BCS} (Eq. (3.33)), one can solve for the critical value g_c of g - i.e.

$$\frac{g_c}{\varepsilon} = \left(\frac{\sin\theta_c}{N/\Omega(1 + \beta - \beta\sec\theta_c)^{\frac{1}{2}}} - \frac{V}{\varepsilon}\right) / \left(\Omega/2 + (\Omega/2 - 1)\sin\theta_c\right).$$

The HFB solution exists for the chosen value of V if $g_c > 0$ and $g < g_c$.

A plot of the BCS - to - HFB (or superconducting - to - deformed - superconducting) transition line in the $\Sigma\chi$-plane for various values of N when $\Omega = 22$ is given in Fig. 3.3. Not surprisingly, this transition has certain features in common with the superconducting - to - deformed transition found in the closed-shell system. Deformation occurs as χ is increased; the larger Σ is, the larger χ must be (which, as before, reflects the competition between monopole and pairing interactions). In the BCS phase, the approximate ground state energy (in units of $-\Omega/2\ \varepsilon$) is $\xi_{BCS} = \xi(\psi = \psi_{BCS},\ \ \phi = \phi_{BCS} = 0)$, where $\xi(\psi,\phi)$ is given in Eq. (3.21), and

$$\frac{\partial\xi}{\partial x}_{BCS} = \left(\frac{\partial\xi}{\partial x}(\psi,\phi)\right)\Bigg|_{\substack{\psi = \psi_{BCS}\\ \phi = 0}} + \left(\frac{\partial\xi}{\partial\psi}\right)\Bigg|_{\substack{\psi = \psi_{BCS}\\ \phi = 0}} \frac{\partial\psi}{\partial x}_{BCS}$$

$$+ \left(\frac{\partial\xi}{\partial\phi}\right)\Bigg|_{\substack{\psi = \psi_{BCS}\\ \phi = 0}} \frac{\partial\phi}{\partial x}_{BCS} = \left(\frac{\partial\xi}{\partial x}(\psi,\phi)\right)\Bigg|_{\substack{\psi = \psi_{BCS}\\ \phi = 0}} , \tag{3.40a}$$

using the fact that ψ_{BCS}, ϕ_{BCS} satisfy Eqs. (3.31) and (3.32). Similarly

$$\frac{\partial\xi}{\partial x}_{HFB} = \left(\frac{\partial\xi}{\partial x}(\psi,\phi)\right)\Bigg|_{\substack{\psi = \psi_{HFB}\\ \phi = \phi_{HFB}}} . \tag{3.40b}$$

Along the BCS - to - HFB transition line,

$$\theta_{BCS} = \theta_{HFB} = \theta_c \rightarrow \psi_{BCS} = \psi_{HFB},\ \phi_{BCS} = \phi_{HFB} = 0 \tag{3.41}$$

which, together with Eq. (3.40), implies that the derivatives of ξ_{BCS} and ξ_{HFB} with respect to interaction strengths are the same on this line. So, in contrast to the superconducting - to -deformed transition in the closed-shell system, the BCS - to - HFB transition is continuous.

Equation (3.41) by itself ensures the continuity of all approximate ground state expectation values at the BCS - to - HFB transition. The continuity of the derivatives of the approximate ground state energy results from the particular nature of the variational principle occurring in zero temperature HFB, and cannot be expected (in general) of the other expectation values. In fact, a difference in the behaviour of ξ and other expectation values at continuous transitions can be seen in the results of Table 3.

Inspection of the general expressions for the ground state expectation values of quasi-spin operators in Appendix 3.1 shows that their behaviour in the BCS and HFB phases of the open-shell system is similar to their behaviour in the BCS and deformed HF phases respectively of the closed-shell system. However, it must be remembered that, in the HFB phase, both $\bar{\kappa} \neq 0$ and $\rho_1^c \neq 0$ (because $\theta_{HFB} > 0$ always), while, in the deformed HF phase, $\bar{\kappa} = \rho_1^c \equiv 0$. Properties of the BCS and HFB solutions in open-shell systems will be studied in subsequent chapters.

A feature of Fig. 3.3 is that the value of χ at which the BCS-to-HFB transition occurs for given Σ decreases with increasing N. This can be stated in another more familiar way: for fixed interaction strengths, changing the number of particles in the valence shell can lead to the onset of deformation, which is characteristic of several sets of isotopes in, for example, the rare earth region (Ra 50, KB 66). Observe that it holds even as the shell closure ($N = \Omega$) is approached. Equation (3.36) implies that, when Σ is small (i.e. $\theta \to 0$ on the transition line), the critical value of χ scales with N like $1/n$, where $n = N + 1 - 2N/\Omega$. When Σ is very large, $\theta_c = \theta_{BCS} \equiv \theta_u$ on the transition line; the critical value of χ is also very large (cf. Fig. 3.3). The dependence of $g(\theta)$ on interaction strengths along with the graphical equivalent of Eq(3.37a) suggests that, under these circumstances, $\theta_o \cong \theta_c$. From the equivalent "equality" $\mathrm{cosec}\theta_o = \mathrm{cosec}\theta_u$, one deduces (using Eq. (3.19)) that, when Σ is large, the values of χ and Σ on the transition line should be approximately related by

$$\chi = \mu\Sigma \tag{3.42a}$$

where

$$\mu = \frac{\Omega/2 \; - N/\Omega\;(1 - N/2\Omega)}{N(1 - N/2\Omega) - 1 + \frac{1}{4}(1 - N/\Omega)^2} \; . \tag{3.42b}$$

When $N = \Omega$, Eq. (3.42) coincides with the expression for the superconducting - to - deformed line in the $N = \Omega$ phase diagram.

In the future, instead of Σ and χ, the variables

$$\chi_N = \eta V/\varepsilon \qquad , \qquad \Sigma_N = \mu \eta g/\varepsilon \tag{3.43}$$

will be used when dealing with systems in which $N < \Omega$. The transition lines in Fig. 3.3 are replotted in Fig. 3.4 using χ_N and Σ_N. The variables χ_N and Σ_N are like the "reduced" variables used in discussing "corresponding" states in thermodynamics, in that the transition lines now almost coincide. In fact, one can go further: the HFB ground state expectation values in systems of different particle number, if appropriately scaled, also have essentially the same functional dependence on χ_N and Σ_N. This is demonstrated in, for example, Fig. 5.3.

APPENDIX 3.1: EXPECTATION VALUES OF QUASI-SPIN OPERATORS IN HFB GROUND STATE

The normalised ground state $|v\rangle$ corresponding to the quasi-particle operators defined by the combination of transformations in Eqs. (3.14) and (3.15) can always be written as

$$|v\rangle = \prod_{\substack{\sigma m \\ m > 0}} (u_\sigma + v_\sigma a^\dagger_{\sigma m} a^\dagger_{\sigma -m}) |-\rangle, \tag{A3.1}$$

where $|-\rangle$ is the state containing no particles or the "bare" vacuum. (It is trivially verified that $\alpha_{\sigma m}|v\rangle = 0$ for all σ and m.) In this appendix, expressions for the expectation values in this state of the combinations of quasi-spin operators considered in Appendix 2.1 are derived. This is facilitated through the use of the expressions in Eq. (A3.9) of Appendix 3.2. (Familiarity with the contents of Appendix 3.2 is assumed in this appendix.) Equation (A3.1) implies that only combinations of the operators in Eqs. (A3.6) and (A3.7) (of Appendix 3.2) which conserve the formal equivalent in the canonical basis of parity (which is defined for the bare basis in Section 2.1), can have non-zero expectation values in the state $|v\rangle$. Thus reference to

Eq. (A3.9) shows that only the expectation values of y_+y_-, x_+x_-, m_+m_-, y_+y_-, j_x^2, j_y^2 and j_o^2 have to be evaluated.

In this appendix, the expectation value of an operator O in the state $|v\rangle$ will be denoted by $\langle O\rangle$.

<u>Expectation values of</u> y_+y_-, x_+x_-, m_+m_-, y_+x_- __:

From the definitions of y_+, x_+, m_+ and their hermitian conjugates, it follows that each of these combinations is a special case of the operator

$$A = \sum_{\substack{(\sigma)\ m\ m' \\ m,\ m' > 0}} S_{\sigma_1\sigma_2\sigma_3\sigma_4}\, a^\dagger_{\sigma_1 m}\, a^\dagger_{\sigma_2 -m}\, a_{\sigma_3 -m'}\, a_{\sigma_4 m'}$$

in which (σ) denotes the sum over σ_1, σ_2, σ_3, σ_4 and

$$S_{\sigma_1\sigma_2\sigma_3\sigma_4} = S_{\sigma_1\sigma_3}\ \delta_{\sigma_1\sigma_2}\ \delta_{\sigma_3\sigma_4} + S_2\ {}'\ \ \delta_{\sigma_3 -\sigma_4}, \tag{A3.2a}$$

where $S_{\sigma_1\sigma_3}$, S_2, are given in Table A3. Using Wick's theorem, Eq. (3.17) and the fact that m, m' > 0,

$$\langle a^\dagger_{\sigma_1 m}\, a^\dagger_{\sigma_2 -m}\, a_{\sigma_3 -m'}\, a_{\sigma_4 m'}\rangle$$

$$= \kappa^c_{\sigma_1}\, \kappa^c_{\sigma_3} \delta_{\sigma_1\sigma_2}\ \delta_{\sigma_3\sigma_4} + \rho^c_{\sigma_1}\ \rho^c_{\sigma_2}\ \delta_{\sigma_1\sigma_4}\ \delta_{\sigma_2\sigma_3}\ \delta_{mm'},$$

implying

$$\langle A\rangle = \Omega/2\{\Omega/2 \sum_{\sigma\sigma'} S_{\sigma\sigma'}\, \kappa^c_\sigma\, \kappa^c_{\sigma'} + \sum_\sigma S_{\sigma\sigma}\ (\rho^c_\sigma)^2 + S_2(2\rho^c_{-1}\ \ \rho^c_1)\} \tag{A3.2b}$$

Specialising Eq. (A3.2b) one deduces

$$\left.\begin{array}{l}\langle y_+ \; y_- \rangle \\ \\ \langle x_+ \; x_- \rangle\end{array}\right\} = \Omega \left\{ \Omega \left(\frac{\kappa^c_{-1} \pm \kappa^c_1}{2}\right)^2 + \frac{1}{2}\left(\frac{N}{\Omega}\right)^2 - \rho^c_{-1} \; \rho^c_1 \right\},$$

$$\langle m_+ \; m_- \rangle = \Omega \quad \rho^c_{-1} \quad \rho^c_1, \tag{A3.3}$$

$$\langle y_+ \; x_- \rangle = -(\delta + N/\Omega) \; \Omega/2 \; (\rho^c_{-1} - \rho^c_1) \, ,$$

where $\delta = (\Omega - N)/2$.

<u>Expectation values of j_x^2, j_y^2 and j_o^2 __:</u>

Using the method above, one finds

$$\left.\begin{array}{l}\langle j_x^2 \rangle \\ \langle j_o^2 \rangle\end{array}\right\} = \Omega/4 \; (N/\Omega - 2\rho^c_{-1} \; \rho^c_1 \pm 2\kappa^c_{-1} \;\; \kappa^c_1)$$

$$\langle j_o^2 \rangle = \Omega/4 \; ((\Omega - 1) \; (\rho^c_{-1} - \rho^c_1)^2 + (\kappa^c_{-1} - \kappa^c_1)^2) + \langle v | (j_x)^2 | v \rangle \tag{A3.4}$$

<u>Expectation values of operators in Eq. (A3.9):</u>

Combining Eqs. (A3.3), (A3.4) and (A3.9),

$$\langle S_+ S_- \; + \; L_+ L_- \rangle = \Omega/2 \; (\Omega/2 \; ((\kappa^c_{-1})^2 + (\kappa^c_1)^2) + (N/\Omega)^2 - 2\rho^c_{-1} \; \rho^c_1)$$

$$- \; \Omega/2 \; (\Omega((\kappa^c_{-1} - \kappa^c_1)/2)^2 + \tfrac{1}{2}(\rho^c_{-1} - \rho^c_1)^2) \sin^2\phi$$

$$\langle S_+ S_- - L_+ L_- \rangle = (\delta + N/\Omega) \; \Omega/2 \; (\rho^c_{-1} - \rho^c_1) \cos\phi$$

$$= -(\delta + N/\Omega) \langle v | J_o | v \rangle$$

$$\langle Y_+ Y_- \rangle = \langle y_+ y_- \rangle$$

$$\langle J_x^2 \rangle = \langle j_x^2 \rangle + \Omega/4 \; ((\Omega - 1) \; (\rho^c_{-1} - \rho^c_1)^2 + (\kappa^c_{-1} - \kappa^c_1)^2) \sin^2\phi$$

$$\langle J_y^2 \rangle = \langle j_y^2 \rangle$$

$$\langle M_+ M_- \rangle = \langle m_+ m_- \rangle + \Omega \{\Omega((\kappa_{-1}^c - \kappa_1^c)/2)^2 + \tfrac{1}{2}(\rho_{-1}^c - \rho_1^c)^2\} \sin^2\phi .$$

The expression for $\langle J_0^2 \rangle$ is obtained by replacing $\sin^2\phi$ by $\cos^2\phi$ in the result for $\langle J_x^2 \rangle$.

Substituting from Eqs. (A3.4) and (A3.5) into Eq. (A3.10), Eq. (3.21) follows trivially.

APPENDIX 3.2: FORM OF QUASI-SPIN OPERATORS IN CANONICAL BASIS

In this appendix the quasi-spin operators defined in Chapter 2 and various combinations thereof are rewritten in terms of the operators $a^\dagger_{\sigma m}$, $a_{\sigma m}$ given by Eq. (3.14). For this purpose, it is convenient to introduce the formal analogues in the canonical basis of the quasi-spin operators - i.e. the set of operators

$$\ell_0 = \tfrac{1}{2}(\sum_m a^\dagger_{1m} a_{1m} - \Omega/2), \qquad s_0 = \tfrac{1}{2}(\sum_m a^\dagger_{-1m} a_{-1m} - \Omega/2),$$

$$\ell_+ = (\ell_-)^\dagger = \sum_{\substack{m \\ m>0}} a^\dagger_{1m} a^\dagger_{1-m}, \qquad s_+ = (s_-)^\dagger = \sum_{\substack{m \\ m>0}} a^\dagger_{-1m} a^\dagger_{-1-m}, \tag{A3.6}$$

$$j_+ = (j_-)^\dagger = \sum_m a^\dagger_{1m} a_{-1m}, \qquad m_+ = (m_-)^\dagger = \sum_{\substack{\sigma m \\ m>0}} a^\dagger_{\sigma m} a^\dagger_{-\sigma -m},$$

as well as the linear combinations

$$j_x = \frac{(j_+ + j_-)}{2}, \quad j_y = \frac{(j_+ - j_-)}{2i}, \quad j_0 = \ell_0 - s_0,$$

$$y_+ = \ell_+ + s_+, \quad x_+ = \ell_+ - s_+, \quad m_0 = \ell_0 + s_0. \tag{A3.7}$$

Clearly the operators in Eq. (A3.6) have the same commutation relations as their formal counterparts in Eqs. (2.3) and (2.4), and so also form an SO(5) algebra.

Quasi-spin operators in Eqs. (2.3) and (2.4):

Using the inverse of the transformation in Eq. (3.14),

$$\left.\begin{matrix} L_o \\ \\ S_o \end{matrix}\right\} = \tfrac{1}{2}(m_0 \pm \cos\phi\ j_o \pm \sin\phi\ j_x)$$

$$\left.\begin{matrix} L_+ \\ \\ S_+ \end{matrix}\right\} = \tfrac{1}{2}(y_+ \pm \cos\phi\ x_+ \pm \sin\phi\ m_+) \tag{A3.8}$$

$$J_+ = \cos\phi\ j_x - \sin\phi\ j_o + i\ j_y$$

$$M_+ = \cos\phi\ m_+ - \sin\phi\ x_+ .$$

Expressions for the remaining operators in Eqs. (2.3) and (2.4) can be obtained by hermitian conjugation.

Combinations of quasi-spin operators (discussed in Appendix 2.1):

Using Eq. (A3.8),

$$S_+S_- + L_+L_- = \tfrac{1}{2}\{y_+ y_- + \cos^2\phi\ x_+x_- + \sin^2\phi\ m_+m_-$$
$$+ \sin\phi\ \cos\phi(m_+x_- + x_+m_-)\}$$

$$S_+S_- - L_+L_- = -\tfrac{1}{2}\cos\phi\ (y_+x_- + x_+y_-) - \tfrac{1}{2}\sin\phi\ (y_+m_- + m_+y_-)$$

$$Y_+Y_- = y_+ y_-$$

$$J_x^2 = \cos^2\phi\ j_x^2 + \sin^2\phi\ j_o^2 - 2\sin\phi\ \cos\phi\ (j_xj_o + j_oj_x) \tag{A3.9}$$

$$J_y^2 = j_y^2$$

$$M_+M_- = \cos^2\phi\ m_+ m_- + \sin^2\phi\ x_+x_- - \sin\phi\ \cos\phi\ (m_+x_- + x_+m_-).$$

The expression for J_o^2 can be inferred directly from Eq. (A3.9), since the transformation to the canonical basis is such that $J^2 = j^2$ (ALM 66).

Inserting the results in Eqs. (A3.8) and (A3.9) into Eq. (2.2), one finds that, under this transformation, the Agassi Hamiltonian becomes

$$H = \varepsilon(\cos\phi j_o + \sin\phi\, j_x) - g\, y_+ y_- - V(j_x^2 - j_y^2)$$
$$- V \sin^2\phi (j_o^2 - j_x^2) + 2V \sin\phi \cos\phi (j_x j_o + j_o j_x). \tag{A3.10}$$

A feature of Eq. (A3.10) is the invariance of the pairing interaction, which emphasizes the fact that the transformation to the canonical basis is designed to accommodate the monopole interaction (and not the pairing interaction).

TABLE 3: EXPECTATION VALUES OF APPROXIMATE GROUND STATE WHEN $N = \Omega$

State / Units	ρ_0	$\bar{\kappa}$	Ground State Energy	Y_+Y_-	J_0	J_x^2	J_y^2
Units	–	–	$-(\Omega/2\epsilon)$	$\Omega/2$	$\Omega/2$	$\Omega/4$	$\Omega/4$
Spherical	0	0	$1 + g/\epsilon$	1	-1	1	1
Deformed	$\frac{1}{2}\sqrt{1-(1/\chi_0)^2}$	0	$\frac{1}{2}(\chi + 1/\chi) + g/\epsilon$	1	$-1/\chi$	A	1
Superconducting	0	$\frac{1}{2}\sqrt{1-(1/\Sigma_0)^2}$	$\frac{1}{2}(\Sigma_0 + 1/\Sigma_0) + g/\epsilon$	B	$-1/\Sigma_0$	1	$1/(\Sigma_0)^2$

$A = (\Omega - 1)(1 - 1/\chi^2) + 1$
$B = (\Omega - 1)/2\ (1 - 1/(\Sigma_0)^2) + 1$

TABLE A3: DEFINITION OF COEFFICIENTS IN EQ. (A3.2a)

	y_+y_-	x_+x_-	m_+m_-	y_+x_-
$S_{\sigma\sigma'}$	1	$\sigma\sigma'$	0	σ'
S_2	0	0	1	0

CHAPTER FOUR

THERMAL SELF-CONSISTENT MEAN-FIELDS

Temperature is no stranger to the description of finite nuclei. Its classic application is to the compound nucleus formed in low-energy neutron scattering, where it is unambiguously determined by the level density (Appendix 2 of chapter 2 of (BM 69)). What is perhaps a little surprising is that it can also be applied to fusion and deep inelastic heavy-ion reactions. These produce nuclei with large intrinsic excitation energies whose decay proceeds through a number of highly-excited intermediate states of different energy and particle number, and is dominated by neutron and γ-ray emission (GN 80). This implies a de-excitation time of the order of 10^{-16}s. On the other hand, the time required to "thermalise" the excitation energy of any of these intermediate states over the various degrees of freedom is of the order of 10^{-21}s (TEC 82), suggesting the methods of equilibrium statistical mechanics could be usefully employed.

The nature of this physical process indicates that it is the grand canonical ensemble which is appropriate, because the members of this type of ensemble have different energies and particle number. The grand canonical ensemble has a well-defined temperature T and chemical potential μ (section 5.1 of (Pa 71)). In quantum statistical mechanics, the measurable properties of this ensemble are determined by a positive definite hermitian operator termed the density operator D, which is such that

$$\mathrm{Tr}\, D \equiv \sum_i \langle i|D|i\rangle = 1,$$

where the sum is over all states in the ensemble. The expectation value of any observable O is given by the ensemble average (chapter 4 of (Pa 71))

$$\langle O\rangle = \mathrm{Tr}\,(DO).$$

The laws of thermodynamics imply that the condition satisfied by the equilibrium state of this ensemble is conveniently expressed in terms of the grand potential

$$\Phi = E - TS - \mu N \tag{4.1a}$$

where

$$E = \mathrm{Tr}\,(DH), \quad S = -k_B\,\mathrm{Tr}\,(D\ \ln D), \quad N = \mathrm{Tr}\,(D\hat{N}), \tag{4.1b}$$

in which H and S are the Hamiltonian and entropy of the system, respectively, $\hat{N}$ is the particle number operator and k_B is Boltzmann's constant. In equilibrium, Φ is minimized (section F of chapter 1 of (Re 80)).

Finite temperature or thermal HFB represents the optimal description in terms of non-interacting quasi-particles (Cl 67, Go 81a) of a grand canonical ensemble containing fermions with a Hamiltonian of the type given in Eq. (3.1). Within this approximation, the ensemble consists of the entire set of states $|n_1, n_2, \ldots, n_m>$, where m is the total number of quasi-particle states (which is finite in applications to nuclei), and n_i is the occupation number of a quasi-particle state (n_i = 0 or 1). As in zero temperature HFB, the quasi-particle operators $\beta_i^\dagger$, β_i are assumed to be related to bare particle operators $b_i^\dagger$, b_i by a unitary transformation of the form in Eq. (3.3).

In this chapter, the foundations are laid for the investigation in chapter 5 of the existence of phase transitions predicted by thermal HFB when it is applied to finite systems. This topic is conveniently addressed within the Agassi model.

A general method for the determination of the transformation in thermal HFB is discussed in section 4.1. In the process, the calculation of ensemble averages within this approximation is demonstrated and, where relevant to subsequent considerations, features which distinguish thermal HFB from zero temperature HFB are pointed out. While it is well known that the operator identity established in Wick's theorem does not hold at finite temperature (BD 58), there is some confusion in the literature over the status of the canonical basis. (See, for example, the conflicting statements made in (Go 84) and (RP 85).) It is shown that, in general, this does not exist.

The application of thermal HFB to the Agassi model is presented in section 4.2. Only closed-shell systems ($N = \Omega$) are considered. The form of thermal HFB appropriate to such systems is discussed, and then the corresponding phase diagram is determined. Like its zero temperature counterpart, it contains no full HFB phase.

SECTION 4.1: ESSENTIAL FEATURES OF THERMAL HFB

The operator identity in Wick's theorem cannot be extended to finite temperature because it is not possible to define, in an ensemble of quasi-particle states, the analogue of a normal product of operators. Nevertheless, Wick's theorem remains valid for the ensemble average $\langle\rangle_o$ of operators in this ensemble (BD 58). It follows that

$$\tilde{\rho}_{ij} = \langle b_j^\dagger b_i \rangle_o \qquad \text{and} \qquad \tilde{\kappa}_{ij} = \langle b_j b_i \rangle_o \tag{4.2}$$

play the same role in the evaluation of ensemble averages in thermal HFB as the contractions ρ_{ij} and κ_{ij} (in Eq. (3.4)) in the calculation of ground state expectation values in zero temperature HFB. The quantities $\tilde{\rho}_{ij}$ and $\tilde{\kappa}_{ij}$ are the matrix elements in the bare basis of the thermal single-particle density $\tilde{\rho}$ and the thermal pairing tensor $\tilde{\kappa}$, respectively.

As in a non-interacting Fermi gas at finite temperature, the independent non-vanishing ensemble averages of bilinear combinations of the quasi-particle operators are (Go 81a)

$$\langle \beta_i^\dagger \beta_j \rangle_o = f_i \, \delta_{ij}, \tag{4.3}$$

where the quasi-particle occupation probabilities f_i lie in the interval $0 < f_i < 1$. It is through these as yet unknown occupation probabilities that the effects of non-zero temperature are taken into account. Employing the anti-commutation relations of the operators $\beta_i^\dagger$, β_i, the ensemble averages in Eq. (4.3) imply the existence of another class of non-zero ensemble averages, namely,

$$<\beta_i \, \beta_j^\dagger>_\circ = (1 - f_i)\delta_{ij} \quad . \tag{4.4}$$

Substitution of the inverse of the transformation in Eq. (3.3) into Eq. (4.2), along with use of Eqs. (4.3) and (4.4) leads to the expressions

$$\begin{aligned} \tilde{\rho}_{ij} &= \sum_k \left\{ V_{ik}^* V_{jk} (1 - f_k) + U_{ik} U_{jk}^* f_k \right\} \\ \tilde{\kappa}_{ij} &= \sum_k \left\{ V_{ik}^* U_{jk} (1 - f_k) + U_{ik} V_{jk}^* f_k \right\} . \end{aligned} \tag{4.5}$$

Equations (3.5) and (4.4) and the formally similar roles of $<v|\beta_i\beta_j^\dagger|v>$ and $<\beta_i\beta_j^\dagger>_o$ imply that the results in Eqs. (4.5) and (3.6) must coincide when $f_i \equiv 0$, and indeed this is the case.

It is obvious that the transformation properties of $\tilde{\rho}_{ij}$ and $\tilde{\kappa}_{ij}$ under a change of single-particle basis are the same as those of ρ_{ij} and κ_{ij} in Eq. (3.4) respectively. Recalling the consequences of these transformation properties in zero temperature HFB, the question arises as to whether there is a single-particle basis in which $\tilde{\rho}$ is diagonal and $\tilde{\kappa}$ is simultaneously canonical. A requirement for the existence of such a basis is that $\tilde{\kappa}\,\tilde{\kappa}^\dagger$ commutes with $\tilde{\rho}$ (BM 62). (This property holds for κ and ρ because of Eq. (3.7)). The unitarity of the transformation in Eq. (3.3) implies that the matrices U and V, with matrix elements U_{ij} and V_{ij} respectively, must satisfy the conditions

$$\begin{aligned} U^\dagger U + V^\dagger V &= UU^\dagger + V^* V^T = I, \\ U^T V + V^T U &= U^* V^T + VU^\dagger = 0. \end{aligned} \tag{4.6}$$

Using Eqs. (4.5) and (4.6), one finds that

$$\begin{aligned} \tilde{\kappa}\,\tilde{\kappa}^\dagger &= \tilde{\rho} - \tilde{\rho}^2 - \gamma_1, \\ \tilde{\rho}\,\tilde{\kappa} &= \tilde{\kappa}\,\tilde{\rho}^* - (\gamma_2 + \gamma_2^T), \end{aligned} \tag{4.7a}$$

where

$$\gamma_1 = V^* F(1 - F)V^T + U F(1 - F)U^\dagger,$$
$$\gamma_2 = V^* F(1 - F)U^T, \tag{4.7b}$$

in which F is the diagonal matrix with entries f_i. With the exception of the special case in which $F = I$, γ_1 and ρ do not commute. Thus, as recognized in (Go 84), there is, in general, no equivalent in thermal HFB of the canonical basis of zero temperature HFB. On the other hand, it is always possible to write the transformation in Eq. (3.3) in terms of three successive transformations along the lines of the Bloch-Messiah decomposition (Section 7.2.1 in (RS 80)) - i.e. one can write

$$U = U_1 \bar{U} U_2 \qquad \text{and} \qquad V = U_1^* \bar{V} U_2 \tag{4.7c}$$

where U_1 and U_2 are unitary matrices and

$$\bar{U} = \begin{pmatrix} 1 & & & & & & & \\ & u_1 & & & & & & \\ & & u_1 & & & & & \\ & & & u_2 & & & & \\ & & & & u_2 & & & \\ & & & & & \ddots & & \\ & & & & & & u_n & \\ & & & & & & & u_n & \\ & & & & & & & & 0 \end{pmatrix}, \quad \bar{V} = \begin{pmatrix} 0 & & & & & & & & \\ & 0 & v_1 & & & & & & \\ & -v_1 & 0 & & & & & & \\ & & & 0 & v_2 & & & & \\ & & & -v_2 & 0 & & & & \\ & & & & & \ddots & & & \\ & & & & & & 0 & v_n & \\ & & & & & & -v_n & 0 & \\ & & & & & & & & 1 \end{pmatrix}$$

in which u_k and v_k are real-valued and satisfy $u_k^2 + v_k^2 = 1$. It is for this reason that there is confusion over the status in thermal HFB of the canonical basis. The point overlooked in certain formal papers (So 83, RP 85) is that, in general, the transformation U_1 cannot be chosen so that it simultaneously diagonalises $\tilde{\rho}$ and brings $\tilde{\kappa}$ to its canonical form.

A related difference between thermal and zero temperature HFB is that the ensemble averages, unlike the ground state expectation values in zero temperature HFB, depend explicitly on the third transformation U_2. For example, the ensemble average of the particle number operator $\hat{N}$ is

$$\langle\hat{N}\rangle_o = \sum_k \tilde{\rho}_{kk} = \sum_k V_k + \sum_{k,l} (1 - 2V_k)\, f_l (U_2)_{kl}\, (U_2)^*_{kl} \qquad (4.8)$$

where V_k denotes any entry of the diagonal matrix $\bar{V}^T\bar{V}$, and use has been made of Eqs. (4.5) and (4.7c) and the fact that $\bar{U}^2 + \bar{V}^T\bar{V} = I$. The lack of dependence of $\langle\hat{N}\rangle_o$ on U_1 is a feature unique to $\hat{N}$ – cf. Eq. (3.9).

The entropy of the thermal HFB ensemble is as in any non-interacting system (Go 81a), given by

$$S_o = -k_B \sum_i \left\{ f_i \ln f_i + (1 - f_i) \ln (1 - f_i) \right\} \qquad (4.9)$$

The expression for the ensemble average of the Hamiltonian is trivially obtained from Eq. (3.11) by replacing ρ_{ij} and κ_{ij} by $\tilde{\rho}_{ij}$ and $\tilde{\kappa}_{ij}$, respectively. Combining the above results, one obtains the thermal HFB approximation to the grand potential $\Phi_o = \langle H\rangle_o - TS_o - \mu\langle\hat{N}\rangle_o$ in terms of the unknown occupation probabilities f_i and transformation coefficients U_{ij} and V_{ij}. These are determined by appealing to the thermodynamic criterion for thermal equilibrium stated in connection with Eq. (4.1). Thus they have to minimize Φ_o, subject to the constraints implied by the unitarity of the transformation in Eq. (3.3) and the condition that $\langle\hat{N}\rangle_o = N$, the number of particles in the system under consideration. (Depending on the nature of the application of the thermal HFB approximation, additional restrictions on other ensemble averages can be introduced.) Note the <u>formal</u> similarity between this criterion and that determining zero temperature HFB solutions.

The consequences of the requirement that the constrained variation of Φ_o vanish are considered in detail in (Go 81a). They are twofold. Firstly, with the exception of certain special cases (which are given in (Go 81a)), it is equivalent to the system of equations

$$\tilde{H}^{20}_{ij} = 0 \qquad \text{and} \qquad \tilde{H}^{11}_{ij} = \tilde{E}_i\, \delta_{ij} \qquad (4.10a)$$

where $\tilde{H}^{20}$, $\tilde{H}^{11}$ are defined in the same way as H^{20} and H^{11} in zero temperature HFB, with $\tilde{\rho}$ and $\tilde{\kappa}$ replacing ρ and κ (as in the calculation of $\langle H\rangle_o$), and $\tilde{E}_i$ is a thermal quasi-particle energy. Observe that the diagonality of $\tilde{H}^{11}$ follows automatically from the variational principle in thermal HFB, whereas, in zero temperature HFB, the demand that H^{11} be diagonal supplements the relevant variational principle. (The reason for this difference is that in zero temperature HFB the variational principle determines only the ground state, whereas in thermal HFB it determines an ensemble - i.e. ground state plus excited states.) The second consequence is the relation

$$f_i = (1 + e^{\beta\tilde{E}_i})^{-1} . \qquad (4.10b)$$

Although formally similar to the expression for occupation probabilities in a non-interacting Fermi gas in equilibrium, it differs subtly in that $\tilde{E}_i$ is temperature dependent.

As in zero temperature HFB, the value of the chemical potential μ is adjusted so that the condition $\langle\hat{N}\rangle_o = N$ is satisfied. The temperature T is strictly another Lagrange parameter, and should be fixed so that the average energy of the ensemble $\tilde{E}_o$ takes on some desired value (Section 5.1 of (Pa 71)). (In a study of heavy-ion reactions, this value can be related to the excitation energy (MZP 74, Fig.1 in Go 81b).) The issues addressed in this work however do not require this, and so T will be treated as a free parameter. In addition, instead of solving the system of Eq. (4.10) subject to the constraint $\langle\hat{N}\rangle_o = N$, the variational principle will be used directly.

Thermal HFB solutions are classified in the same way as zero temperature HFB solutions. Thus, for a thermal HF solution, $\tilde{\kappa} \equiv 0$, while, for a thermal BCS solution, $\tilde{\rho}$ is diagonal and $\tilde{\kappa}$ is non-zero but canonical in the bare basis. Other forms of $\tilde{\rho}$ and $\tilde{\kappa}$ (in the bare basis) correspond to full HFB solutions. There is however one difference, which is revealed by the ensemble average of $(\hat{N} - N)^2$ where $N = \langle\hat{N}\rangle_o$; this is given by

$$(\Delta N)^2 = \langle(\hat{N} - N)^2\rangle_o = \mathrm{Tr}\,(\tilde{\rho} - \tilde{\rho}^2 + \tilde{\kappa}\,\tilde{\kappa}^\dagger) ,$$

which, substituting from Eq. (4.7), becomes

$$(\Delta N)^2 = 2\,\mathrm{Tr}\,(\tilde{\kappa}\,\tilde{\kappa}^\dagger) + \mathrm{Tr}\,(F(1 - F)). \qquad (4.11)$$

So for all bases, including thermal HF bases, $(\Delta N)^2 > 0$. This is a characteristic of any description of a system at finite temperature, which has a fixed chemical potential (section 5.1 of (Pa 71)). In open-shell systems, it leads to the existence of solutions which have no counterpart at T = 0 (Appendix B in (LA 84) and (QM 86)).

SECTION 4.2: APPLICATION OF THERMAL HFB TO THE AGASSI MODEL WHEN $N = \Omega$

Since the purpose of the quasi-particle transformation at finite T is the same as at T = 0, its form is the same. The full HFB transformation appropriate to the Agassi model (and not just that part determining the quasi-particle vacuum) is discussed in Appendix 6.1 of chapter 6. It is shown that, taking advantage of the Bloch-Messiah decomposition, it can be written as

$$\beta^{\dagger}_{\sigma m} = \cos\zeta/2 \; \alpha^{\dagger}_{\sigma m} - \sigma \sin\zeta/2 \; \alpha^{\dagger}_{-\sigma m} \tag{4.12}$$

where $\alpha^{\dagger}_{\sigma m}$ is defined by the two successive transformations in Eqs. (3.14) and (3.15) and $0 \leq \zeta \leq \pi/2$.

Given the equivalence in the Agassi model of the single-particle states within a level of the non-interacting basis, the quasi-particle occupation probability $f_{\sigma m}$ must be independent of m - i.e. $f_{\sigma m} = f_\sigma$. Therefore, substituting from Eqs. (4.12) and (3.15) into Eq. (4.8), the constraint $\langle \hat{N} \rangle_o = N$ becomes

$$\begin{aligned}(1 - N/\Omega) - (1 - v^2_{-1} - v^2_1)\,(1 - f_{-1} - f_1) \\ = (f_{-1} - f_1)\,(v^2_{-1} - v^2_1) \cos\zeta \;.\end{aligned} \tag{4.13}$$

There are two independent contributions to this relation. Terms proportional to f_σ arise from the statistical character of the description and are not inherent in the approximation (cf. the discussion in connection with Eq. (4.11)). On the other hand, terms in Eq. (4.13) containing only v^2_σ, occur because the ensemble used by thermal HFB to approximate the exact ensemble contains states of indefinite particle number. It is desirable to impose the additional constraint

$$v^2_{-1} + v^2_1 = N/\Omega, \tag{3.18}$$

which ensures that the quasi-particle vacuum, at least, has the correct particle number on average. The additional constraint in Eq. (3.18) implies that the coefficients u_σ, v_σ of the second transformation can once again be written as in Eq. (3.19).

As the purpose of the application of thermal HFB is to investigate "phase transitions" at finite temperature, it is sufficient to consider only the case $N = \Omega$, for which various technical simplifications occur. Inserting Eq. (3.18) into Eq. (4.13) one obtains

$$(1 - \frac{N}{\Omega})(f_{-1} + f_1) = (f_{-1} - f_1)\ (v_{-1}^2 - v_1^2)\ \cos\zeta.$$

Thus, when $N = \Omega$, the quasi-particle occupation probabilities $f_{\sigma m}$ must be independent of both σ and m, i.e.

$$f_{\sigma m} = \langle\beta^\dagger_{\sigma m}\ \beta_{\sigma m}\rangle_o = f\ . \qquad (4.14a)$$

It is precisely under these conditions that the first transformation in the Bloch-Messiah decomposition of the transformation in the Eq. (4.12) defines a canonical single-particle basis in which ρ is diagonal and κ canonical.

This is verified by explicit calculation: one finds

$$\rho^c_{\sigma m,\sigma' m'} = \langle a^\dagger_{\sigma' m'}\ a_{\sigma m}\rangle_o = \rho^c_\sigma\ \delta_{\sigma,\sigma'}\ \delta_{m,m'} \qquad (4.14b)$$

and

$$\kappa^c_{\sigma m,\sigma' m'} = \langle a_{\sigma' m'}\ a_{\sigma m}\rangle_o = \mathrm{sgn}(m)\ \kappa^c\ \delta_{\sigma,\sigma'}\ \delta_{m,-m'}, \qquad (4.14c)$$

in which

$$\rho^c_\sigma = \tfrac{1}{2}(1 - \sigma(1 - 2f)\cos\psi), \qquad \kappa^c = \tfrac{1}{2}(1 - 2f)\sin\psi, \qquad (4.14d)$$

where ψ is defined in Eq. (3.19). As $\rho^c_{-1} \geq \rho^c_1$, $f \leq \frac{1}{2}$. The lack of dependence of the ensemble averages in Eq. (4.14) on the third transformation in the Bloch-Messiah decomposition (or, in this case, the parameter ζ), is also a general feature of the case F=I. It holds for all ensemble averages and so the variational principle discussed in section 4.1 does not, in this case, determine the third transformation. (As only ensemble averages are of interest in the present work, this is not a drawback, rather an economy.)

The forms of $\tilde{\rho}$ and $\tilde{\kappa}$ in the bare basis are obtained replacing ρ_σ^c and κ_σ^c in Eq. (3.20) by $\tilde{\rho}_\sigma^c$ and $\tilde{\kappa}_\sigma^c$. Thus they are

$$\tilde{\rho}_{\sigma m,\sigma' m'} = \langle c^\dagger_{\sigma' m'}\, c_{\sigma m}\rangle_o = \tilde{\rho}_{\sigma,\sigma'}\, \delta_{m,m'} \tag{4.15a}$$

and

$$\tilde{\kappa}_{\sigma m,\sigma' m'} = \langle c_{\sigma' m'}\, c_{\sigma m}\rangle_o = \mathrm{sgn}(m)\, \tilde{\kappa}^c\, \delta_{\sigma,\sigma'}\, \delta_{m,m'} \tag{4.15b}$$

with

$$\begin{aligned} \tilde{\rho}_{\sigma,\sigma} &= \tilde{\rho}_\sigma = \tfrac{1}{2}(1 - \sigma(1 - 2f)\cos\psi\cos\phi) \\ \tilde{\rho}_{\sigma,-\sigma} &= -\tilde{\rho}_o = -\tfrac{1}{2}(1 - 2f)\cos\psi\sin\phi \end{aligned} \tag{4.15c}$$

where ϕ is defined in Eq. (3.14). The difference between the expressions in Eq. (3.20) (when $N = \Omega$) and those above is the appearance of the factor $(1 - 2f)$. Its effect is to diminish the magnitudes of $\tilde{\rho}_o$ and $\tilde{\kappa}^c$ as f increases. Thus a rise in the temperature decreases the order parameters and, at the same time, increases the fraction of particles in excited states. These results illustrate that, on a qualitative level, thermal HFB describes correctly the effects of thermal excitation.

The substitution used in deriving expressions for $\tilde{\rho}$ and $\tilde{\kappa}$ in the bare basis, cannot in general be employed to obtain the ensemble averages of combinations of quasi-spin operators from the expressions in Chapter 3 and Appendix 3.1 for the ground state expectation values in zero temperature HFB, because in many of these results use has been made of Eq. (3.7). In particular, this applies to Eq. (3.21) for the ground state expectation value of the Agassi Hamiltonian. If Wick's theorem (for ensemble averages) is applied directly to the Agassi Hamiltonian and Eq. (4.15) is used, one does however obtain an expression for $\langle H\rangle_o$ which is very similar to that for $\langle v|H|v\rangle$ when $N = \Omega$, namely

$$\xi = \frac{2}{\Omega}\frac{\langle H\rangle_o}{\varepsilon} = (1-2f)\cos\psi\cos\phi + \tfrac{1}{2}\chi(1-2f)^2\cos^2\psi\sin^2\phi$$

$$+ \tfrac{1}{2}\Sigma_o(1-2f)^2\sin^2\psi + \tfrac{1}{2}\frac{g}{\varepsilon}(1+(1-2f)^2) \tag{4.16}$$

where χ and Σ_o are defined in Eqs. (3.21) and (3.24).

The variables ϕ, ψ and f have been defined so that all constraints, in particular the particle number constraint, are automatically satisfied. Thus their values are determined by the minimisation of, not the grand potential, but the thermal HFB free energy functional

$$F_o = \langle H_o\rangle - T\, S_o,$$

where $\langle H\rangle_o$ is given in Eq. (4.16) and, using Eqs. (4.9) and (4.14a), the entropy is given by

$$\frac{S_o}{k_B} = -2\Omega\,(f\ln f + (1-f)\ln(1-f)).$$

The equations for the stationary points of F_o are

$$\frac{\partial F_o}{\partial\phi} = 0 = (1-2f)\sin\phi\cos\psi\,(1-\chi(1-2f)\cos\phi\cos\psi) \tag{4.17a}$$

$$\frac{\partial F_o}{\partial\psi} = 0 = (1-2f)\sin\psi\,(\cos\phi + (\chi\sin^2\phi - \Sigma_o)(1-2f)\cos\psi) \tag{4.17b}$$

$$\frac{\partial F_o}{\partial f} = 0 = \cos\phi\cos\psi + (\chi\sin^2\phi\cos^2\psi + \Sigma_o\sin^2\psi + g/\varepsilon)(1-2f)$$

$$+ 2\tau\ln(f/(1-f)) \tag{4.17c}$$

where $\tau = k_BT/\varepsilon$. Equation (4.17c) demonstrates that, when $\tau \neq 0$, there are no stationary points for which $f = 0$. On the other hand, setting $f = \tfrac{1}{2}$, one finds an infinite class of stationary points satisfying the condition

$\cos\psi \cos\phi = 0.$

None of these points however correspond to minima.

The equations for the remaining solutions of Eq. (4.17), for which $0 < f < \frac{1}{2}$, are simplified by introducing the variable x which is related to f by

$$f = 1/(1 + \exp(2x))$$

and lies in the interval $0 < x < \infty$. Discarding those solutions which are never thermodynamically stable (i.e. never minima of Φ_o, or, in this case, F_o), one is left with three.

(1) A spherical thermal HF solution – $\phi = \psi = 0$, $x = x_s$ where x_s is the solution of the equation

$$1 + g/\varepsilon \tanh x = 4\tau x. \tag{4.18}$$

This spherical solution is always present, but is thermodynamically stable only if $\tanh x_s$ satisfies both

$$\tanh x_s < 1/\chi \ , \tag{4.19a}$$

$$\tanh x_s < 1/\Sigma_o \ . \tag{4.19b}$$

(2) A deformed thermal HF solution – $\psi = 0$, $x = x_D$, $\cos\phi = 1/(\chi \tanh x_D)$, where x_D is the non-zero solution of

$$(\chi + g/\varepsilon) \tanh x = 4\tau x \ . \tag{4.20}$$

This deformed solution exists if

$$\tanh x_s \geq 1/\chi$$

and is thermodynamically stable provided $\chi > \Sigma_o$.

(3) A superconducting thermal BCS solution – $\phi = 0$, $x = x_B$, $\cos\psi = 1/(\Sigma_o \tanh x_B)$, where x_B is the non-zero solution of

$$(\Sigma_o + g/\varepsilon)\tanh x = 4\tau x \, . \qquad (4.21)$$

This superconducting solution exists as long as

$$\tanh x_s \geq 1/\Sigma_o$$

and is thermodynamically stable provided $\Sigma_o > \chi$.

These results are very similar to those found at $T = 0$. Again, there is no full HFB solution. At $T = 0$ the deformed and superconducting solutions are formally similar in certain respects, notably existence and stability. This similarity persists at finite temperature. In the Agassi model, the effect of temperature on pairing is the same as it is on deformation.

The results concerning existence and stability are conveniently summarised at constant temperature by phase diagrams like that in Fig. 4.1. The boundaries of the spherical phase are obtained in the following way. Given g and T, x_s can be determined using Eq. (4.18). From Eq. (4.19a) the value of χ at which the spherical-to-deformed transition occurs (ignoring, for the moment, the existence of the superconducting phase), is then

$$\chi_D = \coth(x_s). \qquad (4.22a)$$

Similarly, from Eq. (4.19b), the value of χ at which the spherical-to-superconducting transition occurs is

$$\chi_B = (\Omega - 1)\,(\coth(x_s) - \Sigma) \qquad (4.22b)$$

where $\Sigma = (\Omega - 1)g/\varepsilon$. Since x_s increases with g (cf. a graphical equivalent of Eq. (4.18)), both χ_D and χ_B are decreasing functions of g (or Σ). To generate the boundaries in Fig. 4.1, Eq. (4.22a) is used for $0 \leq \Sigma \leq \Sigma_E$, and Eq. (4.22b) is used for $\Sigma_E \leq \Sigma \leq \Sigma_M$ where $\Sigma_E(\Sigma_M)$ is the value of Σ at which $\chi_B = \chi_D$ $(\chi_B = 0)$. From Eq. (4.22),

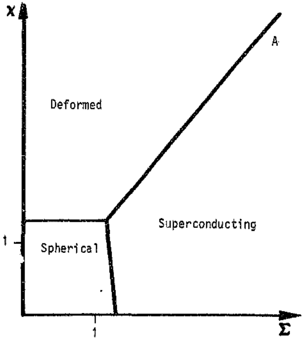

Fig. 4.1 Thermal HFB phase diagram for the Agassi model when $\tau = 0.25$ and $N = \Omega = 20$. The calculation of the boundaries of the spherical phase is discussed in the text; the superconducting - to - deformed transition line is as in Fig. 3.1.

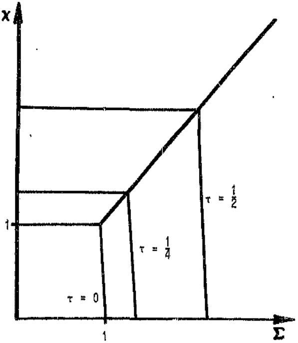

Fig. 4.2 Thermal HFB phase diagrams for the Agassi model at various temperatures when $N = \Omega = 20$.

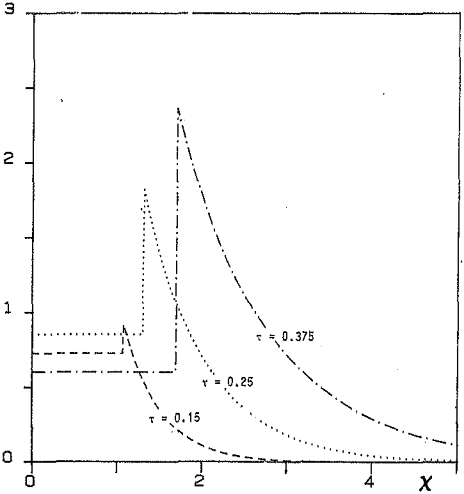

Fig. 4.3 Approximate specific heat C_v (in units of $\Omega\ k_B$) for various temperatures (calculated using Eq. (4.25)); $N = \Omega = 20$, $\Sigma = 0.4$.

$$\Sigma_E \tanh x_s = \frac{\Omega - 2}{\Omega - 1} \tag{4.23a}$$

and

$$\Sigma_M \tanh x_s = 1 . \tag{4.23b}$$

Combining Eq. (4.23) with the relation defining x_s - i.e. $1 + g/\varepsilon \tanh x_s = 4\tau x_s$, one finds

$$\Sigma_E = \left(\frac{\Omega - 2}{\Omega - 1}\right) \coth \left\{\left(1 + \frac{\Omega - 2}{(\Omega - 1)^2}\right)/4\tau\right\},$$

$$\Sigma_M = \coth \left(\frac{\Omega}{\Omega - 1} \frac{1}{4\tau}\right) . \tag{4.24}$$

Observe that, from Eqs. (4.22a) and (4.23a), when $\Sigma = \Sigma_E$, $\chi = (\Omega - 1)/(\Omega - 2)\ \Sigma_E$. Thus the spherical-to-deformed and spherical-to-superconducting transition lines intersect each other on the line $\chi = \Sigma_o$.

The deformed-to-superconducting transition line is given by $\chi = \Sigma_o$ and so temperature has no effect on it (in contrast to other model studies (RP 85)). On the other hand, as Fig. 4.2 demonstrates, the size of the spherical region increases with increasing T. In the absence of the pairing interaction, the value of χ at which the spherical-to-deformed transition occurs is, from Eqs. (4.18) and (4.22a), $\chi = \coth(1/4\tau)$. Even when the pairing interaction is present, this remains a useful estimate of where the spherical-to-deformed transition occurs. From Eq. (4.24), the value of Σ at which the spherical-to-superconducting transition occurs is also approximately equal to $\coth(1/4\tau)$. (These estimates improve with increasing Ω).

Expressions for $\tilde{\xi}$ in the three phases are given in Table 4. The entropy within each phase can be written as

$$\frac{S_o}{k_B} = -2\Omega(\tilde{x} \tanh\tilde{x} - \ln(\cosh\tilde{x}) - \ln 2)$$

where, depending on the phase, $\bar{x} = x_s$, x_D or x_B. If the corresponding expressions for the free energy F_o are considered, it is found that the first derivatives of F_o are continuous through the spherical-to-deformed and spherical-to-superconducting transitions, making these transitions (like their counterparts at $T = 0$) continuous. This does not however apply to all the first derivatives of $\bar{\xi}$ and S_o separately. For example, using Eqs. (4.18), (4.20) and (4.21) and the expressions for $\bar{\xi}$ in Table 4 , one finds that the specific heat C_v (in units of k_B) is given, in each phase by

$$C_v = -\frac{\Omega}{2}\frac{\partial\bar{\xi}}{\partial\tau} = \frac{\Omega}{2}\frac{(2\bar{x}\ \mathrm{sech}\bar{x})^2}{1 - \nu(\mathrm{sech}\bar{x})} \tag{4.25}$$

where ν is defined in Table 4. (Note that a consequence of $\bar{x}$ satisfying any one of Eqs. (4.18), (4.20) and (4.21) is that the denominator in Eq. (4.25) is positive) Because ν changes discontinuously, C_v (and hence $\partial\bar{\xi}/\partial\tau$) is discontinuous at the spherical-to-deformed and spherical-to-superconducting transitions. Figure 4.3 contains a typical plot of C_v and illustrates that the discontinuity is "lambda-shaped". The phenomenological Landau-Ginzberg theory demonstrates that any mean-field description of continuous symmetry-breaking transitions must predict this distinctive type of behaviour in C_v (Section F of chapter 4 of (Re 80)).

Although not required for subsequent developments, certain features of the thermal HFB solutions away from phase boundaries are worth pointing out. For example, when $g = 0$, analytic solution of Eq. (4.18) is possible ($x_s = 1/4\tau$). Because the dependence of x_s on g is weak, the explicit expressions for ensemble averages obtained in this limit are still useful when $g \neq 0$. Furthermore, the decrease of x_s with increasing T is a generally valid property. Since in the spherical phase

$$\bar{\rho}_{-1} - \bar{\rho}_1 = \tanh(x_s),$$

it implies that the excitation of particles to the upper level of the non-interacting basis occurs. By contrast, although x_B and x_D also decrease with increasing temperature, in the superconducting and deformed phases

$$\tilde{\rho}_{-1} - \tilde{\rho}_1 = \begin{cases} 1/\Sigma_o & \text{Superconducting} \\ 1/\chi & \text{Deformed} \end{cases} .$$

The reduction in the fraction of particles in the upper level due to the weakening of correlations (with temperature) exactly cancels the increase due to thermal excitation.

As $T \to 0$, each of x_D, x_B and $x_s \to \infty$. Study of these limits shows that one recaptures the results of zero temperature HFB. So, in this system, the limit $T \to 0$ is continuous.

TABLE 4

	$\tilde{\xi}$	$4\tau\nu$
Spherical	$\tanh x_s + \frac{1}{2}\frac{g}{\varepsilon}(1 + \tanh^2 x_s)$	$\frac{g}{\varepsilon}$
Deformed	$\frac{1}{2}\left(\chi + \frac{g}{\varepsilon}\right)\tanh^2 x_D + \frac{1}{2}\left(\frac{1}{\chi} + \frac{g}{\varepsilon}\right)$	$\chi + \frac{g}{\varepsilon}$

Expressions appropriate to superconducting phase are obtained from expressions in deformed phase by replacing χ and x_D by Σ_o and x_B.

CHAPTER FIVE

EXISTENCE OF PHASE TRANSITIONS

The attitude in the literature towards the use of the HFB approximation in the study of (finite) nuclei is ambivalent. On the one hand, there is the success of phenomenological applications of zero temperature HFB in the description of medium-to-heavy nuclei. The most sophisticated of these to date (DG 80), employing a realistic static effective interaction (a finite-range extension of the Skryme interaction), gives impressive agreement with a broad range of experimental data on ground state properties. On the other hand, aspects of HFB, in particular its prediction of phase transitions, cannot emerge from any <u>exact</u> description of a <u>microscopic</u> many-body system. The HFB approximation incorporates correlations by breaking symmetries of the Hamiltonian of the system. Such dynamical symmetry-breaking is admissible in the thermodynamic limit (La 66) - i.e. for systems in which the particle number $N \to \infty$, subject to the restriction that the particle density remains constant (and whatever other conditions are required to ensure the existence of this limit (Gi 77)). A consistent interpretation is possible in this case because of the presence of classical macroscopic observables (GDM 71). It is therefore not surprising that attempts to lend formal respectability to the broken-symmetry HFB solution in microscopic many-body systems, by identifying it as an intrinsic state, have encountered unresolved problems (VC 70). In the same vein, a rigorous statistical mechanics treatment ((Ho 49), section 12.1 of (Pa 71)) demonstrates that thermodynamic variables derived from a partition function can display singular behaviour only in the thermodynamic limit. (This result was originally proved for classical systems, but it is easily extended to quantum systems - section 15.1 of (Hu 63).) Thus a system has to be macroscopic for its physical variables to display characteristics observationally indistinguishable from singular behaviour. In turn, this means that phase transitions cannot strictly occur in finite nuclei, so that the phase transitions predicted by HFB when applied to a microscopic system can only be valid in a qualitative sense.

This chapter investigates the issue of these phase transitions, both at zero and at non-zero temperature. Consistent with the discussion in the preceding paragraph, it is possible for HFB to be exact in the thermodynamic limit (GF 78, RP 85). In effect, the validity of phase transitions predicted by HFB depends on the extent to which a finite microscopic system still possesses characteristics of the thermodynamic limit. (In what follows, phase transition found in the thermodynamic limit will often be referred to as "thermodynamic phase transitions" to distinguish them from the phase transitions in finite systems predicted by HFB.)

The phenomenological success of <u>zero temperature</u> HFB can be viewed as evidence that the phase transitions it predicts are qualitatively reliable. However, it gives no clue as to what formal mechanism is responsible for this - i.e. how it is that phase transitions found in the thermodynamic limit are already "felt" for finite particle number. Section 5.1 tries to establish what this mechanism is. It considers in detail how the exact solution for open-shell configurations of the Agassi model behaves in the vicinity of the superconducting-to-deformed-superconducting transition predicted by HFB. For the most part, values of N and Ω typical of the valence shells of rare-earth nuclei are chosen. It is shown that this behaviour is consistent with the conjecture that the phase transitions predicted by HFB signal the presence of singularities in the dependence of the exact solution on interaction strengths: in the generic case, these are branch point singularities. Implications of this important insight will be explored in chapter 6.

The state of affairs at finite temperature appears to be far less satisfactory. The behaviour of nuclei at finite temperature and very high spin has been an area of considerable theoretical interest recently (SEN 84). It is hoped that detailed properties of nuclei under these conditions will soon be made <u>experimentally</u> accessible by the new generation of "crystal ball" detectors at Berkeley and Daresbury (DS 84, BBH 85). Semi-realistic applications of thermal HFB indicate that, in nuclei, the neutron and proton pairing gaps (which are the conventional order parameters for superconductivity) decrease rapidly with increasing temperature T. Similarly, a variety of HFB calculations of differing levels of sophistication (BMR 73, MSR 76, GVS 76), indicate that pairing gaps in states along the yrast line decrease with increasing nuclear spin I, disappearing abruptly above some critical spin (Mottelson-Valatin effect (MV 60)). Typical results for both types of calculation are given by curves A and B in Figs. 5.1a and b respectively. Naïvely one would expect that, while the abruptness of the superconducting-to-normal phase transitions predicted is spurious, they are qualitatively valid. However, this is at odds with the results of more elaborate treatments (Go 84, ERI 85). Finite temperature HFB does not directly take into account the effects of thermal fluctuations. When these are included, the pairing gap is given by curve C in Fig. 5.1a instead of curve A: the pairing gap now decreases initially with temperature, but for larger T is essentially constant and non-negligible. Thermal HFB is not even qualitatively correct in this region. Equally evident is the discrepancy, in Fig. 5.1b, between the HFB and FHFB predictions at high nuclear spin. (FHFB employs essentially the same trial state as HFB, except that it is first projected onto the required symmetries and only then is the variational principle invoked. It is an improvement over HFB in that it self-consistently includes the "quantum fluctuations" which automatically restore, in any finite system, the symmetry broken by HFB.)

In section 5.2 the qualitative validity of phase transitions predicted by thermal HFB is reconsidered. This is in part motivated by what are felt to be certain weaknesses in the arguments employed in (Go 84, ERI 85). (A full discussion of these is given in section 5.2.) Equally persuasive is the belief that the singularities discussed in section 5.1 must continue to influence the dynamics of a system at finite temperature. Again, the Agassi model is employed. It is shown by considering the specific heat (as opposed to an order parameter like the pairing gap) that thermal HFB phase transitions are indeed visible within the system. However, the result is a subtle one, for, as will be seen, it is not in conflict with the numerical findings of (Go 84) and (ERI 85), but rather suggests a new interpretation of them.

Conditions under which the Agassi model is soluble analytically are discussed in the appendix to this chapter. These results are required in section 5.1.

SECTION 5.1: ZERO TEMPERATURE PHASE TRANSITIONS

A necessary prelude to a discussion of the mechanism whereby a finite system "feels" phase transitions is a demonstration of to what extent they manifest themselves. This requires the exact evaluation of properties of a finite system, and so the exactly soluble Agassi model is considered. (The subsequent discussion will show that the results obtained are not specific to this model.) The question of interest is not do different phases or regimes exist (as evidence of this has already been given in section 2.2), but is there a rapid change from the one to the other as suggested by HFB? Some of the early model studies of HF, BCS and HFB dealt with the reliability of these approximations (RR 64, Ag 68, BFS 69). However, they concentrated on the quantitative accuracy, considering of the various ground state properties only the energy. As demonstrated in section 3.4, the approximate ground state energy does not display any readily visible singular behaviour at a transition; so nothing more specific can be deduced from these studies than that these approximations are numerically inaccurate in the vicinity of the transitions they predict.

By contrast, other ground state expectation values within the HFB approximation in general change dramatically, in the region of phase boundaries. The behaviour of $\langle v|J_x^2|v\rangle$ at the superconducting-to-deformed-superconducting transition (depicted in Fig. 5.2a in this section) is a typical example. In line with the discussion in section, $\langle v|J_x^2|v\rangle$ is continuous at this transition but its first derivative (with respect to V) is discontinuous. More importantly, the magnitude of this discontinuity is large. Thus $\langle v|J_x^2|v\rangle$ changes abruptly and rapidly. Similar behaviour by expectation values of other quasi-spin operators is evident from Table 3. It is this which makes these expectation values, as opposed to the ground state energy, suitable quantities to study.

Within the Agassi model it is appropriate to consider first the expectation values of Y_+Y_- and J_x^2. There are two reasons for this, both of which hinge on the fact that the Agassi Hamiltonian can be written as

$$H = \varepsilon J_0 - V(J_x^2 - J_y^2) - g\, Y_+Y_- \qquad (2.12)$$

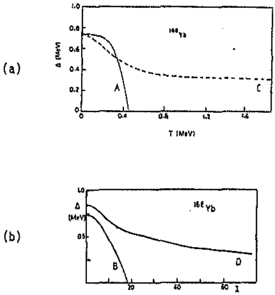

Fig. 5.1 Neutron pairing gaps as a function of temperature (part (a)) and nuclear spin (part (b)). Curves A and B are the results of HFB calculations, while curve C is obtained once thermal fluctuations are included and curve D is the outcome of a number-projected FHFB calculation. Further details are given in (ERI85) from which this figure has been adapted.

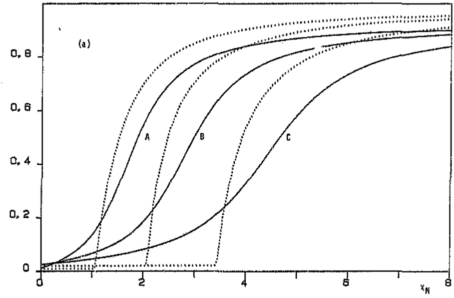

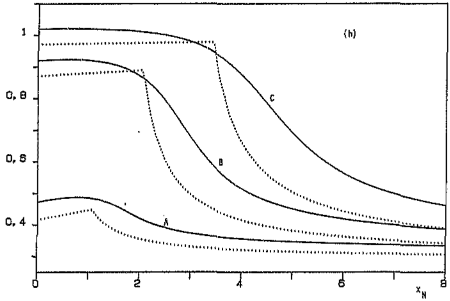

<u>Fig. 5.2</u> Ground state expectation values of J_x^2 (part (a)) and Y_+Y_- (part (b)) scaled as in Eq. (3.1), when $N = 14$, $\Omega = 20$. Curves A–C in each part are the exact expectation value for $\Sigma_N = 0.6, 2.0, 3.4$ respectively. The remaining curves are the approximate expectation values for the same values of Σ_N.

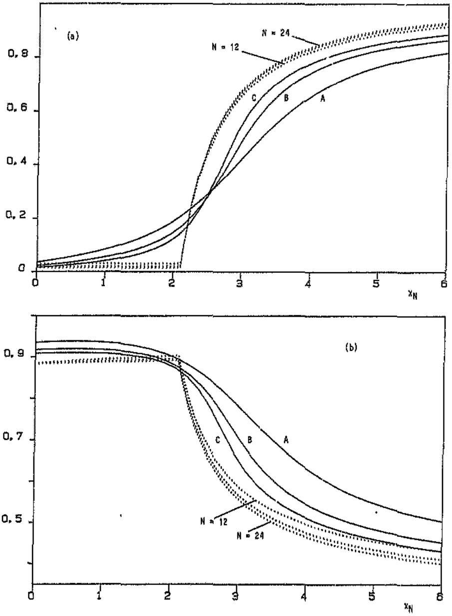

Fig. 5.3 As in Fig. 5.2 except vary N (not E_N); curves A – C are the exact expectation values for N = 12, 18, 24 respectively (E_N = 2.0, N/Ω = 0.6).

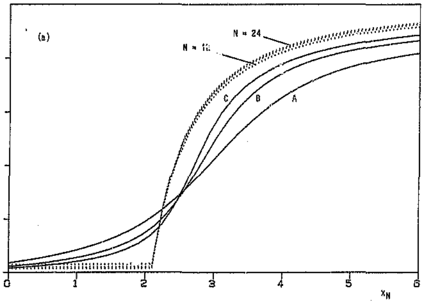

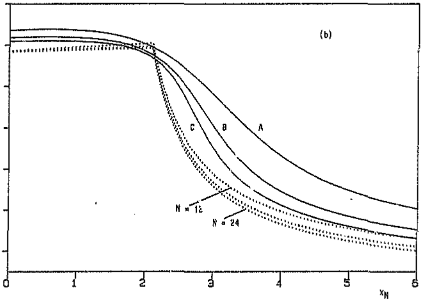

Fig. 5.3 As in Fig. 5.2 except vary N (not ε_N); curves A – C are the exact expectation values for N = 12, 18, 24 respectively (ε_N = 2.0, N/Ω = 0.6).

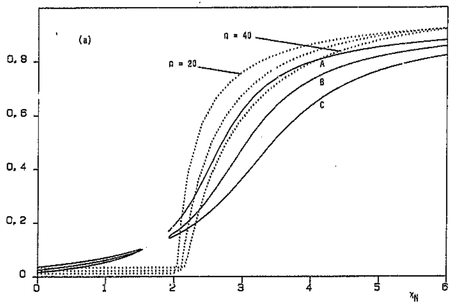

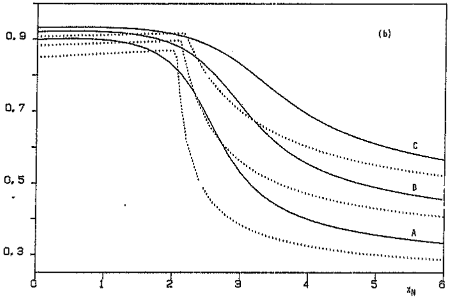

<u>Fig. 5.4</u> As in Fig. 5.2 except vary N/Ω; curves A–C are the exact expectation values for Ω = 20, 26, 40 respectively. (ε_N = 2.0, N = 16).

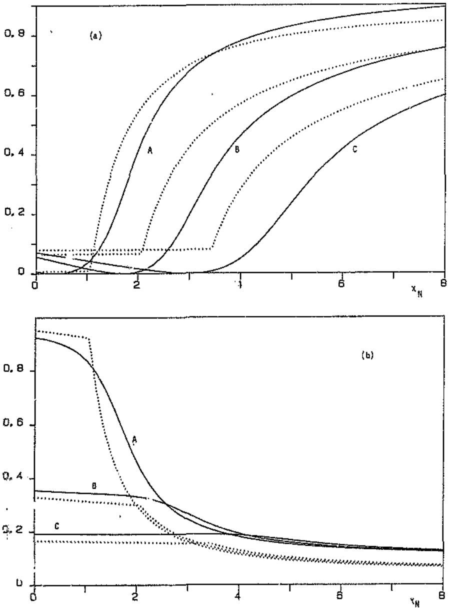

<u>Fig. 5.5</u> Ground state expectation values of M_+M_- (part (a)) and J_o^2 (part (b)) scaled by factors of $2/N(\delta + 1)$ and $4/N^2$ respectively. Other details as in Fig. 5.2.

It was demonstrated in chapter 2 that, as a result, the exact ground state expectation value $\langle 0|J_x^2|0\rangle$ increases with V, from approximately N/4 when V ≅ 0 (g ≅ 0) to of the order of $N^2/4$ as $V \to \infty$ (g fixed), but that, as $g \to \infty$ (V fixed), it becomes of approximately N/4 again. Similarly, it was shown that $\langle 0|Y_+Y_-|0\rangle$ increases with g and decreases with increasing V (cf. Fig. 2.4). Thus, like HFB, $\langle 0|J_x^2|0\rangle$ and $\langle 0|Y_+Y_-|0\rangle$ distinguish between the regimes of large g and V. In addition, the HFB approximation is geared to incorporate the effects of a two-body interaction in a fermion system. Hence the HFB ground state expectation values of 2-body operators which appear directly in the Hamiltonian should in most cases be better than those of any other two-body operators. In the present case, if $\langle 0|J_x^2|0\rangle$ and $\langle 0|Y_+Y_-|0\rangle$ do not follow the trends predicted by $\langle v|J_x^2|0\rangle$ and $\langle v|Y_+Y_-|v\rangle$, then no exact expectation value involving a two-body operator is likely to be qualitatively consistent with its HFB counterpart.

One is of course not restricted to the expectation values of only two-body quasi-spin operators. There are three one-body quasi-spin operators with non-zero expectation values, namely, N_+, N_- and J_o. Of these, just one has independent ground state expectation values (as $\langle 0|\hat{N}|0\rangle = \langle v|\hat{N}|v\rangle = N$). However, a result of section 2.2 is that $\langle 0|J_o|0\rangle$ and hence $\langle 0|N_+|0\rangle$ and $\langle 0|N_-|0\rangle$ do not change significantly between the regimes of large g (V fixed) and large V (g fixed). Thus consideration of these expectation values is also deferred until $\langle 0|J_x^2|0\rangle$ and $\langle 0|Y_+Y_-|0\rangle$ have been studied.

Figures 5.2-4 are graphs of $\langle 0|J_x^2|0\rangle$ and $\langle 0|Y_+Y_-|0\rangle$ in the region where HFB predicts the superconducting-to-deformed-superconducting transition ($N < \Omega$). For convenience, the actual quantities plotted are

$$4\,(\langle 0|J_x^2|0\rangle - N/4)/N^2 \quad \text{and} \quad 4\,\langle 0|Y_+Y_-|0\rangle/N\Omega(2 - N/\Omega). \qquad (5.1)$$

(This choice of scaling is suggested by the results of section 2.2.) Included for comparison are the HFB approximations to these expectation values. Since open-shell systems are considered, the variables χ_N and Σ_N are used instead of V and g (cf. Eq. (3.43).) In all of these figures, the dependence on χ_N is presented. However, all three of the independent variations of Σ_N, N and Ω are also considered. The different curves within a figure correspond to different values of Σ_N (N, Ω fixed) in Fig. 5.2, N (Σ_N, N/Ω fixed) in Fig. 5.3 and N/Ω (N, Σ_N fixed) in Fig. 5.4. Together, then, these figures represent a comprehensive overall survey of the behaviour of $\langle 0|J_x^2|0\rangle$ and $\langle 0|Y_+Y_-|0\rangle$.

The feature common to all the results for $\langle 0|J_x^2|0\rangle$ is that its increase from approximately N/4 to of the order of $N^2/4$, while smooth, is not extended uniformly throughout the interval $0 \leq \chi_N < \infty$. Rather, it occurs essentially in a single small interval. Moreover, this interval coincides approximately with the region just after the superconducting-to-deformed-superconducting transition in which $\langle v|J_x^2|v\rangle$ increases dramatically. Similar observations apply to $\langle 0|Y_+Y_-|0\rangle$: the decrease of $\langle 0|Y_+Y_-|0\rangle$ from its value when $\chi_N = 0$ to its value when $\chi_N \to \infty$, takes place in the same interval in which $\langle v|Y_+Y_-|v\rangle$ decreases rapidly. Thus the present comparison of ground state expectation values of J_x^2 and Y_+Y_- provides unambiguous evidence that the abruptness of the superconducting-to-deformed-superconducting phase transition has a counterpart within the exact solution.

Turning specifically to Fig. 5.2, one can gauge what influence the magnitude of Σ_N has. Two features emerge. For sufficiently small Σ_N (e.g. $\Sigma_N \approx 0.6$), the value of $\langle 0|Y_+Y_-|0\rangle$ when $\chi_N = 0$, is not significantly different from its value when χ_N is large (cf. curve A of Fig. 5.2b). Under these circumstances, it is not really possible to see any effect of the phase transition in the behaviour of $\langle 0|Y_+Y_-|0\rangle$. However, the same is not true of $\langle 0|J_x^2|0\rangle$ for these values of Σ_N (cf. curve A of Fig. 5.2a). This illustrates that any conclusions about phase transitions cannot rest on the behaviour of one expectation value alone; comparison of several expectation values is necessary. Figure 5.2a demonstrates that, as Σ_N becomes large, so the rate of change in $\langle 0|J_x^2|0\rangle$ in the region of the superconducting-to-deformed-superconducting transition decreases gradually. (Equivalently, the width of the interval over which its rate of change is significant becomes larger.) The same trend is seen in curves B and C of Fig. 5.2b. Significantly, HFB fails to reproduce this feature. Thus consideration of the rate of change of quantities calculated within HFB will not by itself indicate when one has escaped the transitional region.

In interpreting the significance of Fig. 5.3, it must be remembered that, as N and Ω are changed, the scale factors for both axes differ for the various curves. The variable χ_N is given by $\chi_N = (N - 0.2)V/\varepsilon$. If the scale for the Y-axis appropriate to curve A (N = 12) were used throughout, curves B and C of both Figs. 5.3a and b would have to be multiplied by factors of 9/4 and 4, respectively. Thus the scaling adopted hides the fact that as N increases $<0|J_x^2|0>$ and $<0|Y_+Y_-|0>$ change more sharply in the vicinity of the superconducting-to-deformed-superconducting transition: not only do the variations in magnitude become greater but they also occur over a smaller variation in the interaction strength V. Nonetheless, the scaling does have an advantage, for Fig. 5.3 shows that the quantities plotted converge to well-defined (finite) limits as N increases with N/Ω fixed. (In fact, it would seem that in the case of $4(<v|J_x^2|v> - N/4)/N^2$ this limit is already attained for $N \cong 20$.) Moreover, the exact results converge to the HFB results (which is true of other systems as well (FGN 79 and references therein, RP 85)).

From Fig. 5.4a, it is seen that the effect of changing N/Ω (N fixed) on the expectation value of J_x^2 is significant only in the transitional region. In this region, decreasing N/Ω causes the rate at which the expectation value changes to decrease. In contrast to Fig. 5.2, this is true of <u>both</u> the exact and the approximate ground state expectation values of J_x^2. The same behaviour in the transitional region is found in Fig. 5.4b. To understand this trend it is helpful to take into account the way in which the expectation values have been scaled. In fact, the expectation value of Y_+Y_- itself increases substantially with Ω or, in this case, as N/Ω decreases; this is consistent with the discussion of $<0|Y_+Y_-|0>$ in connection with Eq. (2.20). (The scaling in Fig. 5.4a is, on the other hand, essentially unaffected by changes in Ω.) As the expectation value of Y_+Y_- is a measure of the extent of pairing correlations, it follows that it is the competition between increased pairing correlations and monopole correlations which is responsible for the pattern in Figs. 5.4a and b.

The expectation values of other combinations of quasi-spin operators confirm that these findings are not fortuitous. The combinations S_+S_-, L_+L_- and L_+S_- can be ignored, since the behaviour of their expectation values in the limits of large V and g is determined by the expectation value of Y_+Y_- (cf. section 2.2.2). The remaining simple (but non-trivial) combinations are J_o, J_o^2, J_y^2 and M_+M_-. The expectation values of M_+M_- and J_o^2 are plotted in Fig. 5.5 as functions of χ_N for the same values of Σ_N, N and Ω as in Fig. 5.2. Like the expectation values of J_x^2 and Y_+Y_-, they behave near the transition point in a way which is qualitatively consistent with the predictions of HFB. This agreement is particularly significant in the case of M_+M_-, as it is not connected to the Agassi Hamiltonian in any way. If Σ_N is <u>large</u> (e.g. $\Sigma_N \gtrsim 3.4$) clearcut change in $<0|J_o^2|0>$ ceases to be visible; however, this behaviour is "forced" on $<0|J_o^2|0>$ since, from section 2.2.2, $<0|J_o^2|0>$ is O(N/4) when g is large and still O(N/4) when V is large. The expectation values $<0|J_o|0>$ and $<0|J_y^2|0>$ also vary rapidly, in general, with χ_N near the superconducting-to-deformed-superconducting transition, but like $<0|J_o^2|0>$ and indeed $<0|Y_+Y_-|0>$ (cf. curve A in Fig. 5.2b), there are certain choices of Σ_N and χ_N for which sharp changes cannot occur. When N and Ω are increased separately for these combinations of quasi-spin operators (as in Figs. 5.3 and 5.4), the patterns found for J_x^2 and Y_+Y_- persist.

If this study of exact ground state expectation values is repeated for the closed-shell system ($N = \Omega$), the findings are similar. Moreover, clear evidence of phase transitions is not restricted to ground state expectation values alone. They are also seen in exact transition matrix elements between the ground state and the excited states, which is illustrated in Fig. 6.5b for the deformed-to-superconducting transition in the $N = \Omega$ system.

Having discussed the behaviour of exact results, it is instructive to digress slightly by considering the agreement between the <u>approximate</u> and <u>exact</u> ground state properties depicted in Figs. 5.2 - 5.5. One sees that HFB scores two notable successes. Firstly, the superconducting-to-deformed-superconducting transition correctly signals the onset of the region in which the exact solution changes. Secondly, the changes in the approximate expectation values mirror those in the exact expectation values. At the same time, however, the phase diagrams deduced in chapter 3 are inadequate. For example, in the open-shell phase diagram, the single transition line can now be seen to mark the beginning of a transitional region and it should ideally be supplemented by a line marking the <u>end</u> of the <u>transitional</u> region. Studies of simpler or more reliable methods for predicting the critical interaction strength for a phase transition (BCP 81, BNP 82) are deficient in that they overlook this point. While it is possible to develop prescriptions for the second line which exploit the qualitative reliability of HFB expectation values, they are inevitably somewhat arbitrary; for example, one candidate is the locus of points at which the partial derivative of an HFB expectation value with respect to χ_N in the deformed-superconducting phase is some particular fraction of its maximum value.

A clue to a possible reason why phase transitions are visible in finite systems is provided by the excitation spectra. Consider the excitation spectrum for the closed-shell configuration of the Agassi model given in Fig. 2.2a. The regions of small and large Σ can be identified with the spherical and superconducting phases of Fig. 3.1, respectively. In fact, the arrow in Fig. 2.2a marks the location of the spherical-to-superconducting phase transition. Figure 2.2a demonstrates that the change from the pattern in the exact spectrum typical of small Σ to the pattern typical of large Σ is accomplished by a set of level repulsions found in the vicinity of this arrow. Similar observations hold for the excitation spectra in Figs. 2.2b and 2.5. (Again, the arrow in each of these diagrams indicates the location of a phase transition predicted by HFB.)

All these figures display the eigenvalues of an operator of the form

$$h(\lambda) = h_o + \lambda h_1, \tag{5.2}$$

where h_o, h_1 are hermitian and λ is a (single) variable interaction strength. The properties of this type of operator when λ is a complex variable are well-known (Ka 66, SW 73, Ku 81). The participation by two eigenvalues e_α and e_β of $h(\lambda)$ in a level repulsion for real values of λ, reflects the existence of an <u>exceptional</u> point $\lambda = \lambda_e$ in an adjacent portion of the complex λ-plane at which $e_\alpha = e_\beta$. In the generic case e_α and e_β are the two branches of a function with a 1^{st} order branch point at $\lambda = \lambda_e$ (SW 73). In the present case, exceptions to this can be ruled out because, by using the quasi-spin group, all symmetries of the Agassi model have been properly taken into account (cf. the discussion in section 3.3 of (SW 73)). Thus, for example, Fig. 2.2a implies that, when χ fixed and $\chi < 1$, the exact solution possesses branch point singularities in the interaction strength Σ for complex values with a modulus of approximately unity - i.e. in the region in which HFB predicts the spherical-to-superconducting phase transition. It is singularities of this type which have been conjectured to be responsible for sudden changes like those observed in Figs. 5.2 - 5.5 (GH 84a).

This observation can be further refined. The spectra in Figs. 2.2 and 2.5 contain several level repulsions. However, as the notion of a zero temperature phase transition refers specifically to the properties of the ground state, it is only the level repulsion involving the ground state which is relevant. These considerations can be cast into concrete terms [illegible] Suppose that one is dealing with a system characterise[illegible]action strengths λ_i, all of which are defined [illegible] at the Hamilt[illegible]s <u>physical</u> only when they are <u>real</u>, and that the g[illegible] state energy E_o is given by $E_o = f(\lambda_1, \ldots, \lambda_n)$, in which the dependence of E_o on other physical parameters (such as, the particle number) is suppressed. In line with the preceding discussion, the conjecture is that it is the [illegible] singularities in functions like

$$g(\lambda) = f(\lambda_1 = \lambda, \lambda_2 = c_2, \ldots, \lambda_n = c_n) \tag{5.3}$$

which are responsible for dramatic changes in the exact ground state when $\lambda_2 = c_2, \ldots, \lambda_n = c_n$, and λ_1 is varied (λ_1 real). Confirmation that the singularities in $g(z)$ affect the ground state wavefunction is seen in those few cases for which the exact many-body ground state wavefunction and energy are explicitly available. A non-trivial example found within the context of the Agassi model is discussed in the appendix to this chapter. In this example, $N = 4$ and $g_1 = 0$ (cf. the Hamiltonian in Eq. (2.12)): from Eq. (A5.1) the ground state energy is

$$\omega_1 = -2\sqrt{\varepsilon^2 + \left(1 - \frac{2}{\Omega}\right)\left(\frac{\Omega}{2}g_2 + V\right)^2 + 2\left(1 + \frac{1}{\Omega}\right)V^2}, \tag{5.4}$$

while from Eq. (A5.2) the ground state wavefunction is

$$v_- = \begin{bmatrix} \frac{1}{2} + \frac{\varepsilon}{\omega_o} \\ \frac{a}{\omega_o} \\ \frac{1}{2} - \frac{\varepsilon}{\omega_o} \\ \frac{b}{\omega_o} \end{bmatrix}.$$

As anticipated, the singularities in v_- are the same as those in ω_o.

Functions like $g(\lambda)$ in Eq. (5.3) are eigenvalues of operators of the form considered in Eq. (5.2). Thus these functions do not possess singularities at any real value of λ (SW 73). From instances where explicit expressions for E_0 are available (e.g. (LMG 65)), one can extrapolate that the number of singularities is O(D), where D is the dimension of the matrix which has to be diagonalised; in the present context, this means their number is at least O(N), N being the particle number. Further information about the way in which these singularities must behave for the conjecture stated in connection with Eq. (5.3) to be valid can be extracted, in the particular case of the Agassi model, from the patterns in Figs. 5.2-5.5. The fact that, when Σ_N is fixed and χ_N is varied, the character of the ground state changes only once suggests that the distribution of the singularities in the complex χ_N-plane is as in Fig. 5.6a rather than as in, for example, Fig. 5.6b. Figures 5.2 and 5.5 imply that as Σ_N is increased from its value in Fig. 5.6a, the point A moves to a point like B also depicted in Fig. 5.6a; similarly, Fig. 5.4 implies that, as N/Ω is decreased, A moves to a point like C. The changes with N are particularly interesting: Fig. 5.3 shows that the singularities must approach the real χ_N-axis - e.g. A moves to D. In addition, the number of singularities increases. It is conceivable that in the limit as $N \to \infty$, they form a set with an accumulation point (not in the set) on the real χ_N-axis. Under these conditions, the Agassi model would really experience a phase transition. The knowledge that HFB is exact in this limit for such systems, suggests that this is in fact what happens.

The discussion above illustrates how the singularities in functions like $g(\lambda)$ can be responsible for real phase transitions in any system. There are interesting parallels with the considerations of Yang and Lee on thermodynamic phase transitions at finite temperature (YL 52, section 15.2 of Hu 63). In a system characterized by temperature T and fugacity z, all other thermodynamic variables can be written in terms of

$$\Phi(z,T) = k_B T \,\ell n Q(z,T)$$

and its derivatives, where $Q(z,T)$ is the grand canonical partition function. The papers by Yang and Lee thus relate the singular behaviour of thermodynamic variables at some temperature to the distribution of zeros of $Q(z,T)$ in the complex z-plane. Much as with the singularities of $g(\lambda)$, none of the zeros of $Q(z,T)$ are located at physical values of z (i.e. $z > 0$), and a phase transition corresponds to a situation in which they form a set with an accumulation point on the positive real axis. It can even be argued that the two approaches are related: as $T \to 0$, the dominating contribution to $Q(z,T)$, because of the absence of thermal fluctuations, comes from the lowest energy state of the system containing strictly the desired number of particles N_0 - i.e.

$$\Phi(z,t) \to E_0\,(N_0) - \mu N_0,$$

where μ is the chemical potential. Hence, at $T = 0$, it is natural to study, instead of the distribution of zeros of $Q(z,T)$, the distribution of singularities in the ground state energy.

The preceding considerations are somewhat academic, but they acquire practical importance when one turns to the HFB approximation. They suggest that one can ascribe the following significance to HFB phase transitions, namely, that they locate singularities in the dependence on interaction strengths of the exact solution for the ground state. Do cases in which these singularities are available explicitly confirm this?

Consider the example introduced earlier in discussing the functions $g(\lambda)$ in Eq. (5.3) for which the exact ground state energy is explicitly available. If g_2 is fixed and real, ω_0 in Eq. (5.4) is singular at

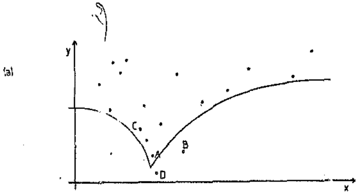

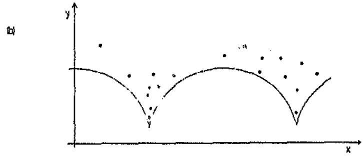

Fig. 5.6 Possible distributions of exceptional points involving the ground state eigenenergy in the complex χ_N-plane ($x = \mathrm{Re}(\chi_N)$, $y = \mathrm{Im}(\chi_N)$) for a given set of values of Σ_N, N and Ω (full dots). The patterns are symmetric about the x - axis, and the curves mark boundaries of regions enclosing this axis in which no exceptional points are found for the given values of Σ_N, N and Ω. The empty circles in part (a) denote the conjectured location of A for other values of Σ_N, N and Ω.

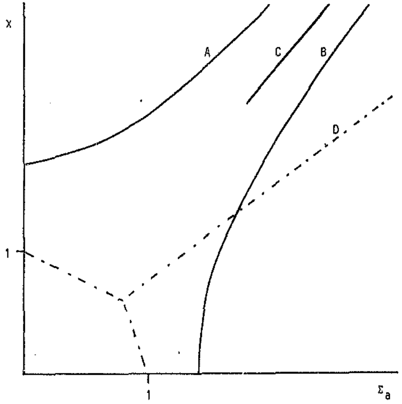

Fig. 5.7 Comparison of "exact" and approximate critical strengths. Curve C is the asymptote to curves A and B and is given by $\chi = (3/2)^{\frac{1}{2}}\ \Sigma_a$; curve D is given by $\chi = 3/4\ \Sigma_a$. See text for further details.

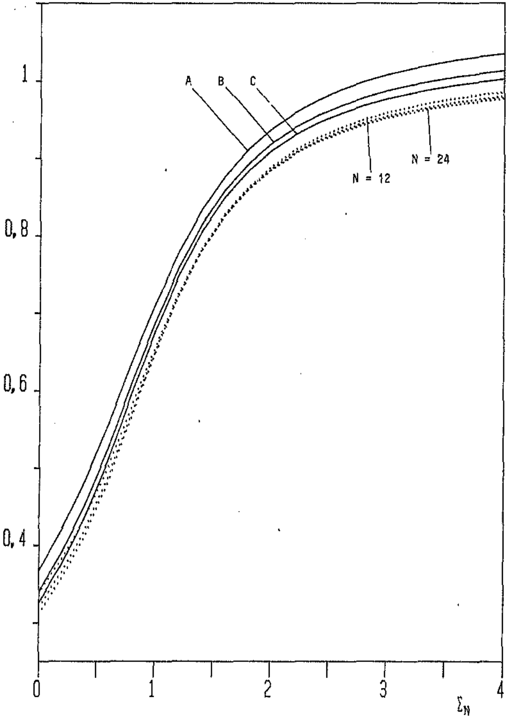

Fig. 5.8 Ground state expectation value of Y_+Y_- scaled as in Eq. (5.1), when $\chi_N = 0.4$, $N/\Omega = 0.6$; curves A-C are the exact expectation values for N = 12, 18, 24 respectively. The remaining curves are the corresponding BCS expectation values.

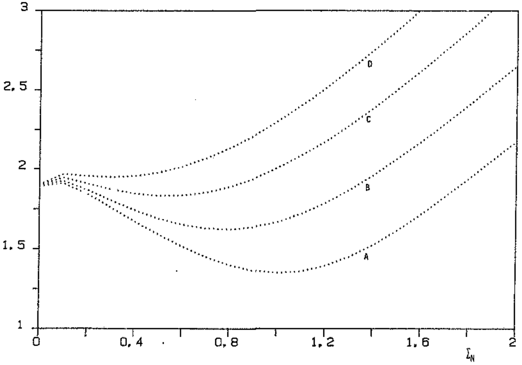

<u>Fig. 5.9</u> Excitation energy of lowest positive parity state when $N = 18$, $\chi_N = 0.4$. For curves A–D, $\Omega = 22$, 28, 40 and 66 respectively.

$$V_s = \frac{1}{3}\left\{ -\left(\frac{\Omega}{2} - 1\right)g_2 \pm \sqrt{3\varepsilon^2 + 2\left(1 + \frac{1}{\Omega}\right)\left(1 - \frac{2}{\Omega}\right)\left(\frac{\Omega}{2}g_2\right)^2}\, \right\} ,$$

and, if V is fixed and real, it is singular at

$$(g_2)_s = \frac{2}{\Omega}\left\{ - V \pm \sqrt{\left(\varepsilon^2 + 2\left(1 + \frac{1}{\Omega}\right)V^2\right) / \left(1 - \frac{2}{\Omega}\right)}\, \right\} .$$

Curves A and B in Fig. 5.7 are plots in the $\Sigma_a\chi$-plane ($\Sigma_a = (\Omega/2)(g_2/\varepsilon)$) of the magnitudes of V_s and $(g_2)_s$, respectively, for the closed-shell configuration ($N = \Omega = 4$). Superimposed on this is the HFB phase diagram appropriate when $g_1 = 0$ (cf. Eq. (3.26)). Although the boundaries do not coincide with curves A and B, there is an encouraging global correspondence between the two sets of curves. However, the same is not true when $N < \Omega$: the explicit example demonstrates that the class of singularities giving rise to curve B persists but, on the other hand, there is no corresponding phase boundary in the $N < \Omega$ diagram.

Figure 5.8 contains typical plots of $\langle 0|Y_+Y_-|0\rangle$ and $\langle v|Y_+Y_-|v\rangle$ when Σ_N is varied and χ_N (< 1) is fixed. (As in Figs. 5.2 – 5.4, these expectation values have been scaled by the factor $4/N\Omega\,(2 - N/\Omega)$). Both the exact and the approximate expectation values of Y_+Y_- increase sharply for $\Sigma_N \lesssim 1$ and remain essentially constant thereafter. The structure in $\langle 0|Y_+Y_-|0\rangle$ is reminiscent of that seen in $\langle 0|J_x^2|0\rangle$ in Figs. 5.3 – 5.5. However, as demonstrated by Fig. 5.8, the behaviour of $\langle 0|Y_+Y_-|0\rangle$ as $N \to \infty$ is different; it remains non-singular, implying that the Agassi model does not experience a phase transition. (In fact, Fig. 5.8 provides further evidence that HFB or, in this case, BCS is exact in the thermodynamic limit for systems like the Agassi model: $\langle 0|Y_+Y_-|0\rangle$ converges to $\langle v|Y_+Y_-|v\rangle$ in this limit.) Nevertheless, the rapid localised increase in $\langle 0|Y_+Y_-|0\rangle$ could signal the presence of singularities in the exact solution.

The plot in Fig. 5.9 of the energy (as a function of Σ_N) of the first excited positive parity state relative to the ground state for different values of N/Ω (N fixed, $\chi_N = 0.4$) is consistent with this. For $N/\Omega = 0.82$, a level of repulsion between these two states in the interval $0 < \Sigma_N < 1$ is clearly visible. The behaviour of the other energies in Fig. 5.9 is compatible with the interpretation that as N/Ω decreases the singularities associated with this repulsion remain, but that their location moves further the positive real Σ_N-axis. A similar trend in the χ_N-plane is implied by Fig. 5.4 (cf. the earlier discussion of Fig. 5.6). The fact that these singularities are not responsible for a phase transition as $N \to \infty$ simply suggests that they do not have an accumulation point on the positive real axis in this limit. (This does not exclude the possibility of an accumulation point elsewhere.)

The difference between the regimes of small Σ_N and large Σ_N is only that, in the former, pairing occurs essentially within the lowest level, whereas in the latter it occurs in all levels. Despite this, the progression from one regime to the other appears to be accompanied by singularities. Inspection of Fig. 5.8 shows that not only does BCS accommodate both regimes (which in itself is remarkable if singularities are present), but also that it rapidly changes precisely where the exact solution changes. Thus, combining the present findings with those obtained earlier (when Σ_N was fixed and χ_N was varied), one is led to a slight revision of the earlier conjecture concerning HFB: the self-consistent mean-field approximation possesses the remarkable property of being sensitive to singularities in the dependence on interaction strengths of the <u>exact</u> solution for the ground state of a <u>many-body</u> system. Furthermore, it would appear as if all of these singularities are responsible for localised changes in the exact ground state properties and some of them for phase transitions in the thermodynamic limit, while HFB attempts to reproduce these changes, and the "phase transitions" predicted by it in a finite system correspond to this latter class of singularities. (This property also allows one to distinguish between the two types of singularities).

This conjecture provides a formal reason for the qualitative validity of the phase transition predicted by HFB in a finite system. It also implies that the stability criterion employed in chapter 3 to deduce the HFB phase diagrams for the Agassi model is not as arbitrary as suggested in the literature (KÜ 79, BCD 81); the quasi-particle bases, which it identifies as physically appropriate, attempt to mimic the relevant features in the exact solution, i.e. the singularities discussed in this section.

SECTION 5.2: FINITE TEMPERATURE PHASE TRANSITIONS

In one of the earliest papers (Mo 72) dealing with the effect of temperature on the mean-field description of a nucleus, it was pointed out that in any consistent (statistical mechanics) treatment of a nucleus which is supposed to be at some non-zero temperature, one should consider, in addition to the equilibrium values of observables, the thermal fluctuations about these values. These can be significant in a finite system and are not directly catered for by the mean-field approximation which gives only the most probable value of an observable (Go 84). Thus the qualitative reliability of zero temperature HFB does not immediately imply that the transitions predicted by thermal HFB are also qualitatively valid. In fact, a variety of studies (Mo 73, Go 84, ERI 85), some of which were discussed in the introduction to this chapter, seem to have shown that thermal fluctuations wash out any sign of phase transitions at finite temperature in finite systems.

On the other hand, the thermal HFB study in chapter 4 indicates the limit $T \to 0$ can be continuous. Furthermore, the singularities present in the exact solution for the eigenvalues of a system which were discussed in the previous section, persist at finite temperature. It is difficult, then, to see how an infinitesimal, non-zero temperature can substantially alter the situation from the zero temperature ca· Rather, one would expect phase transitions to remain visible below some finite (but perhaps small) temperature. In fact, the studies referred to earlier do not exclude this possibility. All considerations in (Mo 73) and (Go 84) are based on the Landau theory description of thermal fluctuations (Th 83), which does not hold for temperatures $T \to 0$. In addition, the exact model study in (ERI 85) deals with a phase transition which has no analogue at $T = 0$.

The obvious way to resolve these doubts is to determine the thermal fluctuations around an exact ensemble average. A particularly appropriate choice is the ensemble average of the Hamiltonian H, for it can be shown, quite generally (p. 70 of (Pa 71)), that the specific heat C_V (in units of k_B) is given by

$$C_V = \frac{1}{(k_B T)^2} \left(\langle H^2 \rangle - \langle H \rangle^2 \right)$$

where <> denotes the canonical ensemble average. Since C_V vanishes in the limit $T \to 0$, it is a direct measure of extent of thermal fluctuations in <H>. More importantly, the behaviour of C_V in thermodynamic phase transitions is very distinctive: it diverges. Such singular behaviour is not possible in a small finite system but the appearance of a smooth peak in C_V would be evidence of a "phase transition" (Wa 72, FF 69). (Recall that the thermal HFB calculation in chapter 4 predicts a peak-like structure in C_V.) Thus, by calculating C_V one can simultaneously extract information about the magnitude of fluctuations and the extent to which phase transitions occur in small finite systems (at $T \neq 0$).

In this section, the behaviour of C_V is studied for closed-shell configurations of the Agassi model. Figure 5.10 contains typical plots of C_V at different fixed temperatures when $\chi = 0.5$ and Σ is varied ($N = \Omega = 20$). The ensemble over which the average has been performed has been restricted to the collective subspace because only the structure in C_V is of interest, and it is determined by this subspace. Two arguments can be presented in support of this contention. The energies of the states omitted change less with interaction strengths than those of states in the collective subspace. In particular, the energies of these states decrease more slowly with increasing interaction strengths than the energy of the ground state. Thus in the regime of large interaction strengths the contribution of these states to the ensemble average is numerically negligible. The difference in the dependence on interaction strengths is, in fact, a consequence of the singularities discussed in detail in the previous section; these only affect states in the collective subspace.

The second argument exploits the presence of these singularities in a more direct way. In the limit as $T \to 0$, contributions to C_V from the lowest-lying excited states dominate, and for T small enough,

$$C_V \approx g\,\beta(\Delta E)^2\, e^{-\beta\Delta E}, \qquad (5.5)$$

where $\beta = 1/k_B T$ and ΔE is the energy of the g-fold degenerate lowest excited level relative to the ground state. The spectrum of the Agassi model when Σ is varied and $\chi = 0.5$ is given in Fig. 2.2a. The essential features of the lowest-lying excited states can be mimicked by supposing there is a single doubly degenerate level with excitation energy

$$\frac{\Delta E}{2\varepsilon} = a(\Sigma - \Sigma_c)^2 + b, \tag{5.6}$$

where a and b are appropriately chosen (dimensionless) constants and Σ_c marks the location of the level of repulsion seen in Fig. 2.2a. Equations (5.5) and (5.6) imply that C_V has the following structure (if regarded as a function of Σ):

1) when τ ($\sim k_BT/\varepsilon$) $< b$, C_V has a single maximum at $\Sigma = \Sigma_c$;
2) when $\tau > b$, C_V has three stationary points - minimum at $\Sigma = \Sigma_c$ and maxima at

$$\Sigma = \Sigma_\pm = \Sigma_c \pm \sqrt{(\tau - b)/a}. \tag{5.7}$$

Features of these results like the precise value of τ at which the bifurcation occurs and the square root appearing in Eq. (5.7), should not be taken seriously, since they depend on the details of the parametrization in Eq. (5.6). Also, the symmetry of the two maxima at $\Sigma = \Sigma_\pm$ is spurious. For convenience, ΔE in Eq. (5.6) has been chosen to be symmetric about $\Sigma = \Sigma_c$. If a more realistic parametrization is used, the peak at $\Sigma = \Sigma_-$ disappears; instead, C_V decreases (slowly) as $\Sigma \to \Sigma_c$. Nevertheless, Eq. (5.6) serves to show in a simple way essentially what is the structure in C_V implied by the level repulsion in Fig. 2.2a.

A remarkable finding is that the changes seen in Fig. 5.10 as the temperature increases are in accord with this pattern, even when the temperature is not small. At the lowest temperature considered in Fig. 5.10 a peak is clearly visible. With a slight increase in temperature it disappears. However, the new shape of C_V could quite conceivably be the sum of two overlapping and unresolved maxima in line with the approximate analysis of the previous paragraph. The appearance of the shoulder in C_V at a still higher temperature ($\tau \cong 0.5$) confirms this. The approximate analysis correctly predicts that these two maxima appear only above a certain temperature (i.e. the bifurcation temperature $\tau_b \cong b$), and that the one maximum becomes clearly resolved from the other and its location moves to larger Σ when the temperature is further

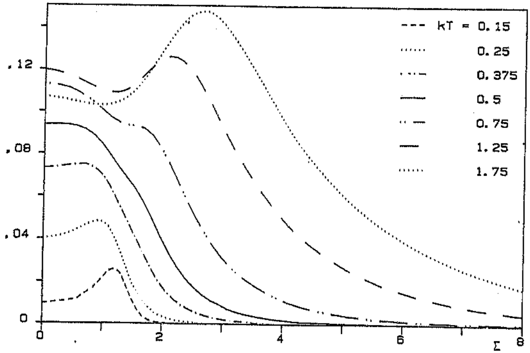

Fig. 5.10 C_V/Ω (in units of k_B) when $N = \Omega = 20$, $\chi = 0.4$.

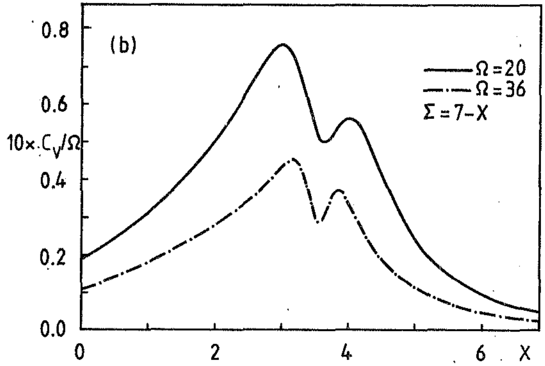

Fig. 5.11 C_V/Ω (in units of k_B) for different interaction strengths when τ = 1.5.

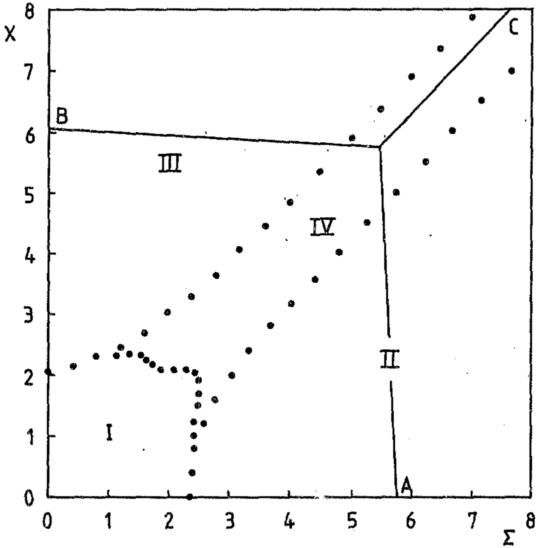

Fig. 5.12 Approximate and "exact" phase diagrams for the Agassi model when $N = \Omega = 20$, $\tau = 1.5$. Curves A-C are the spherical - to - superconducting, spherical - to - deformed and superconducting - to - deformed transition lines respectively in the approximate (i.e. thermal HFB) phase diagram.

increased. This agreement indicates that even the inclusion of other states within the collective subspace in the ensemble average, let alone states outside the collective subspace, does not significantly alter the gross structure of C_V. It also suggests that the structure of C_V is a consequence of the singularities in the exact solution discussed in section 5.1. (Earlier, in section 5.1, the Yang-Lee theory of phase transitions, which also deals with the relationship between singularities and phase transitions, was referred to. To demonstrate the role of the singularities discussed in section 5.1, it is necessary to vary interaction strengths. On the other hand, Yang-Lee Theory is is designed for a situation in which temperature and particle number and not interaction strengths are varied. Hence it will not be considered here.)

One of the maxima found above τ_b corresponds to the peak found below this temperature, and the other to a pronounced increase in thermal fluctuations in the region $\Sigma < \Sigma_c$. Thus the peak seen at the lowest temperatures persists throughout; it simply is not visible for temperatures close to τ_b. The fact that, in this range of temperatures, the magnitudes of C_V for $\Sigma \to 0$ and for $\Sigma \approx \Sigma_c$ become <u>suddenly</u> comparable suggests a change in the properties of the system for $\Sigma < \Sigma_c$. Thermal fluctuations for these interaction strengths are now important, and remain important at higher temperatures. The significance of the change will be returned to later. First it is appropriate to consider the behaviour of C_V for a temperature at which peak structure is clearly visible, and see whether it can be consistently interpreted as the remnant of a phase transition in the thermodynamic limit.

A suitable temperature is $\tau = 1.5$ (cf. Fig. 5.10). In fact, the peak structure of C_V at this temperature is non-trivial. For example, when both Σ and χ are changed, with $\Sigma + \chi = c$ (c some constant) as in Fig. 5.11, one finds that C_V has not one but two peaks. Clarity is gained by plotting the loci in the $\Sigma\chi$-plane of all the peaks in C_V, which is done in Fig. 5.12: the dots in this diagram indicate these loci when $\Omega = 20$ and, for comparison, the phase boundaries predicted by HFB at this temperature (curves A, B and C) have also been included. The peak structure in C_V divides the $\Sigma\chi$-plane into four regions (labelled I to IV in Fig. 5.12). Clearly, regions I, II and III are to be identified with the spherical, superconducting and deformed phases, respectively. Region IV can be associated with a deformed-superconducting or hybrid phase which is not actually predicted by thermal HFB. It is essentially a transitional region linking the superconducting and deformed regions, for, as Ω increases (or the thermodynamic limit is approached), the width of this region decreases - cf. Fig. 5.11. (Recall that, from section 5.1, phase transitions amount in finite systems to transitional regions.) With this in mind, it is possible to associate the peaks in C_V with transitions found in the thermodynamic limit. In turn, this means the phase transitions predicted by thermal HFB are relevant in finite systems. It is even possible to deduce an "exact" phase diagram (i.e. Fig. 5.12). These findings continue to apply at other temperatures. (With the insight afforded by the approximate analysis earlier, it is possible to "guess" the positions of the peaks even when they are not clearly visible.)

Comparison of the exact and approximate phase diagrams in Fig. 5.12 shows that in its gross structure the approximate phase diagram is correct. Further, the location of the approximate superconducting-to-deformed transition is essentially correct. However, the size of the approximate spherical phase at this temperature is grossly overestimated. In fact, it is only for $\tau \leq \tau_b$ that the agreement between the approximate and the exact phase diagrams can be considered everywhere reasonable. (Recalling the significance of τ_b, one sees that, as one might have expected, it is the presence of thermal fluctuations which is responsible for this failure of thermal HFB.) It must therefore be concluded that, in general, thermal HFB does not reliably predict critical interaction strengths or, equivalently, critical temperatures.

This result is not incompatible with the demonstration that thermal HFB is exact in the thermodynamic limit. In (AZ 84) various mean-field approximations differing only by terms of $O(1/N)$ are considered. As these predict very different critical temperatures, one can infer that the critical temperatures and strengths depend sensitively on terms of $O(1/N)$ (which, of course, vanish in the thermodynamic limit).

A remarkable pattern is evident in the magnitude of fluctuations in the regions away from phase boundaries. Fluctuations are always negligible in the superconducting and deformed regions (cf. Fig. 5.11). However, as observed earlier in connection with Fig. 5.10, they can be significant in the spherical region Note that these findings hold when the temperature is fixed and it is interaction strengths which are varied. (Thus the inclusion of more states in the ensemble average does not affect them.)

This difference between the spherical (or, more generally, disordered) phase and the deformed and superconducting (or ordered) phases is very important. It helps to explain why, in the model study of (RP 85), the convergence of the exact grand potential to its thermodynamic limit, as particle number was increased, was slowest in the spherical phase. (A similar trend can be seen in Fig. 1 of (FGN 79).) It also has implications for order-to-disorder transitions (e.g. spherical-to-superconducting).

When thermal fluctuations are significant, the <u>average</u> value of any particular parameter can be quite different from that predicted by the HFB approximation. In particular, order parameters like the pairing gap - which within the mean-field description are automatically zero in the spherical phase - could in a more elaborate treatment be significantly different from zero. Exactly this effect is seen in the results of (Go 84) and (ERI 85). Taken in isolation, it implies that the transitions from spherical-to-deformed and spherical-to-superconducting are washed out. So the results of the present study are compatible with those of (Go 84) and (ERI 85). However, it indicates that a different (and pragmatically advantageous) viewpoint should be adopted: the transitions do occur, but they correspond in general to a progression from a region in which a static self-consistent mean-field by itself is useful to a region in which it is not.

In view of this, the failure of HFB (under the same circumstances) to reproduce this transition point reliably is a serious flaw. A simple remedy would seem to be to calculate (within thermal HFB) the variance in any thermal HFB ensemble average of interest, with the understanding that only if this is large, are more elaborate methods (such as those suggested in, for example, (AZ 84)) indicated.

APPENDIX 5

An interesting feature of the LMG model is that, although no convenient basis which diagonalises the Hamiltonian exists, the eigenenergies can be solved for analytically even when the particle number is as large as $N(=\Omega) = 8$ (LMG 65). In the Agassi model this can only be done in trivial cases for which the matrices involved are at most 2 x 2 - i.e. for positive parity states when $N = 2$, and negative parity states when $N = 4$ (cf. Table 2.1). However, if $g_1 = 0$, 4 x 4 Hamiltonian matrices, which determine the positive (negative) parity states when $N = 4(6)$, can also be treated analytically. (Recall that the interaction with strength g_1 is automatically diagonalised by the basis $|m,z\rangle$.)

Using Eqs. (2.7), (2.9) and (2.10), one deduces that the form of these 4 x 4 matrices is

$$h = \begin{bmatrix} -2\varepsilon & -a & 0 & -b \\ -a & 0 & -a & 0 \\ 0 & -a & 2\varepsilon & -b \\ -b & 0 & -b & 0 \end{bmatrix} ,$$

where a and b are given in Table A5. Explicit calculation shows that the secular equation $\det(\omega I - h) = 0$ is fortuitously quadratic in ω^2, being

$$\omega^2 \left(\omega^2 - 4\varepsilon^2 - 2(a^2 + b^2)\right) = 0.$$

Hence the eigenenergies of h are

$$E = 0 \text{ (twice)}, \pm \omega_o , \tag{A5.1a}$$

where

$$\omega_o = +\sqrt{4\varepsilon^2 + 2(a^2 + b^2)} . \tag{A5.1b}$$

The corresponding orthonormal eigenvectors are

$$v_{\pm} = \begin{bmatrix} \frac{1}{2} \mp \frac{\varepsilon}{\omega_0} \\ \mp \frac{a}{\omega_0} \\ \frac{1}{2} \pm \frac{\varepsilon}{\omega_0} \\ \mp \frac{b}{\omega_0} \end{bmatrix}, \quad v_1 = \frac{1}{\sqrt{2}\,\omega_1} \begin{bmatrix} -a \\ 2\varepsilon \\ a \\ 0 \end{bmatrix}, \quad v_2 = \frac{\sqrt{2}}{\omega_1 \omega_0} \begin{bmatrix} -b\varepsilon \\ -ab \\ b\varepsilon \\ \omega_1^2 \end{bmatrix} \tag{A5.2}$$

where

$$\omega_1 = \underset{+}{\sqrt{2\varepsilon^2 + a^2}}$$

and, as the notation suggests, $v_{\pm}$ has the eigenenergy $\pm\omega_0$; the degenerate eigenvectors v_1 and v_2 have been chosen so that, when $b = 0$ (i.e. $V = 0$), they coincide with members of the natural set of orthonormal eigenvectors in this limit. When g_1 is non-zero, first order perturbation theory indicates that the degeneracy of these two eigenvectors is lifted.

Quite apart from the interesting singularities exhibited, these results provide useful checks of numerical results.

TABLE A.5: ENTRIES IN h

Entry	N = 4	N = 6
a	$2\sqrt{\left(1 - \frac{2}{\Omega}\right)}\left(\frac{\Omega}{2}g_2 + V\right)$	$2\left(1 - \frac{2}{\Omega - 2}\right)\left(\left(\frac{\Omega}{2} - 1\right)g_2 + 3V\right)$
b	$2\sqrt{\left(1 + \frac{1}{\Omega}\right)}V$	$2\sqrt{3\left(1 + \frac{3}{\Omega - 2}\right)}V$

When N = 4, h is the positive parity submatrix, and when N = 6, h is the negative parity submatrix.

CHAPTER SIX

THE RANDOM-PHASE APPROXIMATION IN SELF-CONSISTENT BASES

In the previous chapter the conjecture was put forward that sudden changes in the character of the HFB solution for the ground state, including, in particular, the appearance of broken-symmetry solutions, mimic the presence of algebraic singularities in the dependence on interaction strengths of the exact solution. (In what follows, this will, for convenience, be termed the "singularity" conjecture.) If this is so, then despite the well-known disadvantages of broken-symmetry bases (cf. introduction to chapter 5), approximation schemes employing self-consistent (broken-symmetry) bases in the description of excited states ought to be at least qualitatively successful. In this chapter, this claim will be substantiated by considering the results of random-phase approximation calculations within the self-consistent bases appropriate to the Agassi model.

The random-phase approximation (RPA) is selected [illegible] its simplicity. Within the context of certain systematic [illegible]nsion treatments, it can be viewed as the lowest order correct[illegible]o the independent quasi-particle description of excited states (Ma 74). It is also intimately related to the <u>self-consistent</u> mean-field approximation: RPA in an HFB basis yields the normal modes for the description of small amplitude oscillations on the HFB energy surface about the stationary point to which the basis corresponds (Section 6.5 of (BV 78)).

In section 6.1 there is a discussion of properties of RPA in self-consistent bases. Its purpose is to prepare for the application of RPA to the Agassi model in section 6.2, and so it is essentially a summary of material appealed to in this section. Section 6.2 itself is divided into two subsections: formal aspects of the application of RPA are presented in section 6.2.1; in section 6.2.2, RPA results are compared with both energies and suitable matrix elements of the exact solution, and conclusions emerging from this comparison are discussed. Technical material required in section 6.2 is relegated to two appendices.

SECTION 6.1: FEATURES OF RPA WITHIN A SELF-CONSISTENT BASIS

Within an independent quasi-particle description, the simplest excitations of an even system are the two quasi-particle states $\beta_i^\dagger\beta_j^\dagger|v\rangle$. The random-phase approximation also describes excitations of essentially two quasi-particle character except it allows for the possibility that the ground state differs from the quasi-particle vacuum $|v\rangle$. Whereas $\beta_i|v\rangle \equiv 0$, the RPA ground state $|r\rangle$ can be such that $\beta_i|r\rangle \neq 0$. One of the advantages of RPA is that it permits one to calculate properties of excited states $|a\rangle$ without requiring explicit knowledge of $|r\rangle$ (which may be very complicated.) It starts from the assumption that

$$|a\rangle = \sum_{i<j} (X_{ij}^a \beta_i^\dagger \beta_j^\dagger - Y_{ij}^a \beta_j\beta_i)|r\rangle = Q_a^\dagger|r\rangle, \tag{6.1}$$

and proceeds to determine $Q_a^\dagger$ (approximately). Thus RPA yields information about $|a\rangle$ relative to the ground state, namely:

(1) the excitation energy E_a with respect to $|r\rangle$;

(2) transition matrix elements

$$X_{ij}^a = \langle r|\beta_j\beta_i|a\rangle \text{ and } Y_{ij}^a = \langle r|\beta_i^\dagger\beta_j^\dagger|a\rangle. \tag{6.2}$$

These are obtained by solving the RPA eigenvalue problem (Ba 60)

$$\begin{pmatrix} A & B \\ B^* & A^* \end{pmatrix} \begin{pmatrix} X \\ Y \end{pmatrix} = E \begin{pmatrix} X \\ -Y \end{pmatrix}, \tag{6.3a}$$

where X/Y are the column vectors with components X_{ij}/Y_{ij} $(i < j)$ and A and B are hermitian and symmetric matrices respectively, with matrix elements $(i < j,\ k < l)$

$$\begin{aligned} A_{ij,kl} &= \langle v|\left(\beta_j\beta_i, (H', \beta_k^\dagger\beta_l^\dagger)\right)|v\rangle \\ B_{ij,kl} &= \langle v|\left(\beta_j\beta_i, (H', \beta_k\beta_l)\right)|v\rangle, \end{aligned} \tag{6.3b}$$

in which H' is the "Hamiltonian" operator used in determining the quasi-particle basis; in this work, $H' = H - \mu\hat{N}$ (cf. the discussion following Eq. (3.3)).

The positive eigenergies E of . (6.3a) are the excitation energies E_a, and the components of the corresponding eigenvectors, the transition matrix elements in Eq. (6.2). Within RPA, the excitations are (non-interacting) harmonic vibrations about the quasi-particle vacuum configuration (cf. introduction to this chapter).

If particle number is conserved, then Eq. (6.3a) decouples into the (separate) ph- and pp- RPA equations (Section 8.9 of (RS 80)). The structure of the ph- RPA equations is the same as that of Eq. (6.3a). (This is not true, in general, of the pp- RPA equations.) Thus several properties of solutions to the ph- RPA equations (Th 61), e.g. the fact that for each eigenvector with eigenvalue E ($\neq 0$), there is an eigenvector with eigenvalue $-E^*$, and the orthonormalisation condition for solutions with real non-zero eigenvalues

$$\sum_{i<j} (X_{ij}^{a*} X_{ij}^{b} - Y_{ij}^{a*} Y_{ij}^{b}) = \mathrm{sgn}\,(E_a)\,\delta_{ab}, \tag{6.4}$$

apply also to solutions of Eq. (6.3).

For simplicity, the anti-symmetrised matrix elements $\bar{v}_{ijkl}$ of the interaction in the bare basis and the coefficients in the quasi-particle transformation (Eq. (3.3)) will henceforth be assumed to be real-valued. Under these conditions, A and B are real matrices and, substituting H' expressed in terms of normally-ordered products of the operators $\beta_i^\dagger, \beta_i$ into Eq. (6.3b), one finds that they have matrix elements

$$A_{12,34} = (E_1 + E_2)\delta_{13}\delta_{24} + A^{i}_{12,34} \tag{6.5a}$$

with

$$\begin{aligned} A^{i}_{12,34} = \sum_{5678} \bar{v}_{5678}((U_{51}V_{82}V_{63}U_{74} - (1 \leftrightarrow 2) - (3 \leftrightarrow 4) \\ + U_{51}U_{62}U_{73}U_{84} + V_{71}V_{82}V_{53}V_{64}) \end{aligned} \tag{6.5b}$$

and

$$B_{12,34} = \sum_{5678} \bar{v}_{5678} \left((U_{51}U_{62}V_{83}V_{74} + U_{53}U_{64}V_{81}V_{72}) \right. \tag{6.5c}$$

$$\left. - (1 \leftrightarrow 3) - (1 \leftrightarrow 4) \right),$$

where E_1 and E_2 are quasi-particle energies.

A feature of RPA is its lack of internal consistency. Any derivation of Eq. (6.3) presupposes $|r\rangle$ and $|v\rangle$ are not significantly different - i.e. the coefficients Y_{ij} are small in comparison to the coefficients X_{ij}. It is for this reason that $|v\rangle$ appears in Eq. (6.3b). (Another consequence is that the identity $|a\rangle = Q_a^{\dagger}|r\rangle$ is lost - cf. section 2 of (LM 80).) The actual solution of Eq. (6.3) may not conform with this assumption. Thus an RPA calculation is not a priori meaningful.

The eigenvalue problem in Eq. (6.3a) is not explicitly hermitian and so its eigenvalues are not necessarily real-valued. Provided, however, a self-consistent basis is employed, it is possible to state precisely when complex eigenvalues occur (OS 83); moreover, information about the appropriate mean-field can be extracted (Th 61).

Suppose one is dealing with a self-consistent basis which does not break any symmetries. Then, if this basis is stable (in the sense of section 3.1), the matrix

$$S = \begin{pmatrix} A_{ph} & B_{ph} \\ B_{ph} & A_{ph} \end{pmatrix}$$

appearing in the ph- RPA equations appropriate to this basis, is positive definite (Th 61). This means that a Cholesky decomposition of S exists - i.e. S can be written as $S = L^T L$, where L is a non-singular upper triangular matrix (Chapter 4 of (Wi 65)). The ph- RPA equations can be recast into the real symmetric eigenvalue problem

$$L \begin{pmatrix} 1 & 0 \\ 0 & -1 \end{pmatrix} L^T \begin{pmatrix} \tilde{X} \\ \tilde{Y} \end{pmatrix} = \begin{pmatrix} \tilde{X} \\ \tilde{Y} \end{pmatrix}, \tag{6.6}$$

in which

$$\begin{pmatrix}\tilde{X}\\ \tilde{Y}\end{pmatrix} = c^{-\frac{1}{2}} \; L\begin{pmatrix}X\\ Y\end{pmatrix},$$

where c is some constant. Hence, as long as the basis is stable, all the ph- RPA eigenvalues must be real and, in fact, non-zero. (The determinant of the matrix on the left-hand side of Eq. (6.6) is non-zero.)

What happens if an eigenvalue e_s of S tends to zero as an interaction strength $\lambda \to \lambda_c^-$, and, for $\lambda > \lambda_c$, is negative? Such behaviour means that the quasi-particle vacuum $|v\rangle$ for the basis is not stable for $\lambda > \lambda_c$ and indicates the existence of a new stable quasi-particle vacuum $|v'\rangle$ (with which is associated a new quasi-particle basis), which supplants $|v\rangle$. It also implies that a pair of ph- RPA eigenvalues tend to zero as $\lambda \to \lambda_c^-$, and that, for $\lambda > \lambda_c$, they become complex (Th 61). Thus, complex ph- RPA eigenvalues are found when the basis is unstable. Appealing to Thouless's theorem (Th 60, Ma 75), one can relate $|v'\rangle$ to $|v\rangle$ by an expression of the form

$$|v'\rangle = n \exp\,(\sum_{i<j} Z_{ij}\, \beta_i^\dagger\, \beta_j^\dagger)\; |v\rangle, \tag{6.7}$$

where n is a normalisation constant, and $\beta_i^\dagger$ is an "old" quasi-particle operator corresponding to $|v\rangle$. New correlations are present in $|v'\rangle$ and their character is indicated by the coefficients Z_{ij} in Eq. (6.7). When $\lambda = \lambda_c$, these coefficients coincide with the amplitudes X_{ij} of the soft RPA mode, whose energy $E \to 0^+$ as $\lambda \to \lambda_c^-$ (BB 76). So, the soft mode and the new stable ground state are related: it must contain the correlations that are excited in the old ground state by the soft mode.

The stability of the basis is no longer a guarantee that a Cholesky decomposition of the matrix in the RPA equations exists if one adopts a broken-symmetry basis which is subject to constraints (OS 83) or considers the pp-RPA equations (LM 80). In the case of broken-symmetry bases, the discussion is further complicated by the presence, in general, of "spurious" modes: these have eigenenergies which are identically zero throughout the broken-symmetry phase (TV 62). They reflect the existence of "spurious" states which can be generated by acting on the vacuum state with the operator which maps the quasi-particle Hilbert space onto itself, under transformations of the system corresponding to a broken symmetry. (RPA has thus the ability, unlike, notably, the Tamm-Dancoff approximation (TDA), to distinguish these states from vibrational excitations of the system.) After a technically more elaborate discussion (LM 80, OS 83), one again finds the same relationship between the reality of RPA eigenenergies and the stability of the basis employed, and between the vibrational modes whose energies become complex (when this basis becomes unstable) and the new stable quasi-particle vacuum.

The decrease to zero of the energy of a vibrational mode is undesirable in that, in general, it will no longer be a good approximation to any excited state. (As the energy tends to zero, $|Y_{ij}| + |X_{ij}|$.) However, because this behaviour occurs when a basis becomes unstable, it can be used to predict changes in the mean-field. There are several many-body systems in which a mean-field is readily available (e.g. a plane wave basis), but it is clearly appropriate only for a certain range of the interaction parameters. What is of interest is the precise range of values for which the basis is appropriate and the nature of the new basis that replaces it when going beyond that range. Even in simple models, a complete self-consistent mean-field calculation is a difficult problem because of its <u>non-linear</u> character (HL 82, WH 86). The discussion in the previous paragraphs implies that both issues can be settled by studying the <u>linear</u> problem of the behaviour of the RPA modes in the available quasi-particle basis. Following this approach in the Agassi model, it is possible to eliminate the existence of a full HFB solution when $N = \Omega$ and derive the phase diagram (Fig. 3.1) using only the results of the HF and BCS calculations. This method is valid only when the quasi-particle basis adopted is self-consistent. Nevertheless it is plausible that the method remains useful even when this is not the case (KL 85).

The occurrence and form of spurious modes are entirely determined by the quasi-particle basis. They occur whenever the basis breaks a symmetry of H' which possesses infinitesimal generators that are one-body operators (MW 69). Any of these generators B when expressed in terms of the quasi-particle operators of this basis, will be given by an expression of the following form:

$$B = B_o + \sum_{ij} B^{11}_{ij} \beta^\dagger_i \beta_j + \sum_{i<j} (B^{20}_{ij} \beta^\dagger_i \beta^\dagger_j + B^{02}_{ij} \beta_j \beta_i), \qquad (6.8)$$

where B_o is the ground state expectation value of B (which may be zero), and B^{20}_{ij}, B^{02}_{ij} are non-zero because the basis breaks the symmetry for which B is the generator. Since $[H',B] = 0$, one has the relation

$$<v|[\beta_j\beta_i,[H',B]]|v> = 0,$$

which, using Eqs. (6.3b) and (6.8), leads to the conclusion that

$$B_{sp} = \begin{pmatrix} B^{20} \\ -B^{02} \end{pmatrix} \qquad (6.9)$$

satisfies Eq. (6.3a) with eigenvalue $E \equiv 0$. So the precise form of spurious solutions of the RPA equation can be established from results like Eq. (6.8), without reference to the RPA equations themselves.

The identification of B_{sp} in Eq. (6.9) as a spurious mode hinges on the fact that an exactly self-consistent basis is used. In practical calculations, technical simplifications are necessary which forfeit this property of the basis. Spurious modes no longer have eigenenergies which are identically zero, nor is the corresponding eigenvector as in Eq. (6.9) (UR 71). (The clear-cut division between spurious modes and other modes in a self-consistent basis is another advantage of this type of basis.) The extent of the deviation from these results serves as a check on the simplifications made (RW 70). On the other hand, when the bases are self-consistent, the requirement that B_{sp} satisfy the RPA equations can be used to establish whether the RPA matrix has been correctly calculated.

The presence of spurious modes suggests that RPA respects, in some sense, the symmetries of the Hamiltonian. In fact, while a vibrational RPA mode is interpreted as an excitation of an intrinsic state, a spurious mode can be interpreted as collective (non-vibrational) motion of the intrinsic state (e.g. a rotation or translation) which restores the symmetry broken by it to the accuracy of the random-phase approximation (MW 69 and references therein). However, because RPA is a "small amplitude approximation" and, moreover, does not supply explicit wavefunctions, there are certain ambiguities (MW 69, LM 80). To resolve them it is necessary to go beyond the framework of RPA (MW 69, MW 79, Ma 82), and so, in what follows, the discussion will focus on vibrational modes.

SECTION 6.2: APPLICATION OF RPA TO THE AGASSI MODEL

The RPA calculations considered in this section are performed within the self-consistent quasi-particle bases determined in chapter 3 and appendix 6.1. Detailed comparison of RPA results with exact results (Section 6.2.2) will be presented only for the $N = \Omega$ configuration of the Agassi model, as this is sufficient to establish the points of interest. On the other hand, in dealing with formal aspects of the application of RPA to the Agassi model (Section 6.2.1), the most general appropriate quasi-particle basis, namely, the deformed-superconducting basis, is adopted because it provides a natural framework for the simultaneous discussion of RPA within the spherical and deformed HF bases and RPA within the superconducting basis.

6.2.1: The appropriate collective RPA modes

The form of the transformation relating the quasi-particle operators in the deformed-superconducting phase to the bare operators $c^{\dagger}_{\sigma m}$, $c_{\sigma m}$ is given in Eq. (A6.4), and the anti-symmetrised matrix elements of the Agassi model interaction in the bare basis are obtained by setting $\phi = 0$ in Eqs. (A6.6-7). Substituting these results into Eq. (6.5), one finds that the matrices A and B in the RPA equations appropriate to the deformed-superconducting basis have elements

$$A_{\sigma_1 m_1, \sigma_2 m_2, \sigma_3 m_3, \sigma_4 m_4}$$

$$= (E_{\sigma_1} + E_{\sigma_2})\delta_{\sigma_1\sigma_3}\delta_{\sigma_2\sigma_4}\delta_{m_1 m_3}\delta_{m_2 m_4} - A^{1}_{\sigma_1 m_1, \sigma_2 m_2, \sigma_3 m_3, \sigma_4 m_4} \qquad (6.10a)$$

with

$$A^{i}_{\sigma_1 m_1, \sigma_2 m_2, \sigma_3 m_3, \sigma_4 m_4} = (A_{\sigma_1\sigma_2\sigma_3\sigma_4}\, \delta_{m_1 m_3}\, \delta_{m_2 m_4} - (\sigma_3 m_3 \leftrightarrow \sigma_4 m_4))$$

$$+ \; \mathrm{sgn}(m_2 m_4)\, A'_{\sigma_1\sigma_2\sigma_3\sigma_4}\, \delta_{m_1 -m_2}\, \delta_{m_3 -m_4}, \qquad (6.10b)$$

and

$$B_{\sigma_1 m_1, \sigma_2 m_2, \sigma_3 m_3, \sigma_4 m_4}$$

$$= (\mathrm{sgn}(m_1 m_2)\, \delta_{m_1 -m_3}\, \delta_{m_2 -m_4}\, B_{\sigma_1\sigma_2\sigma_3\sigma_4} - (\sigma_3 m_3 \leftrightarrow \sigma_4 m_4) \qquad (6.10c)$$

$$- (\sigma_1 m_1 \leftrightarrow \sigma_4 m_4)),$$

where E_σ is a quasi-particle energy (the calculation of which is discussed in Appendix 6.1) and detailed expressions for A_{1234}, A'_{1234} and B_{1234} are given in Appendix 6.2.

Consideration of Eq. (6.10) leads to the conclusion that the coherent collective RPA eigenvectors have components

$$X_{\sigma m, \sigma' m'} = \mathrm{sgn}(m)\, \delta_{m\, -m'}\, (\sqrt{2}\, x_\sigma\, \delta_{\sigma\sigma'} + x\delta_{\sigma-\sigma'})/\Omega^{\frac{1}{2}}$$

$$Y_{\sigma m, \sigma' m'} = \;\;'' \qquad '' \quad ('' \;\; y_\sigma \;\; '' \;\; + y \;\; '' \;\;)/'' , \qquad (6.11)$$

where the normalisation condition for positive energy solutions is (cf. Eq. (6.4))

$$\sum_\sigma (x_\sigma^2 - y_\sigma^2) + x^2 - y^2 = 1.$$

The coefficients x_σ, y_σ, x and y satisfy the 6x6 RPA equation

$$\begin{pmatrix} A_c & B_c \\ B_c & A_c \end{pmatrix} \begin{pmatrix} X \\ Y \end{pmatrix} = E \begin{pmatrix} X \\ -Y \end{pmatrix}, \tag{6.12a}$$

where

$$X = \begin{pmatrix} x_1 \\ x_{-1} \\ x \end{pmatrix} \quad , \quad Y = \begin{pmatrix} y_1 \\ y_{-1} \\ y \end{pmatrix}, \tag{6.12b}$$

and A_c and B_c are symmetric matrices. If

$$A_c = \begin{pmatrix} a_1 & -\tilde{a} & -\tilde{a}_1 \\ & a_{-1} & -\tilde{a}_{-1} \\ & & a \end{pmatrix} \quad , \quad B_c = \begin{pmatrix} b_1 & -\tilde{b} & -\tilde{b}_1 \\ & b_{-1} & -\tilde{b}_{-1} \\ & & -b \end{pmatrix}, \tag{6.12c}$$

then

$$a_\sigma = 2E_\sigma - A_{\sigma\sigma\sigma\sigma} - \frac{\Omega}{2} A'_{\sigma\sigma\sigma\sigma}$$

$$b_\sigma = -(\Omega/2 - 1)\, B_{\sigma\sigma\sigma\sigma}$$

$$\tilde{a} = A_{-1-111} + \frac{\Omega}{2} A'_{-1-111}$$

$$\tilde{b} = -B_{-1-111} + \frac{\Omega}{2} B_{-11-11}$$

$$a = E_1 + E_{-1} - A_{-111-1} - A_{-11-11} - \Omega A'_{-11-11} \tag{6.12d}$$

$$b = -B_{-11-11} + (\Omega - 1)\, B_{-1-111}$$

$$\tilde{a}_\sigma = \sqrt{2}\,(A_{\sigma\sigma-11} + \Omega/2\, A'_{\sigma\sigma-11})$$

$$\tilde{b}_\sigma = \sqrt{2}\,(-B_{\sigma\sigma-11} + \Omega/2\, B_{\sigma-1\sigma 1}).$$

As it stands, the system in Eq. (6.12) is formally applicable to all bases appropriate to the Agassi model. However it simplifies still further if the basis is either one of the HF solutions or the BCS solution.

For any of these solutions, $\tilde{a}_\sigma = \tilde{b}_\sigma = 0$, and Eq. (6.12') decouples into the two independent systems

$$\begin{pmatrix} a & -b \\ -b & a \end{pmatrix} \begin{pmatrix} x \\ y \end{pmatrix} = E \begin{pmatrix} x \\ -y \end{pmatrix}, \tag{6.13a}$$

and

$$\begin{pmatrix} A_r & B_r \\ B_r & A_r \end{pmatrix} \begin{pmatrix} X_r \\ Y_r \end{pmatrix} = E \begin{pmatrix} X_r \\ -Y_r \end{pmatrix}, \tag{6.13b}$$

where the definitions of vectors X_r, Y_r and 2x2 matrices A_r, B_r are obvious from Eq. (6.12). In the case of a HF solution, because particle number is conserved, $\tilde{a} = b_\sigma = 0$, and Eq. (6.13b) reduces to

$$\begin{pmatrix} a_1 & -\tilde{b} \\ -\tilde{b} & a_{-1} \end{pmatrix} \begin{pmatrix} x_1 \\ y_{-1} \end{pmatrix} = E_p \begin{pmatrix} x_1 \\ -y_{-1} \end{pmatrix} \tag{6.14a}$$

and

$$\begin{pmatrix} a_1 & -\tilde{b} \\ -\tilde{b} & a_1 \end{pmatrix} \begin{pmatrix} x_{-1} \\ y_1 \end{pmatrix} = E_h \begin{pmatrix} x_{-1} \\ -y_1 \end{pmatrix}, \tag{6.14b}$$

where E_p/E_h is the energy of a $(\Omega + 2)$-/$(\Omega - 2)$-particle RPA state relative to the RPA ground state of the Ω-particle system. The decomposition of Eq. (6.12) into Eqs. (6.13) and (6.14) illustrates <u>precisely</u> how the quasi-particle RPA equations combine the ph-RPA equations (e.g. Eq. (6.13a)) and the pp-RPA equations (e.g. Eq. (6.14)) all under one umbrella. On the other hand, Eq. (6.14) obscures the symmetrical interrelationship between the collective pp-mode (pairon) and the collective hh-mode (holon). These can both be related to solutions of

$$\begin{pmatrix} (a_1 + a_{-1})/2 & -\tilde{b} \\ -\tilde{b} & (a_1 + a_{-1}/2) \end{pmatrix} \begin{pmatrix} \tilde{x} \\ \tilde{y} \end{pmatrix} = E \begin{pmatrix} \tilde{x} \\ -\tilde{y} \end{pmatrix} . \qquad (6.15)$$

If $\tilde{x}$, $\tilde{y}$ satisfy Eq. (6.15) with eigenvalue E, then

$$x_1 = \tilde{x}, \quad y_{-1} = \tilde{y} \qquad (6.16a)$$

satisfies Eq. (6.14a) with eigenvalue $E_p = E - (a_{-1} - a_1)/2$, and, at the same time,

$$x_{-1} = \tilde{x}, \quad y_1 = \tilde{y} \qquad (6.16b)$$

satisfies Eq. (6.14b) with eigenvalue $E_h = E + (a_{-1} - a_1)/2$.

The collective ph-mode in the spherical basis is precisely that found in the LMG model when $\chi < 1$ (MGL 65); similarly, the pairon and holon modes (in the spherical basis) are found in the two-level Pairing model when $\Sigma < 1$ (BB 66). Implicit in RPA is the assumption that the RPA modes do not interact with each other (cf. section 8.4.5 in (RS 80)). Hence, the presence of the pairon and holon states, with energies E_p and E_h, implies the existence of a collective pairon-holon excitation in the Ω-particle system of energy $E_p + E_h$. The studies in (MGL 65) and (BB 66) demonstrate that the collective ph-mode (or monopole mode) and the pairon-holon mode do in fact describe the exact low-lying collective excitations of fixed particle number within the LMG and Pairing models respectively. On the other hand, the discussion in section 2.2.1 of the <u>exact</u> collective excitations of the <u>Agassi model</u> when χ, Σ are small, showed that they can be interpreted as non-interacting superpositions of the (basic) excitations found separately in the LMG and Pairing models. Thus the RPA solutions isolated in Eqs. (6.13a) and (6.14) are indeed those appropriate to the collective excitations of the closed-shell configurations of the Agassi model when $\Sigma, \chi < 1$.

Because of the simplicity of the small interaction strength limit of the Agassi model, the results above (specifically Eqs. (6.13a) and (6.14)) interrelationship between the collective pp-mode (pairon) and the collective hh-mode (holon). These can both be related to solutions of

$$\begin{pmatrix} (a_1 + a_{-1})/2 & -\tilde{b} \\ -\tilde{b} & (a_1 + a_{-1}/2) \end{pmatrix} \begin{pmatrix} \tilde{x} \\ \tilde{y} \end{pmatrix} = E \begin{pmatrix} \tilde{x} \\ -\tilde{y} \end{pmatrix} . \tag{6.15}$$

If $\tilde{x}$, $\tilde{y}$ satisfy Eq. (6.15) with eigenvalue E, then

$$x_1 = \tilde{x}, \quad y_{-1} = \tilde{y} \tag{6.16a}$$

satisfies Eq. (6.14a) with eigenvalue $E_p = E - (a_{-1} - a_1)/2$, and, at the same time,

$$x_{-1} = \tilde{x}, \quad y_1 = \tilde{y} \tag{6.16b}$$

satisfies Eq. (6.14b) with eigenvalue $E_h = E + (a_{-1} - a_1)/2$.

The collective ph-mode in the spherical basis is precisely that found in the LMG model when $\chi < 1$ (MGL 65); similarly, the pairon and holon modes (in the spherical basis) are found in the two-level Pairing model when $\Sigma < 1$ (BB 66). Implicit in RPA is the assumption that the RPA modes do not interact with each other (cf. section 8.4.5 in (RS 80)). Hence, the presence of the pairon and holon states, with energies E_p and E_h, implies the existence of a collective pairon-holon excitation in the Ω-particle system of energy $E_p + E_h$. The studies in (MGL 65) and (BB 66) demonstrate that the collective ph-mode (or monopole mode) and the pairon-holon mode do in fact describe the exact low-lying collective excitations of fixed particle number within the LMG and Pairing models respectively. On the other hand, the discussion in section 2.2.1 of the exact collective excitations of the Agassi model when χ,Σ are small, showed that they can be interpreted as non-interacting superpositions of the (basic) excitations found separately in the LMG and Pairing models. Thus the RPA solutions isolated in Eqs. (6.13a) and (6.14) are indeed those appropriate to the collective excitations of the closed-shell configurations of the Agassi model when $\Sigma,\chi < 1$.

Because of the simplicity of the small interaction strength limit of the Agassi model, the results above (specifically Eqs. (6.13a) and (6.14)) could have been heuristically inferred from a knowledge of the RPA calculations within the LMG and Pairing models - viz. these calculations suggest that a reasonable ansatz for the operator in Eq. (6.1) corresponding to a collective negative parity excitation within the Agassi model is

$$Q_m^+ \propto x J_+ - yJ_- , \tag{6.17}$$

which is consistent with the results above. However the rather formal discussion above has the advantage that it indicates the following extrapolation beyond this "simple" regime to the regimes of large Σ and χ, where the problem appears far more complex (GH 84b): the coherent collective RPA modes given by Eqs. (6.11) and (6.12) are, in general, the modes appropriate to the description of the excitations within the collective subspace of the Agassi model.

The character of these modes in bases other than the spherical HF basis can be summarised as follows.

(1) Deformed HF. In this basis, the modes are formally identical to those in the spherical basis. The physical interpretation of these modes is however radically different. They must now be assumed to describe both members of excited parity doublets built on the parity doublet containing the ground state of the Ω-particle system.

(2) Superconducting (BCS). As in the spherical HF basis, one finds a negative parity "monopole" mode, namely the solution of Eq. (6.13a). The solutions of Eq. (6.13b) possess positive parity. The fact that particle number symmetry is broken implies that the positive parity vector with non-zero components

$$X^{sp}_{\sigma m,\sigma -m} = -Y^{sp}_{\sigma m,\sigma -m} = u_\sigma v_\sigma$$

is a solution of the RPA equations with eigenenergy zero. Observe that this vector is of the same form as the vectors in Eq. (6.11), and so must satisfy Eq. (6.13b), which is confirmed by direct substitution. This mode is of rotational character: as

$Y_o = (\hat{N} - \Omega)/2$, it generates rotations about the z-axis of the quasi-spin space corresponding to the SU(2) group with generators $Y_\pm$ and Y_o. (The absence of a similar "spurious" solution when parity symmetry is broken is a consequence of the fact that it is a discrete symmetry with no infinitesimal one-body generator.) The other mode determined by Eq. (6.13b) is the "pairing" vibration. This is the counterpart of the pairon-holon excitation found in the HF bases, with the difference that, in addition to an energy, one obtains an eigenvector, enabling one to calculate transition matrix elements.

(3) Deformed-superconducting (Full HFB). Not surprisingly, the modes in this basis share features of the modes in the superconducting basis and the deformed (HF) basis. As in the superconducting basis, there are three distinct modes of which one is "spurious". The remaining modes can again be classified as "pairing" and "monopole" modes, but, as in deformed HF, they now describe parity doublets. Because the monopole and pairing modes satisfy the same set of equations, they are identified by their eigenvectors: the dominant components of the monopole (pairing) mode eigenvector are x,y (x_σ,y_σ).

So, independent of the choice of basis, RPA predicts two fundamental excitations in a system of given particle number, a monopole vibration and either a pairing vibration (BCS, HFB basis) or a pairon-holon vibration (HF basis). These have negative and positive parity respectively except when the basis is "deformed", in which they describe both members of excited parity doublets. Observe that these findings are qualitatively consistent with the results of section 2.2.

An interesting aspect of the behaviour of these collective modes is that it is they which are affected by instabilities of the quasi-particle bases. Consider, for example, the pairon-holon mode in the spherical phase of the $N = \Omega$ system. This excites Cooper pairs. On the other hand, in section 3.3 it was shown that the spherical phase becomes unstable with respect to the formation of Cooper pairs for $\Sigma_o \gtrsim 1$. Recalling the discussion of section 6.1, one can conclude that, as $\Sigma_o \to 1^-$, the energy of the pairon-holon mode must tend to zero, and that,

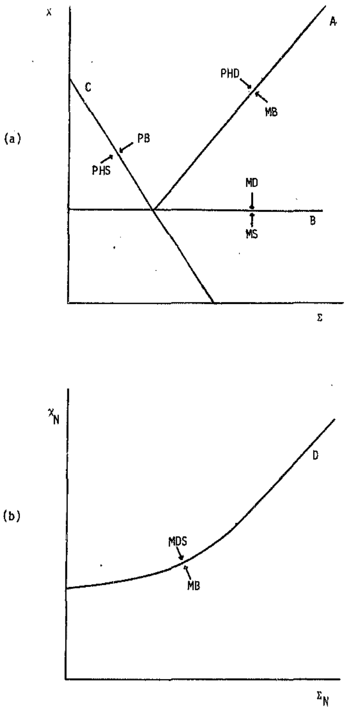

Fig. 6.1 Loci at which energies of RPA modes (indicated by labelled arrows) tend to zero. Curves A and D are the superconducting - to - deformed and superconducting - to - deformed - superconducting transition lines respectively; curve B is given by $\chi = 1$ and curve C by $\chi = (\Omega - 1)(1 - \Sigma)$. In the labels, M, P and PH denote monopole, pairing and pairon-holon modes, and B, D, DS and S the superconducting, deformed, deformed-superconducting and spherical bases respectively.

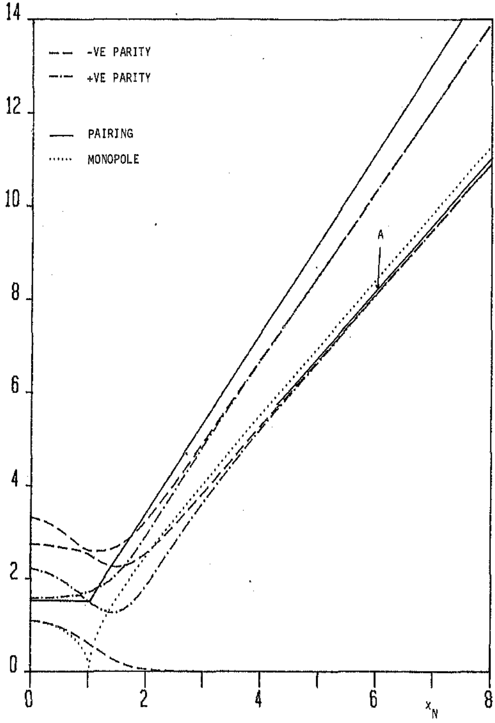

Fig. 6.2 Comparison of exact and approximate excitation energies when $N = 18$, $\Omega = 22$ and $\Sigma_N = 0.5$. Curve A is obtained by using an approximation discussed in section 7.2. The energies of the RPA monopole and pairing vibrational modes within the appropriate quasi-particle bases are identified by the key in the diagram.

for larger values of Σ_o, it is unphysical being no longer real-valued. Furthermore, because, at the spherical-to-superconducting transition, $\phi_{BCS} = \psi_{BCS} = 0$, which are the values of ϕ and ψ in the spherical phase, the pairing mode (in the BCS basis) formally satisfies the same equations as the pairon and holon modes at the transition point, and so the pairing mode energy must tend to zero as $\Sigma_o \to 1^+$. (Because the BCS solution does not exist for $\Sigma_o < 1$, this zero in the pairing vibrational mode energy should not be interpreted as a signal of instability.) The display of similar behaviour by the other collective modes can be anticipated in the same way from the results in chapter 3. This information is conveniently summarised in Fig. 6.1. Explicit confirmation of these patterns in the case of the $N = \Omega$ configuration can be seen in the closed-form analytic results given in section 6.2.2, Eq. (6.19), while numerical calculations are consistent with Fig. 6.1b (cf. Fig. 6.2).

In the next section, comparisons of RPA energies with exact excitation energies will be complemented by comparisons involving RPA matrix elements. Matrix elements of the particle number conserving quasi-spin operators J_o, J_x and J_y will be considered. (The results of section 2.2 indicate that the behaviour of matrix elements of these operators is typical of that displayed by matrix elements of any of the other quasi-spin operators.) Expressions for these matrix elements, applicable to any basis appropriate to the Agassi model, can be obtained by working within the deformed-superconducting basis. Take, for example, the operator J_o: in terms of the quasi-particle operators $\beta^\dagger_{\sigma m}$, $\beta_{\sigma m}$ of the deformed-superconducting basis, it is given by

$$J_o = \tfrac{1}{2} \sum_{\sigma\sigma'} \mathrm{sgn}(m)\, (u_{1\sigma} v_{1\sigma'} - u_{-1\sigma} v_{-1\sigma'})\, (\beta^\dagger_{\sigma m} \beta^\dagger_{\sigma' -m} + \mathrm{h.c.})$$

$$+ \text{(terms which do not contribute to RPA matrix elements)},$$

and so the matrix element between a coherent collective RPA state $|c\rangle$ and the RPA ground state $|r\rangle$ is, from Eqs. (6.2) and (6.11),

$$\frac{2}{\Omega^{1/2}} \langle c|J_o|r\rangle = \sum_\sigma (\eta_{1,\sigma} - \eta_{-1,\sigma}) \frac{(x_\sigma + y_\sigma)}{\sqrt{2}} + (\eta_1 - \eta_{-1})\, (x + y) \tag{6.18a}$$

where

$$\eta_{\sigma,\sigma'} = 2\, u_{\sigma\sigma'}\, v_{\sigma\sigma'} \qquad , \qquad \eta_\sigma = u_{\sigma 1}\, v_{\sigma -1} + (1 \leftrightarrow -1).$$

In the same way, the matrix elements of J_x and J_y between $|c>$ and $|r>$ are

$$\left.\begin{array}{l} \frac{2}{\Omega^{1/2}} <c|J_x|r> \\[2ex] \frac{2}{\Omega^{1/2}}\, i<c|J_x|r> \end{array}\right\} = \sum_\sigma \left(\mu_{1,\sigma} \pm \mu_{-1,\sigma}\right) \frac{(x_\sigma \pm y_\sigma)}{\sqrt{2}} + (\mu_1 + \mu_{-1})\,(x \pm y)$$

(6.18b)

where

$$\mu_{\sigma\sigma'} = 2u_{\sigma\sigma'}\, v_{-\sigma\sigma'} \qquad , \qquad \mu_\sigma = u_{\sigma 1}\, v_{-\sigma -1} + (1 \leftrightarrow -1).$$

The signs of these matrix elements are, of course, not determined by the solution of Eq. (6.12). It is convenient to take $<c|J_x|r>$ and the exact transition matrix elements of J_x to be positive; this determines the signs of the matrix elements of J_y because, independent of the basis, $<c|J_x|r>$ and $<c|J_y|r>$ are to be compared with exact matrix elements between the same pair (or pairs) of states. The phase of matrix elements of J_o however remains arbitrary; they will be assumed to be positive.

6.2.2 Comparison of RPA with exact results

When $N = \Omega$, it is possible to solve for the collective RPA modes analytically. One finds that, independent of the basis, the excitation energy of the monopole vibration can be written as

$$\frac{E_m}{\varepsilon} = \alpha_+ \alpha_- , \qquad (6.19a)$$

where $\alpha_\pm$ is given in Table 6. Similarly, the energy of both the pairon-holon and the pairing vibrations is given by

$$\frac{E_p}{\varepsilon} = 2\beta_+\beta_- , \qquad (6.19b)$$

where $\beta_\pm$ is also defined in Table 6. The transition matrix elements of J_x, J_y and J_o (cf. Eq. (6.18)) can also be written in a compact manner. The matrix elements of J_x and J_y between the pairing vibration $|p\rangle$ (superconducting basis) and the RPA ground state $|r\rangle$ must vanish because both states possess positive parity; in the case of the monopole mode $|m\rangle$ they are given by

$$2/\Omega^{\frac{1}{2}} \langle m|J_x|r\rangle = \mu_x \, (\alpha_+/\alpha_-)^{\frac{1}{2}} , \qquad 2/\Omega^{\frac{1}{2}} \, i\langle m|J_y|r\rangle = \mu_y \, (\alpha_-/\alpha_+)^{\frac{1}{2}} ,$$

where μ_x, μ_y are defined in Table 6. Symmetry considerations imply that the only transition matrix elements of J_o which can be non-zero are $\langle m|J_o|r\rangle$ in the deformed phase and $\langle p|J_o|r\rangle$; they are given by

$$2/\Omega^{\frac{1}{2}} \langle m|J_o|r\rangle = (\alpha_+\alpha_-/\chi)^{\frac{1}{2}} \quad , \quad 2/\Omega^{\frac{1}{2}} \langle p|J_o|r\rangle = (2\beta_+\beta_-/\Sigma_o) .$$

(Matrix elements of J_o involving the pairon-holon excitation are not considered because, as was pointed out in the previous section, no RPA eigenvector is available for this state.) The fact that the matrix elements of all three operators between $|m\rangle$ and $|r\rangle$ are non-zero in the deformed basis may seem contradictory. However, in the deformed phase, the exact spectrum must be treated as if it consists of parity doublets. The RPA matrix elements $\langle m|J_x|r\rangle$ and $\langle m|J_y|r\rangle$ must be compared with the matrix elements of J_x and J_y between the positive and negative parity members of the ground state parity doublet and the negative and positive parity members, respectively, of the appropriate excited parity doublet; $\langle m|J_o|r\rangle$ has to be compared with the matrix elements of J_o between members of these two doublets with the same parity.

The energies of the collective RPA modes are compared with exact excitation energies in Figs. 6.3-4; $N = \Omega = 20$ with Σ being varied and $\chi = \frac{1}{2}$ and 5 respectively (as in Figs. 2.2a and 2.5).

where $\alpha_{\pm}$ is given in Table 6. Similarly, the energy of both the pairon-holon and the pairing vibrations is given by

$$\frac{E_p}{\varepsilon} = 2\beta_+\beta_- , \tag{6.19b}$$

where $\beta_{\pm}$ is also defined in Table 6. The transition matrix elements of J_x, J_y and J_o (cf. Eq. (6.18)) can also be written in a compact manner. The matrix elements of J_x and J_y between the pairing vibration $|p\rangle$ (superconducting basis) and the RPA ground state $|r\rangle$ must vanish because both states possess positive parity; in the case of the monopole mode $|m\rangle$ they are given by

$$2/\Omega^{\frac{1}{2}} \langle m|J_x|r\rangle = \mu_x \, (\alpha_+/\alpha_-)^{\frac{1}{2}} , \qquad 2/\Omega^{\frac{1}{2}} \, i\langle m|J_y|r\rangle = \mu_y \, (\alpha_-/\alpha_+)^{\frac{1}{2}} ,$$

where μ_x, μ_y are defined in Table 6. Symmetry considerations imply that the only transition matrix elements of J_o which can be non-zero are $\langle m|J_o|r\rangle$ in the deformed phase and $\langle p|J_o|r\rangle$; they are given by

$$2/\Omega^{\frac{1}{2}} \langle m|J_o|r\rangle = (\alpha_+\alpha_-/\chi)^{\frac{1}{2}} \quad , \quad 2/\Omega^{\frac{1}{2}} \langle p|J_o|r\rangle = (2\beta_+\beta_-/\Sigma_o) .$$

(Matrix elements of J_o involving the pairon-holon excitation are not considered because, as was pointed out in the previous section, no <u>RPA</u> eigenvector is available for this state.) The fact that the matrix elements of all <u>three</u> operators between $|m\rangle$ and $|r\rangle$ are non-zero in the deformed basis may seem contradictory. However, in the deformed phase, the exact spectrum must be treated as if it consists of parity doublets. The RPA matrix elements $\langle m|J_x|r\rangle$ and $\langle m|J_y|r\rangle$ must be compared with the matrix elements of J_x and J_y between the positive and negative parity members of the ground state parity doublet and the negative and positive parity members, respectively, of the appropriate excited parity doublet; $\langle m|J_o|r\rangle$ has to be compared with the matrix elements of J_o between members of these two doublets with the same parity.

The energies of the collective RPA modes are compared with exact excitation energies in Figs. 6.3-4; $N = \Omega = 20$ with Σ being varied and $\chi = \frac{1}{2}$ and 5 respectively (as in Figs. 2.2a and 2.5).

Naïvely, one expects the collective RPA modes to describe the excited states of lowest energy. This expectation is in fact met for $\chi = \frac{1}{2}$. Figure 6.3a shows that the excitation energy of the lowest negative parity state is well described by the monopole mode in the stable quasi-particle basis. Similarly, except for $\Sigma < 0.15$, the lowest positive parity excited state is approximated first by the pairon-holon mode (in the spherical phase) and then by the pairing vibration (in the superconducting phase). When Σ is small, matters are complicated by the presence of another positive parity state of comparable excitation energy; in fact, as $\Sigma \to 0$, it is lower than the state described by the pairon-holon mode. However it is also an RPA state in that it is approximated by the second harmonic of the monopole vibration.

An important result illustrated by Fig. 6.3a is that it is essential to use a stable basis in an RPA calculation. For $\Sigma_0 > 1$, the spherical HF basis is unstable. Because it is unstable with respect to the formation of Cooper pairs, the energy of the pairon-holon mode becomes complex (in fact, imaginary) beyond this point and it has to be discarded. On the other hand, the properties of the monopole mode within the spherical basis are unaffected. If the results of the RPA calculation of negative parity states (which do not include the pairon-holon mode) are taken in isolation, there is no reason to discard this mode. However Fig. 6.3a demonstrates that it does not have any meaning in this region.

In Fig. 6.3 χ is fixed and Σ is varied. Analogous patterns are found if instead Σ is fixed (at some value less than $(\Omega-2)/(\Omega-1)$) and χ is increased. In this case there is a transition from spherical HF to deformed HF. The roles of the monopole, and pairon-holon and pairing modes are interchanged. A plot of the monopole mode energies would now look like Fig. 6.3b (GH 84b), while the pairon-holon and pairing mode energies would behave as in Fig. 6.3a. When either χ is varied (with Σ fixed) or Σ is varied (with χ fixed), the mode associated with the instability of the spherical HF basis performs poorly in the transition region (as anticipated in section 6.1). The energy of the other mode remains a good approximation if calculated in the stable basis. Outside this region the energies of all modes compare well with the exact energies. This is in particular true in the regime where either χ or Σ is large.

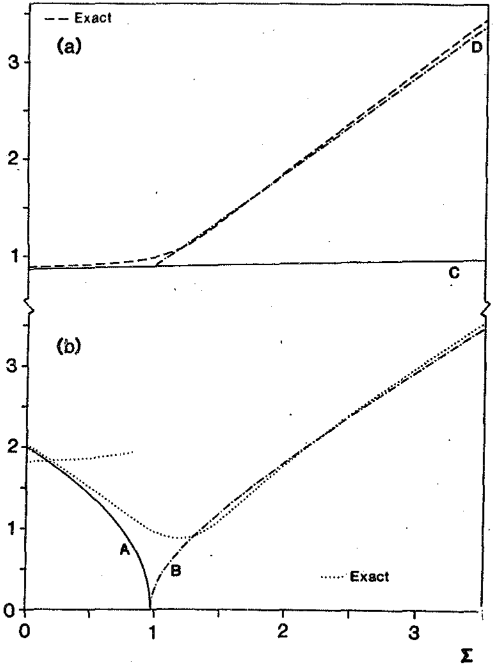

Fig. 6.3 Comparison of exact and RPA excitation energies when $\chi = \frac{1}{2}$, $N = \Omega = 20$. (a) Exact energy of lowest negative parity state and RPA monopole mode energies in: spherical HF basis (curve C); BCS basis (curve D). (b) Exact energies of lowest excited positive parity states and RPA pairon-holon and pairing mode energies in: spherical HF basis (curve A); BCS basis (curve B).

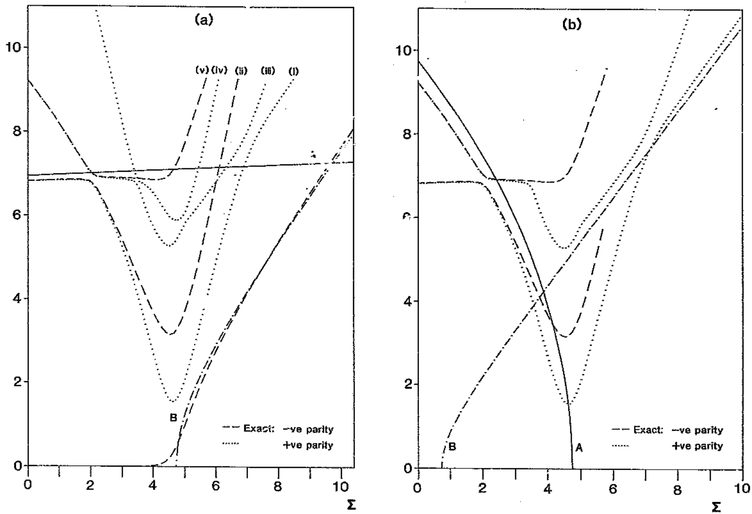

Fig. 6.4 Comparison of RPA energies with exact excitation energies when $\chi = 5$, $N = \Omega = 20$: part (a), monopole mode; part (b), pairon-holon and pairing modes. Results in deformed HF (BCS) basis are labelled by A (B).

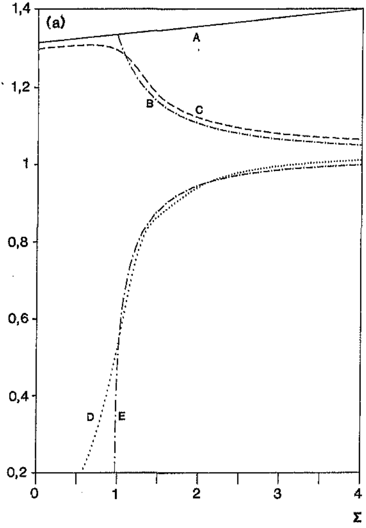

<u>Fig. 6.5</u> Comparison of exact and RPA matrix elements when $N = \Omega = 20$. In all diagrams the matrix elements are scaled by a factor of $2/\Omega^{\frac{1}{2}}$. (a) $\chi = \frac{1}{4}$. The exact and approximate matrix elements of J_x between the ground state and the lowest negative parity state are: curve A, RPA in spherical HF basis; curve B, RPA in BCS basis; curve C, exact. The exact and approximate matrix elements of J_0 between the ground state and the lowest positive parity excited state are: curve D, exact; curve E, RPA in BCS basis. (b) Matrix element of iJ_y between the ground state and lowest negative parity state when $\chi = 5$: curve A, exact; curve B, RPA in BCS basis. (c) Matrix elements of J_x when $\chi = 5$ in the region where the deformed HF is stable. The exact matrix elements are between: the negative parity member of the ground state doublet and the positive parity members of the first, second and third excited parity doublets (curves A, C and E respectively); the positive parity member of the ground state doublet and the negative parity members of the first and second excited parity doublets (curves B and D respectively). Curve F is the RPA result in the deformed HF basis.

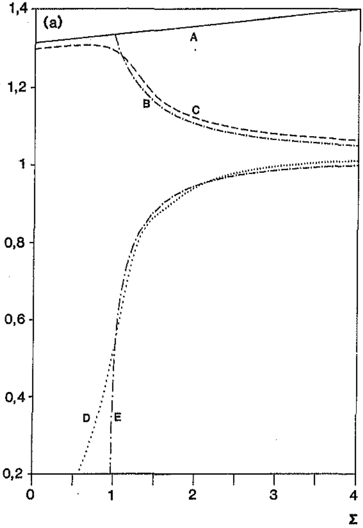

<u>Fig. 6.5</u> Comparison of exact and RPA matrix elements when $N = \Omega = 20$. In all diagrams the matrix elements are scaled by a factor of $2/\Omega^{\frac{1}{2}}$. *(a)* $\chi = \frac{1}{2}$. The exact and approximate matrix elements of J_x between the ground state and the lowest negative parity state are: curve A, RPA in spherical HF basis; curve B, RPA in BCS basis; curve C, exact. The exact and approximate matrix elements of J_0 between the ground state and the lowest positive parity excited state are: curve D, exact; curve E, RPA in BCS basis. (b) Matrix element of iJ_y between the ground state and lowest negative parity state when $\chi = 5$: curve A, exact; curve B, RPA in BCS basis. (c) Matrix elements of J_x when $\chi = 5$ in the region where the deformed HF is stable. The exact matrix elements are between: the negative parity member of the ground state doublet and the positive parity members of the first, second and third excited parity doublets (curves A, C and E respectively); the positive parity member of the ground state doublet and the negative parity members of the first and second excited parity doublets (curves B and D respectively). Curve F is the RPA result in the deformed HF basis.

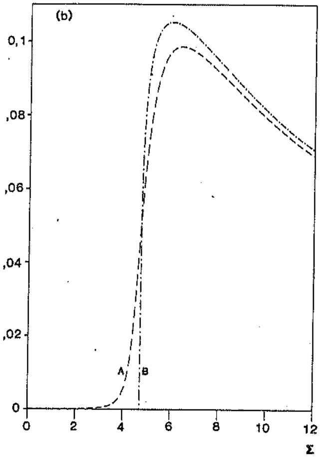
(b)
0,1
,08
,06
,04
,02
0
A
B
0
2
4
6
8
10
12
Σ

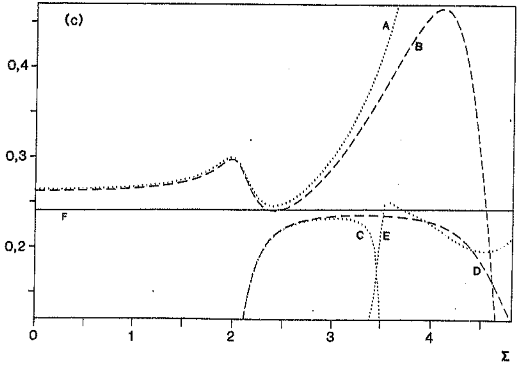
(c)
0,4
0,3
0,2
A
B
C
D
E
F
0
1
2
3
4
Σ

As spherical HF is not stable when $\chi = 5$ (see Fig. 3.1), only the results of RPA calculations in the deformed HF and BCS bases are compared with exact energies in Fig. 6.4. The RPA states calculated in the deformed HF basis must be interpreted as parity doublets, and indeed, the low-lying members of the exact excitation spectrum for $\chi = 5$ do form parity doublets in the deformed phase provided one is not too close to the deformed-to-superconducting transition point. For $\Sigma < 2.5$, the members of the two lowest excited parity doublets cannot be resolved on the scales of Figs. 6.4a and b. In this interval they are reasonably approximated by the monopole and pairon-holon modes respectively in the deformed HF basis. Although the members of the lower of these two parity doublets separate for larger values of Σ, they can still be viewed as belonging to a "doublet". It continues to be approximated by a mode in the deformed HF basis, namely, the pairon-holon mode, but the level of agreement deteriorates (Fig. 6.4b). The other parity doublet is far more clearly defined until the level repulsion at $\Sigma \cong 3.5$ (Fig. 6.4b); up to this point it is well described by the monopole mode in the deformed HF basis. To the extent that states (i) and (ii) in Fig. 6.4a form a "doublet", so do states (iv) and (v) immediately after $\Sigma \cong 3.5$. This doublet is described by the monopole mode in the deformed HF basis. By contrast, the positive parity state (iii), which has a lower excitation energy than this doublet, cannot be a RPA state in this basis because it does not belong to a parity doublet. As the transition region is approached, not only does the quality of the RPA description of "doublets" worsen, but it also fails to describe all the low-lying collective states. When $\chi > 5$ this feature of the spectrum is seen more clearly.

At $\Sigma = \Sigma_c = 4.74$, the deformed HF basis becomes unstable and the BCS basis, which exists provided $\Sigma > 0.74$, becomes stable. The RPA modes in the deformed HF basis behave in the same way at this point as the corresponding RPA modes in the spherical HF basis at the spherical-to-superconducting transition (cf. Fig. 6.1a). The monopole mode in the deformed HF basis remains well-behaved even when the basis is not stable, but, as in Fig. 6.3a, it is completely meaningless (Fig. 6.4a). Likewise the pairing mode (in the BCS basis), although formally acceptable when the BCS basis is unstable, cannot be taken seriously in this region (Fig. 6.4b). This applies in particular to the vanishing of the pairing mode energy at $\Sigma = 0.74$. It is tempting to infer from this the occurrence of a phase transition, but it would be wrong to do so.

In the region in which the BCS basis is stable, the energies of its RPA modes compare well with the energies of exact states. It can be seen from Fig. 6.4a that the negative parity monopole mode approximates the lowest negative parity state, and that the approximation remains remarkably good as the transition point is approached. In the limit of large Σ (i.e. $\Sigma > 7$), the positive parity pairing mode, like the monopole mode, describes the lowest excited state with the same symmetry. However, between the transition point and the level "crossing" at $\Sigma \approx 7$, the pairing mode corresponds to the second excited state of positive parity. The lower excited positive parity state can be viewed as the second harmonic of the monopole vibration.

Through the comparison of energies the exact state or group of states which can be identified with a collective RPA mode have been determined. It is now possible to compare the RPA predictions for transition matrix elements with their exact values.

Figure 6.5 contains comparisons of the RPA predictions for matrix elements with their exact values. As before $N = \Omega = 20$ with $\chi = \frac{1}{2}$ and 5, and Σ is varied. Results for $\chi = \frac{1}{2}$ are all contained in Fig. 6.5a which shows that the two relevant exact matrix elements are well described; the level of quantitative agreement deteriorates in the transition region but still remains fair. This also applies to the matrix element of J_y not shown. A comparison of these results for the matrix elements with those for the energies (Fig. 6.3) in the case of the pairing mode shows surprisingly that the former are significantly better in the transition region: even when the energy of a soft mode is a poor approximation, the matrix elements can still be good. Figures 6.5b and c demonstrate that the RPA results are also reasonable approximations when $\chi = 5$. The discrepancies can become significant as the transition point is approached, but, as is most clearly shown in Fig. 6.5b, the behaviour of the RPA matrix elements remains at least qualitatively correct. Such findings lend support to the methods employed in other investigations (LG 85).

The parity doublet described by the monopole mode in the deformed HF basis is involved in two level repulsions (Fig. 6.4a). This makes the comparisons in Fig. 6.5c rather complex, but they confirm the assignments made in discussing Fig. 6.4a. The intervals of poor agreement in Fig. 6.5c at $\Sigma \approx 2$ and 3.5 coincide with the intervals in which the exact states repel each other. The RPA "ignores" the level repulsions. On the other hand, the exact results in Fig. 6.5c demonstrate that the level repulsions between excited states amount, in effect, to nothing more than level crossings. Thus this is a desirable characteristic of RPA.

When these calculations are repeated for smaller values of χ, namely $1 < \chi < 3$, the RPA in the deformed HF basis is poor (GH 84b) while it still performs well in the BCS basis - i.e. the width of the region of poor agreement in the deformed HF basis parallel to the χ-axis is broader than in the BCS basis parallel to the Σ-axis. This is a peculiarity of the model. For the RPA in the deformed HF basis to work well it is necessary that the exact excited states with quite different unperturbed energies form almost exactly degenerate parity doublets. This pattern only emerges once χ is quite large - much larger than the value at which the ground state parity doublet first appears. In contrast, the RPA in the BCS basis does not require rigid patterns in the excitation spectrum of the $N = \Omega$ system.

The overall pattern to emerge from the comparison of RPA and exact results can be summarised as follows. First and foremost, RPA calculations are meaningful only in <u>stable</u> quasi-particle bases. This can be interpreted as further support for the singularity conjecture of section 5.1, which suggests that the singularities inherent in the exact solution are adequately mimicked by stable bases, but not by unstable bases. The connection with the singularity conjecture in turn suggests this finding is not specific to the Agassi model. It has thus practical significance for calculations within realistic systems in which, for reasons of economy, only some of the collective RPA modes are considered. While these modes may be well-behaved, an instability of the basis may be associated with a mode not under consideration. If so, the results will be invalid, and this will not be obvious by considering them alone.

As regards the quality of the RPA (in a stable basis), this depends on how close one is to a "phase transition". Well away from a phase transition, the RPA is adequate (except at points where excited states are involved in level repulsions among themselves), but it becomes, in general, poor (although still qualitatively correct) in the immediate vicinity of a phase transition. This is also true of the HFB description of ground state properties. So, in the treatment of the collective low-lying states and the ground state, one can identify the vicinity of a phase transition as a region in which the "mean-field approach" (i.e. HFB and RPA) fails, while on either side of a transition it is adequate. More elaborate treatments are required primarily in the region of phase transitions. The same conclusions emerge from realistic applications (see, for example, chapter 11 of (RS 80)).

Model studies show that the solution to a many-body problem, when expressed in terms of the quasi-particle basis appropriate to the non-interacting limit, becomes (in general) extremely complicated with increasing interaction strength, and patterns within the solution are not transparent (GH 84b). The success of the mean-field approach in the region beyond a phase transition is thus remarkable: it identifies a structure which, for example, enables one to express some of the complicated states of the solution to the many-body problem as simple RPA states built on a new "vacuum".

The singularity conjecture can account for the deteriorating quality of the mean-field approach as the location of phase transitions is approached: the inadequacies of the way in which the singularities involved are mimicked now show up. This suggests that improved agreement in the transition region can be obtained by simulating these singularities more accurately. The implementation of crossing-symmetry may be just such a method.

Within the Green's function formulation of the many-body problem, a central role is played by the 4-point vertex function Γ (EHH 77). Crossing-symmetry is one the formal properties required of any exact Γ (EHH 77, He 80). It is a very stringent requirement, being non-perturbative and non-linear in character (HB 68), and attempts at constructing, in the general case, a crossing-symmetric Γ for fermions (He 80,81, DH 84) have to date been unsuccessful. (Studies of crossing-symmetry with bosons seem to have been far more successful (JLS 82).) The purpose of these studies was to establish the physical significance of crossing-symmetry. The results of the model study in (GH 83, GH 84a), in which the exact Γ appropriate to the LMG model with two particles is calculated, seem to shed some light on this issue. This vertex function possesses algebraic singularities in the interaction strength parameter V which occur suggestively for values of V such that $|V/\varepsilon| = |\chi| = 1$. At the same time, these singularities arise because this Γ, being exact, possesses crossing-symmetry (chapter 3 of (Ge 85)). The implication is that it is precisely in the troublesome transitional region where crossing-symmetry is relevant.

APPENDIX 6.1: THE APPROPRIATE QUASI-PARTICLE STATES

In this appendix, the form of the third and final member of the decomposition of the full HFB transformation appropriate to the Agassi model is determined. This yields the quasi-particle states which are necessary for the description of excitations. In addition, the calculation of the quasi-particle energies of these states is discussed.

To accomplish this, the expressions for H^{20} and H^{11} (appropriate to the Agassi model) found in the quasi-particle basis defined by Eqs. (3.14) and (3.15) are required (cf. discussion following Eq. (3.10)). These are

$$H^{20}_{\sigma m,\sigma' m'} = \mathrm{sgn}(m)\, H^{20}_{\sigma\sigma'}\, \delta_{m,-m'} \qquad \text{(A6.1a)}$$

$$H^{11}_{\sigma m,\sigma' m'} = H^{11}_{\sigma\sigma'}\, \delta_{m,m'}, \qquad \text{(A6.1b)}$$

in which

$$H^{20}_{\sigma\sigma'} = \gamma_{\sigma\sigma'}\, h^{c}_{\sigma\sigma'} - \bar{\gamma}_{\sigma\sigma'}\, \Delta^{c}_{\sigma\sigma'} \qquad \text{(A6.2a)}$$

$$H^{11}_{\sigma\sigma'} = \bar{\gamma}_{\sigma\sigma'}\, h^{c}_{\sigma\sigma'} + \gamma_{\sigma\sigma'}\, \Delta^{c}_{\sigma\sigma'}, \qquad \text{(A6.2b)}$$

where

$$\gamma_{\sigma\sigma'} = u_\sigma v_{\sigma'} + u_{\sigma'} v_\sigma \qquad \bar{\gamma}_{\sigma\sigma'} = u_\sigma u_{\sigma'} - v_\sigma v_{\sigma'} ,$$

and use has been made of the fact that the matrix elements in the canonical basis of the equivalent within HFB of the HF Hamiltonian and Pairing field can be written as

$$h^c_{\sigma m,\sigma' m'} = h^c_{\sigma\sigma'} \, \delta_{m,m'}$$

and

$$\Delta^c_{\sigma m,\sigma' m'} = -\mathrm{sg}\cdots \; \Delta^c_{\sigma\sigma'} \, \delta_{m,-m'} ,$$

respectively. Explicit expressions for $h^c_{\sigma\sigma'}$ and $\Delta^c_{\sigma\sigma'}$ will be given below (Eq. (A6.8)).

<u>Form of the 3rd transformation:</u>

The third transformation U_2 is required to be such that $U_2^\dagger H^{11} U_2$ is diagonal. Hence, from Eq. (A6.1b), it can be chosen to be

$$\beta^\dagger_{\sigma m} = \Sigma \, c_{\sigma'\sigma} \, \alpha^\dagger_{\sigma' m} ,$$

where $\alpha^\dagger_{\sigma m}$ are the quasi-particle operators defined by Eqs. (3.14) and (3.15) and

$$C_\sigma = \begin{pmatrix} c_{1\sigma} \\ c_{-1\sigma} \end{pmatrix}$$

is an eigenvector of $H^{11}_{\sigma\sigma'}$ with eigenvalue E_σ; E_σ is the quasi-particle energy corresponding to the quasi-particle state created by $\beta^\dagger_{\sigma m}$. (By choice, $E_1 \geq E_{-1}$.)

Since $H^{11}_{\sigma\sigma'}$ is symmetric and real-valued, the third transformation exists and can be chosen to be orthogonal. It can be parametrised in a manner very similar to the first transformation (Eq. (3.13)), namely

$$\beta^{\dagger}_{\sigma m} = \cos\zeta/2\ \alpha^{\dagger}_{\sigma m} - \sigma \sin\zeta/2\ \alpha^{\dagger}_{-\sigma m}, \tag{A6.3}$$

where $0 \le \zeta \le \pi/2$. The determination of ζ is trivial once $H^{11}_{\sigma\sigma'}$ is known.

In terms of the bare operators $c^{\dagger}_{\sigma m}$, $c_{\sigma m}$, the quasi-particle operator $\beta^{\dagger}_{\sigma m}$ can be written as

$$\beta^{\dagger}_{\sigma m} = \sum_{\sigma'} (r_{\sigma'\sigma}\ c^{\dagger}_{\sigma' m} - \mathrm{sgn}(m)\ v_{\sigma'\sigma}\ c_{\sigma'-m}). \tag{A6.4}$$

<u>Expressions for</u> $h^{c}_{\sigma\sigma'}$, $\Delta^{c}_{\sigma\sigma'}$:

In a canonical basis, h and Δ have matrix elements

$$\begin{aligned} h^{c}_{ij} &= t^{c}_{ij} + \Sigma\ \bar{v}^{c}_{ikjk}\ \rho^{c}_{k} \\ \Delta^{c}_{ij} &= \tfrac{1}{2}\ \Sigma'\ \bar{v}^{c}_{ijk\bar{k}}\ \kappa^{c}_{k}, \end{aligned} \tag{A6.5}$$

where t^{c}_{ij} is a matrix element (in the canonical basis) of the 1-body part of H', $\bar{v}^{c}_{ijkl}$ an anti-symmetrised matrix element of the (2-body) interaction in H' and Σ' denotes the sum over paired states. In the Agassi model, these matrix elements are, from Eq. (A3.10),

$$t^{c}_{\sigma m,\sigma' m'} = (\varepsilon/2\ t^{c}_{\sigma\sigma'} - \mu\delta_{\sigma\sigma'})\ \delta_{mm'} \tag{A6.6a}$$

$$\begin{aligned} \bar{v}^{c}_{\sigma_1 m_1,\sigma_2 m_2,\sigma_3 m_3,\sigma_4 m_4} &= -v^{c}_{\sigma_1\sigma_2\sigma_3\sigma_4}\ (\delta_{m_1 m_3}\ \delta_{m_2 m_4} - (3 \leftrightarrow 4)) \\ &\quad - \mathrm{sgn}(m_1 m_3)\ g\ \delta_{\sigma_1\sigma_3}\ \delta_{\sigma_2\sigma_4}\ \delta_{m_1 -m_2}\ \delta_{m_3 -m_4}, \end{aligned} \tag{A6.6b}$$

where μ is the chemical potential,

$$t^{c}_{\sigma\sigma} = \sigma \cos\phi \quad , \quad t^{c}_{\sigma-\sigma} = -\sin\phi \tag{A6.7a}$$

and

$$v^{c}_{\sigma_1\sigma_2\sigma_3\sigma_4} = V(\delta_{\sigma_1\sigma_2}\ \delta_{\sigma_3\sigma_4} - S_{\sigma_1\sigma_2\sigma_3\sigma_4}), \tag{A6.7b}$$

in which

$$S_{\sigma_1\sigma_2\sigma_3\sigma_4\sigma} = \sum_{\sigma} (U_1)_{\sigma\sigma_1} (U_1)_{\sigma\sigma_2} (U_1)_{\sigma\sigma_3} (U_1)_{\sigma\sigma_4},$$

and $(U_1)_{\sigma\sigma'}$ appears in the transformation to the canonical basis, Eq. (3.13). The independent entries in $S_{\sigma_1\sigma_2\sigma_3\sigma_4}$ are

$$S_{\sigma\sigma\sigma\sigma} = 1 - \tfrac{1}{2}\sin^2\phi \qquad S_{\sigma\sigma-\sigma-\sigma} = \tfrac{1}{2}\sin^2\phi$$
$$S_{\sigma\sigma\sigma-\sigma} = -\tfrac{1}{2}\sigma\sin\phi\cos\phi. \tag{A6.7c}$$

Substituting Eqs. (A6.6)-(A6.7) into Eq. (A6.5), one finds that

$$h^c_{\sigma\sigma'} = \varepsilon/2\; t^c_{\sigma\sigma'} - \mu\,\delta_{\sigma\sigma'} + \Gamma^c_{\sigma\sigma'} \tag{A6.8a}$$

with

$$\Gamma^c_{\sigma\sigma} = \tfrac{1}{2}\sigma(\Omega - 1)\, V\, (\rho^c_{-1} - \rho^c_1)\sin^2\phi - g\,\rho^c_\sigma$$
$$\Gamma^c_{\sigma-\sigma} = \tfrac{1}{2}(\Omega - 1)\, V\, (\rho^c_{-1} - \rho^c_1)\sin\phi\cos\phi \tag{A6.8b}$$

and

$$\Delta^c_{\sigma\sigma} = \tfrac{1}{2}(\Omega g + V)(\kappa^c_1 + \kappa^c_{-1}) + \tfrac{1}{2}\sigma V(\kappa^c_{-1} - \kappa^c_1)\cos^2\phi$$
$$\Delta^c_{\sigma-\sigma} = -\tfrac{1}{2} V\,(\kappa^c_{-1} - \kappa^c_1)\cos\phi\sin\phi, \tag{A6.8c}$$

where ρ^c_σ and κ^c_σ are given in Eq. (3.17).

Quasi-particle energies:

In the superconducting basis, $H^{11}_{\sigma\sigma'}$ is automatically diagonal (as substitution of $\phi = 0$ in Eq. (A6.8) confirms). As, from Eq. (A6.2b), the quasi-particle energy

$$E_\sigma = (1 - 2\rho^c_\sigma)\, h^c_{\sigma\sigma} + 2\kappa^c_\sigma\, \Delta^c_{\sigma\sigma}, \tag{A6.9}$$

and $h^c_{\sigma\sigma}$ depends on μ, it would seem necessary to know μ in order to evaluate E_σ. In fact, this is not the case; using the condition

$$H^{20}_{\sigma\sigma} = 0 \quad \text{(BCS equations)},$$

Eq. (A6.9) can be rewritten as

$$E_\sigma = \Delta^c_{\sigma\sigma}/2\kappa^c_\sigma . \tag{A6.10}$$

(In Eqs. (A6.9-10), it is assumed $\phi = 0$.)

Similarly, in the deformed-superconducting basis, by combining Eq. (6.2) and the condition $H^{20} = 0$, one finds

$$H^{11}_{\sigma\sigma'} = \Delta^c_{\sigma\sigma'}/\gamma_{\sigma\sigma'}.$$

In the HF basis ($N = \Omega$, $\mu = 0$), H^{11} is again automatically diagonal and

$$\begin{aligned} E_\sigma &= \sigma\, h^c_{\sigma\sigma} \\ &= \varepsilon/2\ (\cos\phi + \chi \sin^2\phi) + g\ \delta_{\sigma,-1}, \end{aligned}$$

using Eq. (A6.8).

<u>APPENDIX 6.2: COEFFICIENTS IN EQ. (6.10)</u>

$$\begin{aligned} A_{1234} = {} & V(S^u_{1234} + S^v_{1234} - (\bar{\bar{S}}_{1234} + (1 \leftrightarrow 2,\ 3 \leftrightarrow 4))) \\ & + g((\sum_{\sigma\sigma'} u_{\sigma_1} v_{\sigma_3} u_{\sigma'_2} v_{\sigma'_4}) + (1 \leftrightarrow 2,\ 3 \leftrightarrow 4))) \end{aligned}$$

$$\begin{aligned} A'_{1234} = {} & V(S_{1234} + (1 \leftrightarrow 2) + (3 \leftrightarrow 4) + (1 \leftrightarrow 2,\ 3 \leftrightarrow 4)) \\ & + g \sum_{\sigma\sigma'} (u_{\sigma_1} u_{\sigma_2} u_{\sigma'_3} u_{\sigma'_4} + v_{\sigma_1} v_{\sigma_2} v_{\sigma'_3} v_{\sigma'_4}) \end{aligned}$$

where $u_{\sigma\sigma'}$, $v_{\sigma\sigma'}$ are defined in Eq. (A6.4),

$$\overline{S}_{1234} = \sum_{\sigma} v_{\sigma 1}\, u_{-\sigma 2}\, v_{-\sigma 3}\, u_{\sigma 4}$$

$$S^{u}_{1234} = \sum_{\sigma} u_{\sigma 1}\, u_{\sigma 2}\, u_{-\sigma 3}\, u_{-\sigma 4}$$

and S^{v}_{1234} is obtained from S^{u}_{1234} by replacing u's by v's.

$$B_{1234} = V((\sum_{\sigma} u_{\sigma_1}\, u_{\sigma_2}\, v_{-\sigma_3}\, v_{-\sigma_4}) + (1 \leftrightarrow 3) + (2 \leftrightarrow 4)$$

$$+ (1 \leftrightarrow 2,\ 3 \leftrightarrow 4))$$

$$- g((\sum_{\sigma\sigma'} v_{\sigma_1}\, v_{\sigma_3}\, u_{\sigma'_2}\, u_{\sigma'_4}) + (1 \leftrightarrow 2,\ 3 \leftrightarrow 4)),$$

TABLE 6

Basis	$(\alpha_+)^2$	$(\alpha_-)^2$	$(\beta_+)^2$	$(\beta_-)^2$	μ_x	μ_y
Spherical HF	$1 + \chi + 2g'$	$1 - \chi$	$1 + g' + V'$	$1 - \Sigma_0$	1	1
BCS	$\Sigma_0 + g' + \chi'/(\Sigma_0)^2$	$\Sigma_0 - \chi$	$\frac{1}{2}(\Sigma_0 + g' + V')$	$\frac{1}{2}(\Sigma_0 - 1/\Sigma_0)$	1	$1/\Sigma_0$
Deformed HF	$2\chi'$	$\chi - 1/\chi$	$\chi' + V'/\chi^2$	$\chi - \Sigma_0$	$1/\chi$	1

$g' \equiv g/\varepsilon \quad V' \equiv V/\varepsilon \quad \chi' \equiv \chi + g/\varepsilon$

CHAPTER SEVEN

SIDE-EFFECTS OF SYMMETRY-BREAKING AND THEIR TREATMENT

Not only is the symmetry-breaking of HFB formally undesirable, it also affects the quality of agreement with experiment. The obvious extension of HFB, in which a state with the desired symmetries is projected out of the HFB trial state, leads to improved agreement, even when the projection is performed after the variational parameters in the trial state have been determined (PHFB) (SGF 84 and references therein). (In a fully self-consistent treatment, projection should be performed before variation (FHFB).) Projection, particularly the projection of states of good angular momentum, is however computationally expensive (HHR 82); to date, calculations incorporating projection have largely been confined to semi-realistic models, like the Pairing-plus-Quadrupole model and even these are by no means complete (WAM 85). (Compounding this is the fact that performing PHFB and FHFB does not remove the need in the description of excited states for treatments like TDA or RPA or their symmetry-conserving analogues (FR 85).)

The question arises whether or not the same physical insight cannot be attained by much simpler and technically less demanding methods. This has motivated the Hartree-Fock Seniority (HFS) approximation (GP 86), which is designed for open-shell systems. Realistic calculations have been performed within this approximation but it has not been compared in any detail with its rival approximations - i.e. HFB or PHFB.

This chapter is devoted to a discussion of the effects of symmetry-breaking and their treatment. Section 7.1 reports what can be learnt about the consequences of broken particle number symmetry within the Agassi model. Only the ground state energy is considered because, unlike other HFB expectation values, it is expected to be reliable. The most significant finding is that the HFB ground state energy can be lower that the exact ground state energy, which contradicts a belief implicit in the literature (cf., for example, section 8.4.6 in (RS 80)) that, as HFB can be derived using a Rayleigh-Ritz variational principle, it must always yield an upper bound to the ground state energy. In section 7.2, the HFS approximation will be discussed, with the aim of seeing to what extent it can simulate a projected HFB calculation. The technicalities of particle number projection within the Agassi model are described in an appendix to this chapter (Appendix 7).

SECTION 7.1: CONSEQUENCES OF BROKEN PARTICLE NUMBER SYMMETRY

Within the Agassi model, the mean-fields break two symmetries. Parity symmetry is broken when the monopole interaction is dominant, and the naïve interpretation for the corresponding solution is that it describes both members of a ground state parity doublet. Indeed, under the same conditions the exact positive parity ground state does become degenerate with the lowest negative parity state (Figs. 2.2b, 2.5), and the exact expectation values of this doublet do coincide (Fig. 2.4). Thus, the breaking of parity symmetry is a posteriori justified. On the other hand, particle number symmetry is broken whenever $N < \Omega$, independent of the valu[illegible] interaction strengths. (This is a characteristic of the mean [illegible] description of any open-shell nucleus (LA 84).) [illegible] breaking part[illegible] number symmetry, the mean-field can accommodate t[illegible] pairing interaction. In fact, the comparison of approximate and exact ground state expectation values of Y_+Y_- in Fig. 5.8 demonstrates that the particle number-breaking BCS solution continues to perform adequately even as $g \to 0$ (V small). However, when in isolation, the monopole interaction is accommodated by a particle number-conserving mean-field. So, in this section, the particle number dispersion of the HFB solutions appropriate to open-shell configurations of the Agassi model will be considered, particularly when V is large.

The form of any HFB ground state appropriate to the Agassi model is given by (Appendix 3.1)

$$|v\rangle = \prod_{\substack{\sigma m \\ m > 0}} (u_\sigma + v_\sigma a^\dagger_{\sigma m} a^\dagger_{\sigma -m})|-\rangle, \tag{A3.1}$$

from which it is clear that the distribution of components of different particle number in $|v\rangle$ is determined by the transformation within the canonical basis (cf. Eq. (3.10)), and it is (formally) the same as the distribution corresponding to a BCS state. This distribution can be derived from the observation that $\langle -|a_{\sigma -m}\, a_{\sigma m}|v\rangle = v_\sigma$. Thus, v_1^2 (v_{-1}^2)

is the probability that a specific pair of time-reversed states in the upper (lower) level is occupied; similarly, $u_1^2 = 1 - v_1^2$ ($u_{-1}^2 = 1 - v_{-1}^2$) is the probability that this pair of states is unoccupied. The probability that a component with k specific pairs in the upper level and $\frac{1}{2}N - k$ specific pairs in the lower level is present in $|v\rangle$ is

$$P_k = (u_1^2)^{\Omega/2 - k} (v_1^2)^k (u_{-1}^2)^{\Omega/2 - N/2 + k} (v_{-1}^2)^{N/2 - k}. \qquad (7.1a)$$

The number of such components is

$$n_k = \binom{\Omega/2}{k}\binom{\Omega/2}{N/2 - k} \qquad (7.1b)$$

Thus, the probability that $|v\rangle$ contains a component with particle number N is

$$P_N = \sum_{k=0}^{N/2} n_k P_k. \qquad (7.1c)$$

(This result is also a spin-off of the number projection calculation in Appendix 7.) Because of the constraints in Eq. (3.15), P_N may be regarded as a functional of $\rho_1^c = v_1^2$ alone.

The mathematical properties of this type of distribution have been studied at some length in the literature ((Hø 65) and references therein). Nevertheless, the full extent of the symmetry-breaking by $|v\rangle$ in the <u>present</u> <u>case</u> is best gauged by evaluating P_N explicitly. Typical numerical values, when Σ_N is fixed and χ_N is varied, are given in Table 7; in this example, the number of particles in the system is $N_o = 14$ ($\Omega = 22$). It has the following notable features.

(1) The distribution has a single maximum and this occurs for the component with particle number equal to the desired average N_o. The property is, of course, highly desirable and is, in fact, a general feature of the particle number distribution corresponding to a BCS state (Hø 65).

(2) The distribution is approximately symmetric about this maximum; this is a consequence of the large N_o limit (in which P_N is given by a Gaussian (Hø 65)).

(3) The probabilities P_N are essentially constant in the deformed-superconducting phase and remain appreciable for components with particle number $N \neq N_o$ even when χ_N is very large. The changes in P_N with χ_N (which are confined to the superconducting-to-deformed-superconducting transition region), are consistent with the behaviour of ρ_1^c (cf. Fig. 7.1). (Likewise, changes with Σ_N are restricted to the interval $0 \leq \Sigma_N \leq 2$, if $\chi_N \leq 1$.)

From Fig. 7.1, as $\chi_N \to \infty$, $\rho_1^c \to 0$ (in effect) and so $\rho_{-1}^c \to N_o/\Omega$. Substituting into Eq. (7.1) one finds

$$P_N \to P_N^a = \binom{\Omega/2}{N/2}\left(1 - \frac{N_o}{\Omega}\right)^{(\Omega - N)/2}\left(\frac{N_o}{\Omega}\right)^{N/2}$$

Table 7 shows that the binomial distribution P_N^a is a good approximation to P_N even when $\chi_N \approx 2$. Thus the dispersion seen in P_N for large χ_N is typical of any HFB description of an open-shell nucleus, which admits pairing within a single valence shell.

It is not only in the realm of large χ_N that P_N is of binomial character. The distribution P_N^a is also a good approximation to P_N if both χ_N and Σ_N are small (when $\rho_1^c \approx 0$ again - cf. the curve for which $\Sigma_N = 0.5$ in Fig. 7.1). In addition, when $\Sigma_N \geq 1$ (χ_N small and fixed), the distribution P_N is satisfactorily approximated by the binomial distribution obtained by setting $v_1^2 = v_{-1}^2 = N_o/2\Omega$.

A more succinct, quantitative measure of the indefinite particle number of $|v\rangle$ is the variance in the expectation value of $\hat{N}$ - i.e.

$$(\Delta N)^2 = \langle v|(\hat{N} - N_o)^2|v\rangle,$$

where $\langle v|\hat{N}|v\rangle = N_o$. For the Agassi model this is given by

$$(\Delta N)^2 = 2\Omega\left(\frac{N_o}{\Omega}\left(1 - \frac{N_o}{\Omega}\right) - 2\rho_1^c\,\rho_{-1}^c\right)$$

which, in the limit of large χ_N, becomes

$$\Delta N = (2\Omega)^{\frac{1}{2}} ((N_o/\Omega)(1 - N_o/\Omega))^{\frac{1}{2}}.$$

The dependence of particle number dispersion on N_o and N_o/Ω is easily seen in this result. For example, the dispersion is greatest when the valence shell is half-full (as in Table 7).

The effects of the significant particle dispersion of $|v\rangle$ can be established by comparing the predictions of HFB and PHFB. The particle number projection of $|v\rangle$, which yields the N-particle states $|N,N_o\rangle$ (where $N_o = \langle v|\hat{N}|v\rangle$) and the calculation of the expectation values of quasi-spin operators in these states are discussed in Appendix 7. This material will be used in subsequent considerations. However, it is instructive to consider first an approximate but simple scheme relating the results of HFB and PHFB calculations, which allows one to infer some of the <u>qualitative</u> consequences of restoring symmetry by projection without actually performing the projection (Ni 64, Appendix B in MPR 65, Go 79b). This scheme is particularly useful when the almost intractable angular momentum projection is desirable (Go 79b), but in what follows it will be specialised to the case of particle number projection.

Suppose that $\hat{A}$ is an observable which does not change the particle number and let

$$A_H = \langle v|\hat{A}|v\rangle \qquad , \qquad A_P(N) = \langle N,N_o|\hat{A}|N,N_o\rangle.$$

(The PHFB expectation value of $\hat{A}$ is $A_{PH} = A_P(N_o)$.) The starting point of the approximate scheme is the relation

$$A_H = \sum_N P_N A_P(N) \tag{7.2}$$

where P_N is given in Eq. (7.1c). If N is treated as a continuous variable, and the expansion of $A_P(N)$ about the point $N = N_o$ is inserted into Eq. (7.2), then one finds

$$A_H = A_{PH} + \frac{1}{2}\frac{\partial^2 A_p}{\partial N^2}\bigg|_{N = N_o} \Delta N^2 + \frac{1}{6}\frac{\partial^3 A_p}{\partial N^3}\bigg|_{N = N_o} \Delta N^3 + \ldots \tag{7.3}$$

which is an expansion of A_H in terms of moments of P_N about N_o. (Observe that since the expansion is about the point of $N = N_o$, the first moment vanishes while, because P_N is almost symmetric about this point, other odd moments are negligible.) To convert Eq. (7.3) into a relation between A_{PH} and A_H which can be used without explicit knowledge of $A_p(N)$, two assumptions are made concerning the derivatives it contains. Firstly, it is assumed that

$$\frac{\partial^{(m)} A_p}{\partial N^{(m)}}\bigg|_{N = N_o} \approx \frac{\partial^{(m)} A_p}{\partial N_o^{(m)}}\bigg|_{N = N_o} \tag{7.4a}$$

which appears to be physically reasonable (Ni 64) and not grossly unreliable numerically (MPR 65). The second assumption made is that, although the numerical value of A_H may be incorrect, its derivatives with respect to N_o are essentially correct; more precisely, it is assumed that

$$\frac{\partial^{(m)} A_H}{\partial N_o^{(m)}} \approx \frac{\partial^{(m)} A_p}{\partial N_o^{(m)}}\bigg|_{N = N_o} \tag{7.4b}$$

If the HFB approximation is at least qualitatively valid, this relation should be satisfied. Thus, one arrives at the following approximate relationship between A_H and A_{PH}:

$$A_{PH} \approx A_H - \tfrac{1}{2}\frac{\partial^2 A_H}{\partial N_o^2}\Delta N^2 + \text{higher order terms.} \tag{7.5}$$

Given the somewhat drastic approximations made, and the heuristic use to which Eq. (7.5) will be put, the higher-order terms in Eq. (7.5) will be ignored. In this regard, use of these higher-order terms and suggestions that the rate of convergence of this expansion be studied (Go 79b) seem somewhat misguided. (Such studies are more appropriate to formally consistent but far more complex treatments like the Kamlah expansion (Ka 68).)

The advantage of Eq. (7.5) lies in its simplicity. It makes very clear that discrepancies between A_H and A_{PH} occur when the dependence of A_H on N_o is non-linear. This conclusion is perhaps better expressed the other way round - i.e. if A_H depends linearly on N_o, there will be no significant discrepancies, no matter what the fluctuation in particle number is. Observe also that the sign of correction is determined not, as one might naïvely have thought, by the first derivative of A_H with respect to N_o but by the second. These features can be interpreted as inevitable consequences of the linear particle number constraint employed in HFB, which lends further substance to the validity of Eq. (7.5).

What do these considerations imply for the HFB ground state energy within the Agassi model? In the limit of large χ_N, the dominant contribution to the ground state energy of the deformed-superconducting solution (appropriate to an open-shell configuration of the Agassi model with N_o particles) is, from Eq. (3.21),

$$\frac{E^a}{-\varepsilon} \approx \tfrac{1}{2} N_o \chi_{N_o} = \tfrac{1}{2} N_o (N_o + 1 - 2N_o/\Omega) \frac{V}{\varepsilon} \tag{7.6}$$

and so, because of the non-linear dependence of E^a on N_o, projection ought to yield a substantially different value when the number dispersion in $|v\rangle$ is not negligible (i.e. $N_o \neq \Omega$). More interestingly, Eqs. (7.5) and (7.6) imply that the projected energy will be higher than the unprojected energy $(\partial^2 E^a/\partial N_o^2 < 0)$, and precisely this is seen when the actual PHFB energy is compared with the HFB energy as in Fig. 7.2 (curves A and B respectively). (Note that the absolute magnitudes of the ground state energies are plotted in Fig. 7.2.) This finding is at odds with a commonly accepted belief about projection which has arisen (despite isolated counter-examples, e.g. Table 9 of (AB 71)) from studies of the BCS treatment of pairing correlations within nuclei, namely, that the energies of projected states are lower than the energies of unprojected states. (This has often been cited as the reason why PHFB must be an improvement over HFB (GK 80).) However, as Eq. (7.5) makes clear, this is true only of systems with interactions which imply that the binding energy per particle does not increase monotonically with particle-number - e.g. systems with saturating interactions. The scarcity of nuclei for which the projected ground state energy has been found to be higher than the HFB ground state energy is a fortuitous consequence of the fact that saturation is, in principle, required of any realistic effective nuclear interaction and is therefore a property of most interactions employed in applications including the pairing interaction. (As the monopole interaction is a residual interaction acting only within the valence shell, its failure to possess any saturation properties is not a serious drawback. In fact, the quadruple interaction of the Pairing-plus-Quadrupole model also does not possess saturation properties (BK 68).)

A related observation is that the HFB ground state energy can even be lower than the exact ground state energy (cf. curves A and C of Fig. (7.2)). The HFB ground state is determined by appealing to the Rayleigh-Ritz variational principle, which usually yields an upper bound to the lowest eigenvalue of an operator. The apparent contradiction is resolved by the realisation that the eigenvalue referred to is fixed by a set of "boundary conditions", of which one is the particle number of the system. In HFB, however, the trial states have indefinite particle number. Thus, the HFB ground state ansatz can take advantage of the fact that an eigenenergy of a system with particle number $N \neq N_o$ may be lower than the lowest eigenenergy of the N_o-particle system to predict a spuriously low ground state energy. A pedestrian analysis using the results of the PHFB calculation confirms this in the present example. Plotted in Fig. 7.3 is the absolute magnitude of $\langle N,N_o|H|N,N_o\rangle/N$ ($N_o = 14$). (This choice of scaling permits the dependence of $E_N = \langle N,N_o|H|N,N_o\rangle$ on N to be read off from Fig. 7.3.) It demonstrates that, when χ_{N_o} is large,

$$E_{N_o} - E_{N_o + 2k} > E_{N_o - 2k} - E_{N_o}$$

(k = 1,2). On the other hand, from Table 7, $P_{o+2k} \approx P_{o-2k}$ (where P_o denotes the probability of $|v\rangle$ containing N_o particles). From Eq. (7.2), this ensures that the HFB ground state energy is spuriously low. (Closer inspection of P_N in Table 7 shows that P_{o+2k} is actually slightly greater than P_{o-2k}. It is tempting to interpret this as evidence of how the HFB solution capitalises on the lower energies found in systems of adjacent particle number. However, the presence of the same asymmetry in P_N^a shows that its origin is not related to dynamics.)

It was demonstrated in Chapter 5 that the requirement of stability for a mean-field to be appropriate is reliable. (This, in turn, supports the use of the Rayleigh-Ritz principle in deriving HFB.) The findings of this section are relevant to the selection between <u>different</u> <u>stable</u> mean-fields. Usually the stable mean-field which predicts the lowest ground state energy is adopted. However, care has to be taken to ensure that none of these energies are lowered spuriously by symmetry-breaking, a point which has been overlooked in several realistic applications of HFB (e.g. (GSB 70)). (This possibility can be excluded by resorting the PHFB.) In this section, it has been shown that this can happen when particle number symmetry is broken; it can also occur when translational invariance is broken (MV 83). Fortunately for nuclear physics applications, these considerations are unnecessary in the case of particle number symmetry-breaking when <u>realistic</u> interactions (which have reliable saturation properties) are employed.

<u>SECTION 7.2: HARTREE-FOCK SENIORITY APPROXIMATION (HFS)</u>

Because in an open-shell system there are several Slater determinants of lowest energy, in order to construct a <u>unique</u> ground state wave function within a number-conserving approximation, the use of just one Slater determinant has to be relinquished (cf. the discussion following Eq. (3.19)) - i.e. one cannot work within a mean-field approach. Nevertheless, it is possible to retain several features of the approach by employing the Hartree-Fock Seniority approximation (GP 86).

As in HF, HFS assumes that the particles occupy (unknown) single-particle states $|k\rangle$ which accommodate in an average way the long-range correlations between the particles. Likewise, a natural generalisation of the HF prescription for the ground state of a closed-shell system is adopted: the HFS approximation to the ground state $|s\rangle$ is assumed to be spanned by <u>only</u> the lowest energy Slater determinants formed with the single-particle states $|k\rangle$. To accommodate the short-range correlations between particles, $|s\rangle$ is taken to be that combination of these determinants which has seniority zero (Section 5 of chapter 1 of (La 80)); this particular (fixed) combination also satisfies the requirement of being

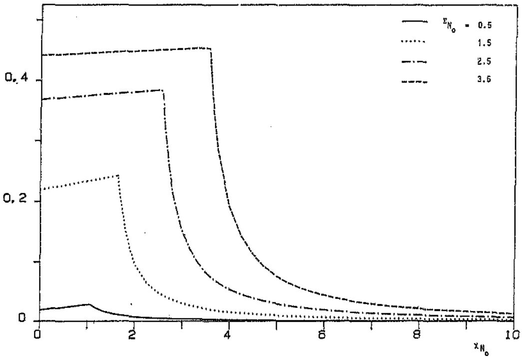

<u>Fig. 7.1</u> Plot of $2\rho_1^c$ (cf. Eq. (3.17)) for different values of Σ_N when $N_0 = 14$, $\Omega = 22$.

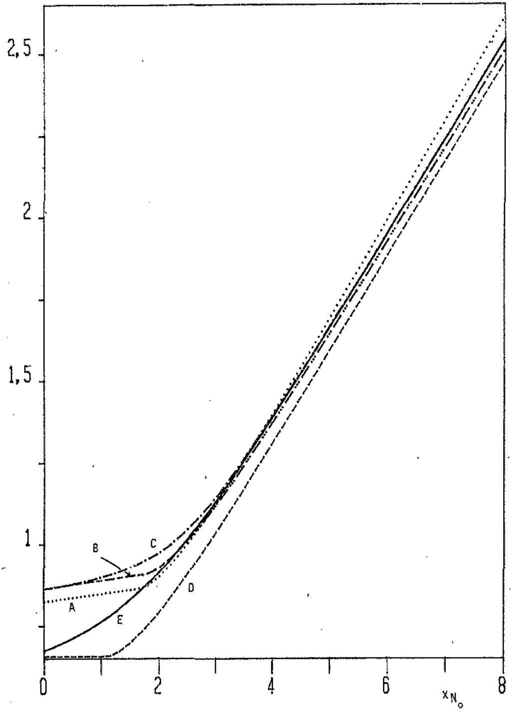

<u>Fig. 7.2</u> Comparison of various approximations to the ground state energy. (For convenience, the absolute moduli in units of $\frac{\Omega}{2}\varepsilon$ are plotted). The various curves are: A, HFB; B, PHFB; C, exact; D, HFS; E, exact energy of the lowest negative parity state. (N_o = 14, Ω = 22, Σ_N = 1.5).

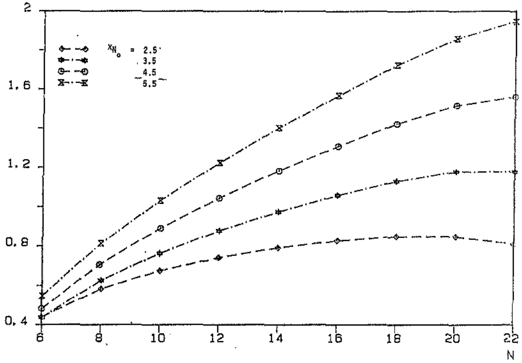

<u>Fig. 7.3</u> The absolute magnitude of $\langle N, N_o|H|N, N_o\rangle/N$ versus N for different values of χ_N; $N_o = 14$, $\Omega = 22$, $\Sigma_N = 1.5$ (as in Fig. 7.2).

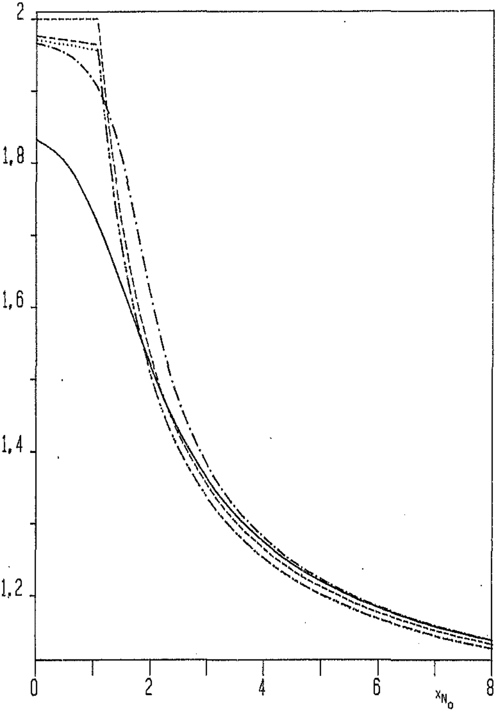

Fig. 7.4 Comparison of various approximations to the ground state expectation value of $\hat{N}_-$ (scaled by a factor of 4/N) when Σ_N = 0.5. The significance of the different line types is the same as in Fig. 7.2. (N_0 = 14, Ω = 22).

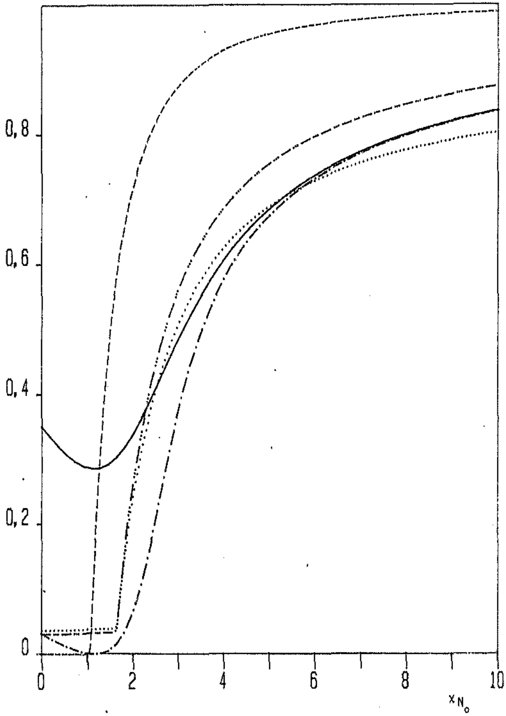

<u>Fig. 7.5</u> Comparison of various approximations to the ground state expectation value of M_+M_- (scaled by a factor of $2/N(\Omega+1)$). Other details are as in Fig. 7.4.

unique (Ke 61). The appropriate single-particle states $|k\rangle$ are those which minimise $\langle s|H|s\rangle$ (where H is the Hamiltonian of the system). For a closed-shell system, HF and HFS are equivalent.

The unknown single-particle basis appropriate to the Agassi model must have particle creation operators whose form is that of $a^{\dagger}_{\sigma m}$ in Eq. (3.14), while $|s\rangle$ is spanned by those Slater determinants containing only particles in the $\sigma = -1$ level of this basis. Thus $|s\rangle$ is the seniority zero state

$$|s\rangle = \frac{1}{n}(s_+)^{N/2}\;|-\rangle \tag{7.7a}$$

where

$$s_+ = \sum_{m>0} a^{\dagger}_{-1m}\, a^{\dagger}_{-1-m}$$

and

$$n = \frac{N}{2}!\begin{pmatrix}\Omega/2\\ N/2\end{pmatrix}^{\frac{1}{2}}$$

is the normalisation constant.

The operator s_+ is a member of the SO(5) Lie algebra involving the operators $a^{\dagger}_{\sigma m}$, $a_{\sigma m}$ introduced in Appendix 3.2. The corresponding quasi-spin, $SO_a(5)$, has, of course, the same formal properties as the SO(5) group introduced in cha‾ter 2 ($SO_c(5)$). In particular, it is possible to introduce the formal analogue of the collective subspace with basis $|m,z\rangle_a$. From the explicit form of those states (Section 4 of (He 65)) it can be inferred that

$$|s\rangle = |m = 0,\, z = -z_u\rangle_a \tag{7.7b}$$

Observe that, if in Eq. (3.14) [illegible] then $|m,z\rangle_a = |m,z\rangle$ and $|s\rangle$ coincides with the ground st[illegible] Hamiltonian in Eq. (2.12) when $V = g_2 = 0$. This by itsel[illegible] that Eq. (7.7a) is a reasonable ansatz for the ground stat[illegible] at [illegible]hen V, g are small.

The identification of $|s\rangle$ as a member of the basis for an irreducible representation of $SO_a(5)$ greatly facilitates the calculation of expectation values. Given a particular combination of the quasi-spin operators in Eqs. (2.3) and (2.4), the first step is to re-express them in terms of the quasi-spin operators in Eqs. (A3.6) and (A3.7) (as in Eqs. (A3.8) and (A3.9)). The expectation value in $|s\rangle$ of a combination q of the operators in Eqs. (A3.6) and (A3.7) can be evaluated by exploiting the formal similarity of $SO_a(5)$ and $SO_c(5)$. If Q is the operator obtained by replacing $a^{\dagger}_{\sigma m}$, $a_{\sigma m}$ in q by $c^{\dagger}_{\sigma m}$, $c_{\sigma m}$, then, from Eq. (7.7b),

$$\langle s|q|s\rangle = \langle m = 0, z = -z_u|Q|m = 0, z = -z_u\rangle, \tag{7.8}$$

and these last expectation values are easily inferred from Appendix 2.1 or Table 2.2. For example, if $q = j_x^2$, then $Q = J_x^2$, and $\langle s|j_x^2|s\rangle = N/4$ from Table 2.2.

The form of the Agassi Hamiltonian H in terms of the operators in Eqs. (A3.6) and (A3.7) is given in Eq. (A3.10). Applying the prescription in Eq. (7.8) to Eq. (A3.10), one finds

$$\langle s|H|s\rangle = -\frac{N\varepsilon}{2}\left(\cos\phi + \frac{\chi_o}{2}\sin^2\phi + (\delta + 1)\frac{g}{\varepsilon}\right)$$

where $\chi_o = (N - 1)V/\varepsilon$. This has minima at:

(1) $\phi = 0$ if $\chi_o < 1$ – a spherical HFS solution;
(2) $\phi \neq 0$, $\cos\phi = 1/\chi_o$ if $\chi_o > 1$ – a deformed HFS solution.

The properties of the spherical and deformed HFS solutions are essentially the same as those of the spherical and deformed HF solutions in the $N = \Omega$ system respectively. Also, like its HF counterpart, the HFS spherical-to-deformed transition is continuous. Observe that the HFS transition occurs at $\chi_o = 1$ independent of the value of g. (In this respect, HFS is again similar to HF.) This is not consistent with the findings of chapter 5 which show that the location of the changes in the exact solution associated with a phase transition do depend on the value of g. Except in the limit of small g ($\Sigma_N \lesssim 1$), the location of the HFS transition is spurious.

A typical example of the HFS ground state energy is given by curve D in Fig. 7.2. (The spherical-to-deformed HFS transition occurs at $\chi_N = 1.06$, and the superconducting-to-deformed-superconducting HFB transition at $\chi_N = 1.63$.) Observe that the PBCS energy becomes exact as $\chi_N \to 0$, in agreement with the results of (KLM 61). By contrast, the spherical HFS ground state energy is not a good approximation for this value of Σ_N. Not only is it quantitatively inaccurate but it is also qualitatively misleading in that it does not reflect the slight decrease in the ground state energy with increasing χ_N (χ_N small); even the symmetry-breaking BCS solution is superior to HFS in this regime. On the other hand, the HFS approximation is much more accurate in the deformed-superconducting region. (Despite this, HFS is only closer to the exact energy than HFB for very large χ_N, which bears testimony to the power of HFB.) Although the HFS energy is still not as accurate as the PHFB energy, the rate of change of both these energies with χ_N is essentially the same. The property is particularly significant because the rate of change of the HFB energy is different; it suggests that HFS can indeed indicate what the effect of projection will be.

Representative comparisons of HFS ground state expectation values not appearing directly in the Agassi Hamiltonian with the corresponding HFB and PHFB expectation values are given in Figs. 7.4 and 7.5. (The significance of this distinction has been discussed in section 5.1.) In the spherical HFS phase, $<s|\hat{N}_-|s> = N$ always. Hence the results of section 2.2.2 indicate that, with the exception of the regime of small Σ_N, χ_N, the <u>spherical</u> HFS solution is inadequate. However, Fig. 7.4 provides further evidence that, in the limit of large χ_N (Σ_N fixed), HFS can be a good approximation. In this instance, it is even marginally better than PHFB. As in Fig. 7.2, the rate of change of the HFS and PHFB expectation values with χ_N is the same. A remarkable feature of Fig. 7.4, which does not detract from the success of HFS, is that the HFB and PHFB results coincide for large χ_N. This is consistent with Eq. (7.5): the non-linearity in the dependence of $<v|\hat{N}_-|v>$ on N in this limit is very weak and so Eq. (7.5) implies that the PHFB and HFB expectation values cannot be significantly different. By contrast, the expectation value of M_+M_- (cf. Fig. 7.5) demonstrates that HFS is not always successful when χ_N is large (Σ_N fixed). Although it predicts correctly that the expectation value in this regime is increased when particle number projection is implemented, it grossly overestimates the magnitude of this correction. In fact, while HFB is a reasonably good approximation to $\langle o|M_+M_-|o\rangle$ in this regime, HFS is not. The spurious location of the HFS phase transition is also evident from Fig. 7.5.

The results in Figs. 7.2, 7.4 and 7.5 show that HFS can simulate the behaviour of the PHFB ground state energy and PHFB expectation values of one-body operators. This is all that can be reasonably expected to be reliable when dealing with a mean-field-like approximation such as PHFB anyway. However, despite the fact that the HFS ground state ansatz has seniority zero, HFS has essentially the same domain of applicability as a full HFB solution, being inadequate when a BCS solution is appropriate - i.e. HFS can simulate PHFB, but not PBCS unless the pairing interaction strength is small. The inability of HFS to cope with a pairing interaction is already evident from the (in general) spurious location of the HFS phase transition. This finding implies that the suggestion implicit in (GP 86), namely that HFS can be employed to establish whether the pairing properties of the phenomenologically successful Skryme interaction (GS 81) are adequate, is incorrect. The characteristic of a pairing interaction which HFS cannot accommodate is the (well-known) associated diffuseness of the Fermi surface. A suitable extension of the HFS ground state ansatz is suggested by the form of the exact ground state of the Agassi model in the limit when $g \to \infty$ (cf. Eq. (2.18)). (Note that the PHFB ground state does in fact possess this structure - cf. Eq. (A7.3).)

In mitigation of its flaws, HFS has the advantage that it allows one to perform a straightforward "open-shell" RPA calculation (PW 70) of excited states. In its formulation, open-shell RPA is completely analogous to quasi-particle RPA (QRPA). Since QRPA has been considered in some detail in the previous chapter, the discussion of open-shell RPA can be confined to the following remarks.

The immediate obstacle to RPA calculations in open-shell nuclei is the disappearance of the distinction between particle-states and holestates. This rules out the extension of pp- and hh-RPA to such systems. However it is possible to introduce a (limited) replacement of the ph- (hp-) operators $c_p^\dagger c_h$ ($c_h^\dagger c_p$) employed in ph-RPA, namely the pairs $c_\alpha^\dagger c_\beta$, $c_\beta^\dagger c_\alpha$ whose members have opposite (spatial) parity (RW 70); in the generic case, these opposite parity pairs satisfy the requirement of having non-zero unperturbed excitation energies - i.e. the unperturbed energies of the single-particle states $|\alpha>$ and $|\beta>$, e_α and e_β, satisfy the inequality $e_\alpha > e_\beta$. (In analogy with the terminology of ph- RPA, $c_\alpha^\dagger c_\beta$ ($c_\beta^\dagger c_\alpha$) is an opposite-parity ph - (hp-) pair.) Open-shell RPA thus caters only for negative (spatial) parity excitations of nuclei.

The range of application of open-shell RPA is further restricted to open-shell systems for which a suitable "uncorrelated" approximation $|\phi_o>$ to the ground state exists; a typical example of a suitable $|\phi_o>$ is given in Table 1 of (RW 70). (A notable feature of this example is that there is configuration-mixing present in $|\phi_o>$; however it is uncorrelated in the sense that configurations containing opposite-parity hp-pairs are excluded.) The approximation scheme yielding $|\phi_o>$ must also supply a single-particle basis from which the opposite-parity pairs can be constructed. One such approximation scheme is HFS.

Given all these ingredients, the derivation of the open-shell RPA equations proceeds as for the QRPA equations. They therefore possess the same structure, which, in turn, means that the (non-spurious) solutions of the open-shell RPA equations also occur in pairs with energies ±E, and are subject to the same orthonormality conditions.

Within the Agassi model, open-shell RPA can describe excitations of negative (LMG model) parity. The appropriate uncorrelated approximation to the ground state is given by $|s>$ in Eq. (7.7). The results of chapter 6 imply that, in an RPA description based on a particle number-conserving ground state, the <u>collective</u> monopole excitation is created by the "quasi-boson" operator (cf. Eq. (6.17))

$$Q_m^\dagger = \frac{1}{(\Omega)^{\frac{1}{2}}} (x\, j_+ - y\, j_-)$$

where $j_\pm$ are given in Eq. (A3.6) and $x^2 - y^2 = 1$. The coefficients x and y, and the monopole excitation energy E_m are found by solving the "linearised" equations of motion (or open-shell RPA equations)

$$<s|[\delta Q_m, (H, Q_m^\dagger)]|s> \;=\; E_m <s|[\delta Q_m,\; Q_m^\dagger]|s>, \tag{7.9}$$

where the variation in δQ_m is with respect to x and y. (The expectation values in Eq. (7.9) are evaluated by employing Eq. (7.8).)

The behaviour for large χ_N of the (positive) eigenvalue E_m which emerges from this calculation, is depicted by curve A in Fig. 6.2. Its accuracy is comparable to if not better than that of the corresponding QRPA eigenvalue. In fact, it becomes significantly better than the QRPA eigenvalue as N decreases. Since, in the general case, the open-shell RPA calculation is less tedious than the QRPA calculation, this is a considerable triumph. It also indicates that, although the HFB description of ground state properties is in general superior to the HFS description, because of its symmetry-breaking character, HFB is not necessarily the best starting point for the description of excited states, this despite the fact that QRPA possesses the property of restoring symmetry to the order of the approximation. Applications of the symmetry-conserving analogues of TDA and RPA are still in their infancy, but this example suggests that they should yield significant improvements over QRPA even in the region away from a transition point.

APPENDIX 7: NUMBER PROJECTION OF THE HFB GROUND STATE

A variety of sophisticated projection techniques have been developed (AG 74, HI 79) in order to facilitate projected TDA calculations in a BCS basis. However, in the present context, it is advantageous to proceed in a pedestrian manner (following the treatment in section 3 of chapter 5 of (So 71)), because it permits one to use the SO(5) group algebra to calculate expectation values.

The HFB ground state is, from Eq. (A3.1),

$$|v> \;=\; \eta \prod_{\substack{\sigma m \\ m > 0}} (1 + b_{\sigma m}^\dagger)|->$$

where

$$b^\dagger_{\sigma m} = \frac{v_\sigma}{u_\sigma} a^\dagger_{\sigma m} a^\dagger_{\sigma -m}, \quad \eta = (u_1 u_{-1})^{\Omega/2}, \quad v_1^2 + v_{-1}^2 = \frac{N}{\Omega}o.$$

As the operators $b^\dagger_{\sigma m}$ commute among themselves and $(b^\dagger_{\sigma m})^2 = 0$, it can be more compactly written as

$$|v\rangle = \eta\, e^{A^\dagger} |-\rangle \qquad (A7.1)$$

with

$$A^\dagger = \frac{v_1}{u_1} \ell_+ + \frac{v_{-1}}{u_{-1}} s_+ .$$

Expanding the exponential in Eq. (A7.1), one finds that the N-particle component in $|v\rangle$ ($N = 0, 2, \ldots, 2\Omega$) is

$$|N\rangle_v = \frac{\eta}{(N/2)!} (A^\dagger)^{N/2} |-\rangle,$$

or, using the binomial theorem (ℓ_+ and s_+ commute),

$$|N\rangle_v = \frac{1}{(N/2)!} \sum_{k=0}^{N/2} \binom{N/2}{k} (p_k)^{\frac{1}{2}} \ell_+^k s_+^{N/2-k} |-\rangle, \qquad (A7.2)$$

where p_k is defined in Eq. (7.1a).

Equation (A7.2) can be rewritten in terms of the states $|m,z\rangle_a$ which form the basis of the analogue for $SO_a(5)$ of the collective subspace (cf. the discussion immediately preceding Eq. (7.7b)). From (He 65),

$$|m = 0, z = -z_u + 2k\rangle_a = \frac{1}{(N/2)!} n_k^{-\frac{1}{2}} \binom{N/2}{k} \ell_+^k s_+^{N/2-k} |-\rangle$$

where n_k is defined in Eq. (7.1b). Hence

$$|N\rangle_v \;=\; \sum_{k=0}^{N/2} (n_k\, p_k)^{\frac{1}{2}}\, |m = 0,\ z = -z + 2k\rangle_a \;. \tag{A7.3}$$

The norm of $|N\rangle_v$ follows immediately - i.e.

$$\langle N|N\rangle_v \;=\; \sum_{k=0}^{N/2} n_k\, p_k \;=\; P_N \qquad \text{(cf. Eq. (7.1c))},$$

and so $|v\rangle$ can be decomposed in terms of normalised N-particle states $|N,N_o\rangle$ as

$$|v\rangle \;=\; \sum_N (P_N)^{\frac{1}{2}}\, |N,N_o\rangle$$

where $|N,N_o\rangle \;=\; (P_N)^{-\frac{1}{2}}\, |N\rangle_v$.

The PHFB ground state is $|N_o,N_o\rangle$. To calculate expectation values of quasi-spin operators in this state, one can exploit the fact that it can be rewritten in terms of the states $|m,z\rangle_a$ (cf. Eq. (A7.3)), and proceed as described in section 7.2 in connection with the calculation of expectation values in $|s\rangle$.

TABLE 7: P_N (cf. Eq. (7.1)) when $\Sigma_{N_o} = 1.5$

X_N \ N	8	10	12	14	16	18	20
1.5	0.066	0.126	0.180	0.200	0.173	0.118	0.064
2.5	0.051	0.116	0.193	0.232	0.201	0.122	0.050
3.5	0.048	0.114	0.194	0.239	0.208	0.124	0.049
4.5	0.047	0.113	0.195	0.241	0.210	0.124	0.045
P_N^a	0.045	0.111	0.195	0.244	0.213	0.124	0.044

CHAPTER EIGHT

CONCLUSION

The results presented in the preceding chapters represent a vindication of the sometimes questioned relevance (Ma 75) in finite systems of the notion of phase transitions and the associated occurrence of dynamical symmetry-breaking. In this regard, there are two particularly important (novel) results. Firstly, evidence has been found which suggests that the phase transitions predicted by zero temperature HFB mimic the effect of singularities (or exceptional points) in the dependence on interaction strengths of the exact solution. (A more precise statement of this conjecture is given at the end of section 5.1.) Secondly, it has been demonstrated that, despite the presence of thermal fluctuations, the effects of phase transitions can be discerned in the exact solution of a many-body problem at finite temperature (DM 86).

The qualitative reliability of broken-symmetry bases is seen in the calculations performed in chapters 6 and 7. The symmetry-breaking accommodates the emergence of a ne[illegible]n within the exact solution, whose clearest manifestation is the [illegible]e of specific degeneracies within the excitation spectrum (GH [illegible] This insight facilitates the interpretation of the results of an RPA calculation in a broken-symmetry basis; for example, the breaking of parity symmetry within the Agassi model indicates the existence of parity doublets, and so the RPA modes in the parity-mixed bases represent excited parity doublets built on the ground state parity doublet (a point which does not seem to have been perceived in (Ag 68)). In chapter 6, it was concluded that RPA calculations are meaningful only in a stable basis and the pragmatic implications of this conclusion were discussed. This result may be reinterpreted as follows: under certain circumstance, RPA calculations will fail unless performed in a basis with broken symmetry. This is true even when the symmetry broken has undesirable consequences, such as a spuriously low ground state energy. (The fact that performing RPA within the HFS approximation yields better results (Section 7.2) does not contradict this conclusion; HFS is not a mean-field approximation. Moreover it also breaks the relevant symmetry - i.e. parity.) Furthermore the results in broken-symmetry bases can be successfully employed to predict the qualitative character of changes introduced by projection calculations (Section 7.1).

The nature and location of the phase transitions discussed in this work have been determined by the requirement that the appropriate solution minimise the zero or finite temperature HFB variational functionals. (When two or more solutions are simultaneously local minima and some of them break symmetries, care must be taken to ensure that the lowest minimum is not spuriously lower than the others (cf. section 7.1), but, fortunately, this eventuality does not arise in the present work.) The gross structures of the corresponding phase diagrams are essentially correct. However, the changes associated with a phase transition in a finite system are spread out over an interval of interaction strengths, and this is not reflected by the single critical interaction strength yielded by HFB. In addition, while at zero temperature the critical strengths do fall within these transitional regions, at finite temperature, this is not the case in general.

The reliable location of the transitional region is important. The results of the HFB and RPA calculations considered in this work illustrate the well-known fact (BFS 69) that these approximations fail to be quantitatively accurate in precisely this region. (This is consistent with the conjectured function of these transitions, namely to mimic the effects of certain singularities.) At finite temperature, one of the distinctions between various phases is that the magnitude of thermal fluctuations differs; in particular, the present study suggests that they are in general significant in "disordered" phases like the spherical phase in the Agassi model, and so the mean-field description is not reliable in these regions. Compounding this problem is the fact that the mean-field approximation seems to grossly overestimate their extent. At finite temperature, the extent of thermal fluctuations within the disordered phases must be evaluated (using, say, Landau theory (Go 84 and references therein)) to assess the validity of the predictions of thermal HFB.

To what use can the identification of the role played by exceptional points be put? Just as in this work these singularities are credited for the qualitative reliability of "phase transitions" predicted in finite systems by HFB, so they should also lie at the root of any success in the transitional region of more elaborate methods - for example, the FHFB approximation and related techniques (SGF 84). Note that this point of view differs from the standard rather vague interpretation of the advantages of FHFB, namely that it accommodates "quantum fluctuations" (FR 85). Two (inter-related) challenges, which go beyond the scope of this work, are raised by these speculations:

(1) firstly, to derive an approximation scheme in which the role of these singularities can be seen explicitly;

(2) secondly, to develop some reliable method for locating these singularities which does not, in effect, entail solving the related many-body problem exactly.

A promising point of departure may be the "uniform" approximation scheme (LS 77 and references therein), which exploits analytic structure within the exact solution and is claimed to be valid in the transition region (AZ 84).

REFERENCES

AB 71 K. Allaart and B. Boeker, Nucl. Phys. A168 (1971) 630

Ag 68 D. Agassi, Nucl. Phys. A116 (1968) 49

AG 74 K. Allaart and W.F. van Gunsteren, Nucl. Phys. A234 (1974) 53

ALM 66 D. Agassi, H.J. Lipkin and N. Meshkov, Nucl. Phys. 86 (1966) 321

AW 85 A.Y. Abul-Magd and H.A. Weidenmüller, Phys. Lett. 162B (1985) 223

AZ 84 Y. Alhassid and J. Zingman, Phys. Rev. C30 (1984) 684

Ba 60 M. Baranger, Phys. Rev. 120 (1960) 957

BB 66 D.R. Bès and R. A Broglia, Nucl. Phys. 80 (1966) 289

BB 76 D.R. Bès and R.A. Broglia, Varenna Lectures 69 (1976) 55

BBH 85 J.R. Beene, F.E. Bertrand and M.L. Halbert, in 5th International Symposium on X-ray spectroscopy and Related Topics, Ed. S. Raman, AIP Conference Preceedings (AIP, New York, 1985), Vol. 125, p. 623

BCP 81 G. Bozzolo, M.C. Cambiaggio and A. Plastino, Nucl. Phys. A356 (1981) 48

BCS 57 J. Bardeen, L.N. Cooper and J.R. Schrieffer, Phys. Rev. 108 (1957) 1175

BD 58 C. Bloch and C. de Dominicis, Nucl. Phys. 7 (1958) 459

BFS 69 K. Bleuler, A. Friederich and D. Schütte, Nucl. Phys. A216 (1969) 628

BGG 69 J. Bar-Touv, A. Goswani, A.L. Goodman and G.L. Struble, Phys. Rev. 178 (1969) 1670

BK 68 M. Baranger and K. Kumar, Nucl. Phys. A110 (1968) 490

BKN 76 P. Bonche, S.E. Koonin and J.W. Negele, Phys. Rev. C13 (1976) 1226

BL 55 K.A. Brueckner and C.A. Levinson, Phys. Rev. 97 (1955) 1344

BLM 79 O. Bohigas, A.M. Lane and J. Martorell, Phys. Rep. 51C (1979) 267

BM 62 C. Bloch and A. Messiah, Nucl. Phys. 39 (1962) 95

BM 69 A. Bohr and B.R. Mottelson, Nuclear Structure, vol. 1 (Benjamin, New York, 1969)

BMP 58 A. Bohr, B.R. Mottelson and D. Pines, Phys. Rev. 110 (1958) 936

BMR 73 B. Banerjee, H.J. Mang and P. Ring, Nucl. Phys. A215 (1973) 366

BNP 82 G. Bozzolo, J. Núnez and A. Plastino, Phys. Rev. C26 (1982) 2692

Br 55 K.A. Brueckner, Phys. Rev. 97 (1955) 1353

BS 68 D.R. Bès and R.A. Sorenson, Adv. Nucl. Phys. 2 (1968) 129

BV 78 M. Baranger and M. Vénéroni, Ann. Phys. (NY) 114 (1978) 123

Ca 65 P. Camiz, Nuovo Cim 40A (1965) 1220

Cl 67 J. des Cloizeaux, in Many-body Physics, Eds. D. de Witt and R. Balian, (Gordan and Breach, New York, 1968), p. 5

CMM 78 R.Y. Cusson, J.A. Maruhn and H.W. Meldner, Phys. Rev. C18 (1978) 2589

Da 67 B.D. Day, Rev. Mod. Phys. 39 (1967) 719

DDK 85 K.T.R. Davies, K.R.S. Devi, S.E. Koonin and M.R. Strayer, in Treatise on Heavy-Ion Science, Ed. D.A. Bromley (Plenum, New York, 1985), vol. 3, p.1

DG 80 J. Dechargé and D. Gogny, Phys. Rev. C21 (1980) 1568

DH 84 E.D. Davis and W.D. Heiss, J. Math. Phys. 25 (1984) 812

DH 86 E.D. Davis and W.D. Weiss, J. of Phys. G: Nucl. Phys., in press

DM 86 E.D. Davis and H.G. Miller, "Phase transitions" at finite temperature in finite systems, NRIMS Technical Report TWISK 446, CSIR

DMP 66 K. Dietrich, H.-J. Mang and J. Pradal, Z. Phys. 190 (1966) 357

DS 84 R.M. Diamond and R.S. Stephens, Nature 310 (1984) 457

EHH 77 C.A. Engelbrecht, F.J.W. Hahne and W.D. Heiss, Ann. Phys. (NY) 104 (1977) 221

EK 71 J.A. Evans and N. Kraus, Phys. Lett. 37B (197') 455

ER 82a J.L. Egido and P. Ring, Nucl. Phys. A383 (1982) 189

ER 82b J.L. Egido and P. Ring, Nucl. Phys. A388 (1982) 19

ERI 85 J.L. Egido, P. Ring, S. Iwasaki and H.-J. Mang, Phys. Lett. 154B (1985) 1

FF 69 A.E. Ferdinand and M.E. Fischer, Phys. Rev. 185 (1969) 832

CMM 78 R.Y. Cusson, J.A. Maruhn and H.W. Meldner, Phys. Rev. C18 (1978) 2589

Da 67 B.D. Day, Rev. Mod. Phys. 39 (1967) 719

DDK 85 K.T.R. Davies, K.R.S. Devi, S.E. Koonin and M.R. Strayer, in Treatise on Heavy-Ion Science, Ed. D.A. Bromley (Plenum, New York, 1985), vol. 3, p.1

DG 80 J. Dechargé and D. Gogny, Phys. Rev. C21 (1980) 1568

DH 84 E.D. Davis and W.D. Heiss, J. Math. Phys. 25 (1984) 812

DH 86 E.D. Davis and W.D. Weiss, J. of Phys. G: Nucl. Phys., in press

DM 86 E.D. Davis and H.G. Miller, "Phase transitions" at finite temperature in finite systems, NRIMS Technical Report TWISK 446, CSIR

DMP 66 K. Dietrich, H.-J. Mang and J. Pradal, Z. Phys. 190 (1966) 357

DS 84 R.M. Diamond and R.S. Stephens, Nature 310 (1984) 457

EHH 77 C.A. Engelbrecht, F.J.W. Hahne and W.D. Heiss, Ann. Phys. (NY) 104 (1977) 221

EK 71 J.A. Evans and N. Kraus, Phys. Lett. 37B (1971) 455

ER 82a J.L. Egido and P. Ring, Nucl. Phys. A383 (1982) 189

ER 82b J.L. Egido and P. Ring, Nucl. Phys. A388 (1982) 19

ERI 85 J.L. Egido, P. Ring, S. Iwasaki and H.-J. Mang, Phys. Lett. 154B (1985) 1

FF 69 A.E. Ferdinand and M.E. Fischer, Phys. Rev. 185 (1969) 832

FGN 79 D.H. Feng, R. Gilmore and L.M. Narducci, Phys. Rev. C19 (1979) 1119

FKW 78 H. Flocard, S.E. Koonin and M.S. Weiss, Phys. Rev. C17 (1978) 1682

FN 75 J.L. Friar and J.W. Negele, Adv. Nucl. Phys. 8 (1975) 219

FR 85 C. Federschmidt and P. Ring, Nucl. Phys. A435 (1985) 110

GD 66 M.R. Gunye and S. Das Gupta, Nucl. Phys. 89 (1966) 443

GDM 71 A.A. Grib, E.V. Damaskinskii and V.M. Maksimov, Sov. Phys. Usp. 13 (1971) 798

Ge 81 H.B. Geyer, Boson Mappings for Elementary Excitations in Fermion Systems, AEB Report PIN - 584 (B/R), Chapter 5

Ge 85 M.Z.I. Gering, PhD Thesis, University of the Witwatersrand, 1985

GF 78 R. Gilmore and D.H. Feng, Phys. Lett. 76B (1978) 26

GH 83 M.Z.I. Gering and W.D. Heiss, S. Afr. J. Phys. 6 (1983) 44

GH 84a M.Z.I. Gering and W.D. Heiss, J. Math. Phys. 25 (1984) 327

GH 84b M.Z.I. Gering and W.D. Heiss, Phys. Rev. C29 (1984) 1113

Gi 77 R. Gilmore, Physica 86A (1977) 137

GK 80 M.R. Gunye and A. Kumar, Phys. Rev. C22 (1980) 869

GLM 65 A. Glick, H.J. Lipkin and N. Meshkov, Nucl. Phys. 62 (1965) 133

GN 80 A. Gobbi and W. Nörenberg, in Heavy Ion Collisions, Ed. R. Bock (North-Holland, New York, 1980)

Go 79a A.L. Goodman, Adv. Nucl. Phys. 11 (1979) 263

Go 79b A.L. Goodman, Nucl. Phys. A325 (1979) 171

Go 81a A.L. Goodman, Nucl. Phys. A352 (1981) 30

Go 81b A.L. Goodman, Nucl. Phys. A352 (1981) 45

Go 84 A.L. Goodman, Phys. Rev. C29 (1984) 1887

GP 86 J.M.G. Gómez and C. Prieto, Nucl. Phys. A452 (1986) 462

GS 81 N. van Giai and H. Sagawa, Phys. Lett. 106B (1981) 379

GSB 70 A.L. Goodman, G.L. Struble, J. J. Bar-Touv and A. Goswani, Phys. Rev. C2 (1970) 380

GVS 76 A.L. Goodman, J.P. Vary and R.A. Sorenson, Phys. Rev. C13 (1976) 1674

HB 68 R.W. Haymaker and R. Blankenbecler, Phys. Rev. 171 (1968) 1581

He 65 K.T. Hecht, Nucl. Phys. 63 (1965) 177

He 80 W.D. Heiss, J. Math. Phys. 21 (1980) 848

He 81 W.D. Heiss, J. Math. Phys. 22 (1981) 1182

HHR 82 K. Hara, A. Hayashi and P. Ring, Nucl. Phys. A385 (1982) 14

HI 79 K. Hara and S. Iwasaki, Nucl. Phys. A332 (1979) 61

Ho 49 L. van Hove, Physica 15 (1949) 951

Hø 65 J. Høgaasen, Nuovo Cim. 36 (1965) 773

Hu 63 K. Huang, Statistical Mechanics, (Wiley, New York, 1963)

JLS 82 A.D. Jackson, A. Lande and R.A. Smith, Phys. Rep. 86C (1982) 55

Ka 66 T. Kato, Perturbation Theory for Linear Operators, (Springer, New York, 1966)

Ka 68 A. Kamlah, Z. Phys. 216 (1968) 52

KB 66 K. Kumar and M. Baranger, Phys. Rev. Lett. 17 (1966) 1146

KCL 82 A. Klein, T.D. Cohen and C.-T. Li, Ann. Phys. (N.Y.) 141 (1982) 382

Ke 61 A.K. Kerman, Ann. Phys. (N.Y.) 12 (1961) 300

KG 84 K. Kumar and J.B. Gupta, J. Phys. G: Nucl. Phys. 10 (1984) 525

KG 85 S.E. Koonin and H.B. Geyer, in Hadrons and Heavy Ions, Ed. W.D. Heiss, Lecture Notes in Physics (Springer, Berlin, 1985), vol. 231, p.1

KL 85 S.P. Klevansky and R.H. Lemmer, J. Phys. G: Nucl. Phys. 11 (1985) 1103

KLM 61 A.K. Kerman, R.D. Lawson and M.H. Macfarlane, Phys. Rev. 124 (1961) 162

Kü 79 H.G. Kümmel, Nucl. Phys. A317 (1979) 199

Ku 81 T.T.S. Kuo, in Topics in Nuclear Physics I, Eds. T.T.S. Kuo and S.S.M Wong, Lecture Notes in Physics (Springer, Berlin, 1981), vol. 144, p. 248

La 66 R.V. Lange, Phys. Rev. 146 (1966) 301

La 80 R.D. Lawson, Theory of the Nuclear Shell Model, (Oxford University Press, New York, 1980)

LA 84 S. Levit and Y. Alhassid, Nuc. Phys. A413 (1984) 439

LG 85 R.H. Lemmer and W. Greiner, Phys. Lett. 162B (1985) 247

LM 80 A.M. Lane and J. Matorell, Ann. Phys. (NY) 129 (1980) 273

LMG 64 H.J. Lipkin, N. Meshkov and A.J. Glick, Nucl. Phys. 62 (1965) 188

LS 77 S. Levit and U. Smilansky, Ann. Phys. (NY) 108 (1977) 165

Ma 75 H.-J. Mang, Phys. Rep. 18C (1975) 325

Ma 74 E.R. Marshalek, Nucl. Phys. A224 (1974) 245

Ma 82 E.R. Marshalek, Ann. Phys. (NY) 143 (1982) 191

MGL 65 N. Meshkov, A.J. Glick and H.J. Lipkin, Nucl. Phys. 62 (1965) 199

Mo 72 L.G. Moretto, Nucl. Phys. A185 (1972) 145

Mo 73 L.G. Moretto, Nucl. Phys. A216 (1973) 1

MPR 65 H.-J. Mang, J.K. Poggenburg and J.O. Rasmussen, Nucl. Phys. 64 (1965) 353

MSR 76 H.-J. Mang, B. Samadi and P. Ring, Z. Phys. A279 (1976) 325

MV 60 B.R. Mottelson and J.G. Valatin, Phys. Rev. Lett. 5 (1960) 511

MV 83 H.G. Miller and J.P. Vary, Phys. Lett. 131B (1983) 271

MW 69 E.R. Marshalek and J. Weneser, Ann. Phys. (NY) 53 (1969) 569

MW 79 Y. Miyanishi and G. Watanuki, Prog. Theor. Phys. 61 (1979) 680

MZP 74 U. Mosel, P.-G. Zint and K.H. Passler, Nucl. Phys. A236 (1974) 252

Ne 82 J.W. Negele, Rev. Mod. Phys. 54 (1982) 913

Ni 64 S.G. Nilsson, Nucl. Phys. 55 (1964) 97

NV 72 J.W. Negele and D. Vautherin, Phys. Rev. C5 (1972) 1472

OS 83 K. Okamoto and K. Suzuki, Prog. Theor. Phys. 70 (1983) 606

Pa 65 J.C. Parikh, Nucl. Phys. 63 (1965) 214

Pa 71 R. Pathria, Statistical Mechanics, (Pergamon, Oxford, 1971)

QM 86 R.M. Quick and H.G. Miller, submitted for publication

Ra 50 J. Rainwater, Phys. Rev. 79 (1950) 432

Re 80 L.E. Reichl, A Modern Course in Statistical Physics, (Arnold, London, 1980)

RP 85 R. Rossignoli and A. Plastino, Phys. Rev. C32 (1985) 1040

RR 64 M. Rho and J.O. Rasmussen, Phys. Rev. 135 (1964) B1295

RS 80 P. Ring and P. Schuck, The Nuclear Many-body Problem, (Springer, Berlin, 1980)

RW 70 D.J. Rowe and S.S.M. Wong, Nucl. Phys. A153 (1970) 561

Sc 72 H. Schmidt, Varenna Lectures 53 (1971) 144

SEN 84 Spin Excitations in Nuclei, Conference Proceedings, Eds. F. Petrovich et al., (Plenum, New York, 1984)

SGB 69 S.L. Salpathy, D. Goss and M.K. Banerjee, Phys. Rev. 183 (1969) 887

SGF 84 K.W. Schmid, F. Grümmer and A. Faessler, Phys. Rev. C29 (1984) 291, 308

So 71 V.G. Soloviev, Theory of Complex Nuclei, (Pergamon, Oxford, 1971)

So 83 H.M. Sommermann, Ann. Phys. (NY) 151 (1983) 163

SW 73 T.H. Schucan and H.A. Weidenmüller, Ann. Phys. (NY) 76 (1973) 483

TBC 82 I. Tseruya et al, Phys. Rev. C26 (1982) 2509

Th 60 D.J. Thouless, Nucl. Phys. 21 (1960) 225

Th 61 D.J. Thouless, Nucl. Phys. 22 (1961) 78

Th 83 H. Thomas, in Critical Phenomena, Ed. F.J.W. Hahne, Lecture Notes in Physics (Springer, Berlin, 1983), vol. 186, p. 141

TV 62 D.J. Thouless and J.G. Valatin, Nucl. Phys. 31 (1962) 211

UR 71 N. Ullah and D.J. Rowe, Nuc. Phys. A163 (1971) 257

Va 61 J.G. Valatin, Phys. Rev. 122 (1961) 1012

VC 70 F. Villars and G. Cooper, Ann. Phys. (NY) 56 (1970) 224

Wa 72 P.G. Watson, in Phase Transitions and Critical Phenomena, Eds. C. Domb and M.S. Green (Academic, London, 1972), vol. 2, p. 101

WAM 85 E. Wüst, A. Ansori and U. Mosel, Nucl. Phys. A435 (1985) 477

WH 86 G.M. Welke and W.D. Heiss, Phys. Rev. D 33 (1986) 2047

Wi 65 J.H. Wilkinson, The Algebraic Eigenvalue Problem, (Clarendon, Oxford, 1965)

YL 52 C.N. Yang and T.D. Lee, Phys. Rev. 87 (1952) 404, 410

YLV 62 A.P. Yutsis, I.B. Levinson and V.V. Vanagas, Mathematical Apparatus of the theory of Angular Momentum, (Israel Program for Scientific Translations, Jerusalem, 1962)

Zu 62 B. Zumino, J. Math. Phys. 3(1962) 1055